D. Koopman

The Topology Optimised Glass Bridge

TUDelft

The Topology Optimised Glass Bridge

By

D. Koopman

in partial fulfilment of the requirements for the degree of

Master of Science
in Civil Engineering

at the Delft University of Technology,
to be defended publicly on Friday, July 2, 2021, at 3:00 PM.

The graduation committee consists out of:

prof.dr. M. Overend
Chairman graduation committee - Architectural Engineering + Technology
T: (+31) (0)15 2784094
E: M.Overend@tudelft.nl

Dr.ir. R. Schipper
Supervisor Delft University of Technology - Civil Engineering/Building Engineering
T: (+31) (0)15 2789933
E: H.R.schipper@tudelft.nl

Dr.ir. F.A. Veer
Supervisor Delft University of Technology - Architecture and the Built Environment / Architectural Engineering + Technology / Structural Design & Mechanics
T: (+31) (0)15 2781358
E: F.A.Veer@tudelft.nl

Dr. F. Oikonomopoulou
Supervisor Delft University of Technology - Architectural Engineering + Technology
T: (+31) (0)15 2785835
E: F.Oikonomopoulou@tudelft.nl

Ir. C. Noteboom
Supervisor Delft University of Technology - Civil Engineering/Building Engineering
T: (+31) (0)15 2783332
E: C.Noteboom@tudelft.nl

This master thesis was created by:

D. Koopman, BSc
Student Civil Engineering – Building Engineering, Structural Design

Preface

The document in front of you represents the closing of a chapter and the beginning of a new one. This thesis is the final assessment for completing the program Building Engineering (specialisation in structural design) within the Master of Civil Engineering at the Delft University of Technology.

During the duration of my master program, one course, in particular, got stuck in my mind. This was the course about structural glass. With this topic in mind, I ended up with Faidra Oikonomopoulou. She encouraged me to continue the exciting and cool research done by several students on the use of 3D-printed sand moulds and topology optimisation to design and produce cast glass elements and structures of complex mass-optimised geometries. Thank you for making me enthusiastic about the topic.

I want to thank Mauro Overend, Roel Schipper, Fred Veer, Faidra Oikonomopoulou, and Chris Noteboom for their feedback, time, advice, and for their critical view throughout the process. Additionally, I would like to thank my parents, boyfriend, and friends for supporting me in the crazy time I wrote this thesis in. Also, for giving me motivation, insight, and feedback during my graduation process.

Daan Koopman
Delft, June 2021

Table of Contents

List of figures

List of tables

Abstract

This research investigates how to design a glass pedestrian bridge that is structurally optimised for multiple load scenario's and feasible in terms of fabrication and construction.

Linear glass elements such as panes have limited freedom of shape. On the other hand, cast glass can be produced into any shape possible. When glass is used in large quantities with large cross-sections, the annealing process can take a long time and require a significant amount of energy. The annealing time must be kept to a minimum to make cast glass a viable option. This is where topology optimisation can play its part.

During topology optimisation, the layout of an element is optimised on the given constraints for the specified design domain. In this design domain, optimisation generally occurs on an objective function based on compliance (strain and displacement) or an objective function based on stresses (Von Mises). A compliance-based optimisation is found to be the most suitable objective function. The software package Ansys and the plugins for McNeel Rhinoceros/Grasshopper: Ameba, Karamba 3D, Millipede, Peregrine and tOpos are compared on their topology optimisation tool during the software research. During this comparison, Ansys is found to be the most suitable software. This is mainly because of the possibility of implementing a cross-sectional constraint during the optimisation, which is needed for implementing a maximum annealing time. The topology optimisation method 'Level Set' is used to obtain an optimised design with clear edges and smooth contours. The most suitable production method for topology optimised cast glass elements is found to be kiln casting with a 3D printed sand mould.

Glass is a brittle material with a low tensile strength compared to its compressive strength. The only type of bridge that can be made entirely in compression, without pre-tensioning, is an arch bridge. This bridge type is used for the final design. The new bridge spans a canal of 6 meters, has a total length of 10 meters, and has a width of 2 meters. Furthermore, the design is made such that maintenance to the waterway is possible. The design life of the bridge is 50 years with consequence class 3.

The loads considered during structural analysis are the vertical traffic load (distributed and point) and the vertical wind load. The parallel and perpendicular loads from the wind are found to be negligible compared to the structure's weight. The bridge is made from borosilicate glass. This type of glass is used to reduce the effect of temperature on the cast structure of the bridge. Additionally, the supports and connections are designed so that they do not restrain deformation from temperature. Furthermore, the shape and place of the connections and supports ensure the possibility of unequal settlement without the formation of unacceptable stresses.

Multiple variant studies are carried out. In the first variant study, optimisation is done on several 2D models to determine the best shape for the bridge's final design. The second variant study focuses on the 3D shape of the bridge and how the bridge is split into manageable segments. The final bridge comprises four cast outer elements, one cast keystone, and a float glass bridge deck. The bridge is simply supported on both sides of the canal. The connections and supports are based on compression and friction and use a polyurethane interlayer. The weight of the final optimised bridge is reduced from 32t to 11.2t with a maximum cross-sectional thickness of 210 mm to get an annealing time of approximately one month.

Due to symmetry in the design, only one-fourth of the bridge is optimised. During the optimisation, seven different distributed load scenarios are implemented. For the point load, a region is excluded from optimisation. After optimisation, finite element analysis and manual verifications are performed. The point load was found to have a significant impact on the topology of the structure. The final design of the bridge is given in Figure 1.1.
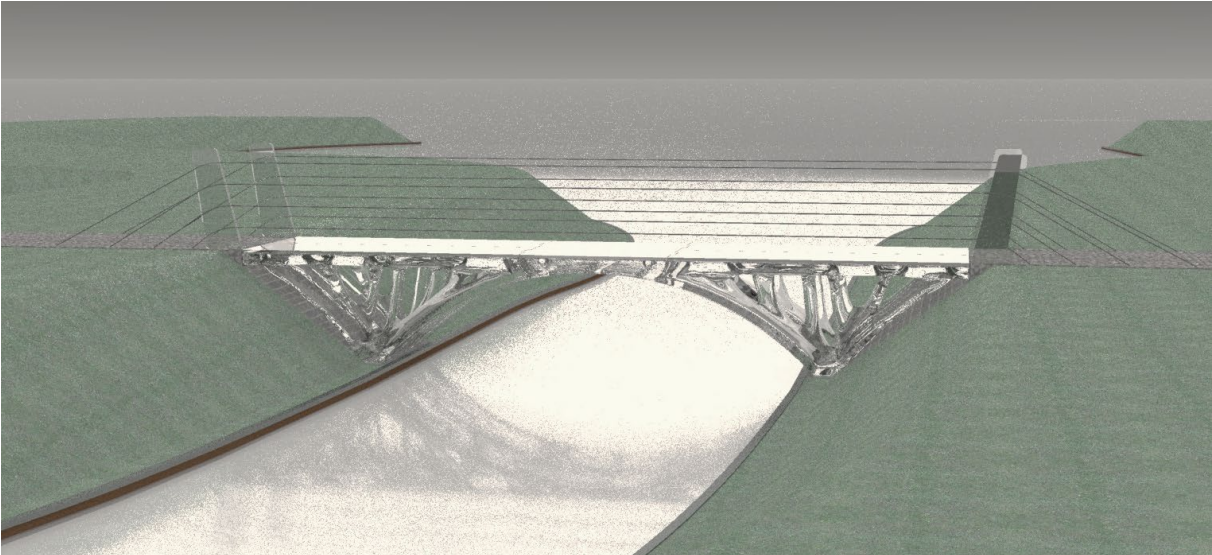
Figure 1.1 3D impression of the bridge

Part 1

Introduction into the research

Part 1 of this document contains the outline of this research. This description includes the problem description, research goals, research questions, and methodology.

1. Introduction

1.1 Introduction

In the past few years, several students from the master Architecture (Track: Building Technology) researched the possibility of using 3D-printed sand moulds and topology optimisation to design cast glass elements and structures of perplex mass-optimised geometries. This research continues with these subjects by investigating how to design and build a glass bridge that is structurally optimised and feasible in terms of fabrication.

Glass has been used since the stone age and has had different applications. Such as cutting tools, weapons, beads, vessels, vases, pottery, lenses, and windows. The reduced manufacturing costs due to the new mass-production techniques developed throughout the 20th century resulted in the increased use of glass. The development of the float glass process in the 1950s resulted in flat sheets of high quality (Freiman, 2007). Due to its translucent property and refraction of light, it is very suitable to use in the construction industry. Glass in structures is mainly used for windowpanes. In the past decades, an increasing number of structures have been designed and built using glass as a structural component. Structures like the Atocha Memorial built in 2004 (esmadrid, 2004), Crown Fountain built in 2004 (Chicago, n.d.), The Optical House built in 2012 (Fuji, 2013), and Crystal Houses built in 2016 (Scagliola & Brakkee, 2019) used structural components made from cast glass. These structures can be seen in Figure 1.1.

Figure 1.1 Top left: Atocha Memorial located in Madrid by (esmadrid, 2004); Top right: Crown fountain located in Chicago by (Matthews, 2017); Bottom left: Optical Glass House located in Hiroshima by (Fuji, 2013); Bottom right: Crystal Houses located in Amsterdam by (Scagliola & Brakkee, 2019).

2

Besides the development of the structural glass industry, there has also been a development in bridges. The use of new materials and design methods resulted in new types of bridges. For example, the Catharina bridge in Leiden made out of ultra-high performance concrete (Wilde, 2018), the MX3D bridge constructed using 3D printing of stainless steel (MX3D, n.d.), the Symbiobridge in Delft built with an unusual shaped steel load-bearing structure and bridge deck made of composite fibreglass (Starink, 2016), and the glass truss bridge constructed with struts made of bundled extruded glass and nodes made out of cast glass components (A.H. Snijder, Nijsse, & Louter, 2018). See Figure 1.2 for an overview of these bridges.

Figure 1.2 Top left: Catherina bridge in Leiden by (Hummel, 2018); Top right: MX3D bridge by (MX3D, n.d.); Bottom left: Symbio Bridge; Bottom right: Glass truss bridge.

1.2 Problem description

Glass is characterised by high compressive strength, low tensile strength and low ductility. There are four main possibilities when using structural glass: flat, corrugated, extruded, or solid (3D) elements. Glass in the building industry is mainly used for windows. However, over the past decades, an increasing amount of structural glass is being used, mainly as flat sheets. A disadvantage is that these elements have a limited thickness and freedom of shape. Cast glass, on the other hand, can be produced in any shape possible. Oikonomopoulou (2019) showed that cast glass could be used structurally. The development of structural glass is still at an early stage and needs lots of research to explore its aspects. In this thesis, the focus is on solid cast glass elements.

Glass has the disadvantage that when used in large quantities with large cross-sections, the annealing time takes up a lot of time, money and energy. Oikonomopoulou (2019) explains that shape optimisation of cast glass elements can result in more feasible structures. The most important aspect is to reduce the annealing time of the elements, the larger and thicker the glass piece, the (exponentially) longer the annealing time. Massive cast glass elements sometimes have an annealing time of more than 12 months to reduce the chance of cracking, as was the case with the biggest solid mirror. More information about this cast glass element follows in part 2. A solution must be found on using the full compressive strength of glass and minimising the annealing time. This is where topology optimisation (TO) can play its part. TO can reduce the weight and maximum size of the components. With this weight and size reduction, the annealing time is also reduced.

Topology Optimisation (TO) can be used to optimise the layout of a structure. This way, one can create a form that utilizes the material more efficiently while considering the crucial constraints during a glass bridge's design and construction phase. Topology optimised structures result in complex shapes that are challenging to manufacture. Producing steel moulds could be very time consuming and expensive. Powder bed 3D printing is a form of additive manufacturing that can realise a topology optimised structure.

TO for cast glass is still at an early stage of development. Previous research has shown that cast glass can be used for structural application. Additionally, various structures have been designed that used topology optimisation combined with cast glass and additive manufacturing. It shows that the combination could be a viable option in producing large cast glass elements. Since glass is not a typical building material and elaborate design regulations are missing, the cast elements should be modelled, verified, and tested on structural behaviour.

Multiple factors should be studied when designing a glass bridge. This master thesis focuses on the use of topology optimisation during the design phase. The following aspects are further considered during the design phase: limiting factors for glass, topology optimisation, and the production and construction process.

1.3 Research goals

This research aims to be useful for the field of glass engineering. Therefore, a meta-goal has been set up. It is not possible to achieve this goal in one thesis. Therefore, based upon the meta-goals, more specific research goals are drafted. The main research goal is answered within this thesis.

The meta-goal is as followed:
- *To show how large full glass structures can be produced for the building industry using glass, additive manufacturing, and topology optimisation.*

The main research goals are as followed:
- *To show how topology optimisation can be used for the design of a glass pedestrian bridge.*
- *To show which and in what way constraints should be considered during a glass bridge's design and construction phase.*

1.4 Research questions

This thesis investigates the use of topology optimisation on the design of a glass bridge. The main research question follows from the main research goals.
- *How can a virtually monolithic glass pedestrian bridge be designed and constructed feasibly by using topology optimisation while considering external influences?*

This research question is answered in two parts. For the first part, a literature review is done to acquire all relevant theory. The second part goes into detail on the design development and construction of the bridge. Below an overview is given of the sub-questions that are answered in this thesis.

SQ1:   What are the characteristic properties of glass, and how can it be used as a structural material in a cast glass structure?

SQ2:   What are the fundamental principles of additive manufacturing, and how can it be used for glass structures?

SQ3:   What are the fundamental principles of topology optimisation, and how can it be used for glass structures?

SQ4:   What are the structural design principles of the new pedestrian bridge made from cast glass?

SQ5:   How does the weather affect the bridge, and how should this be incorporated in the bridge design?

SQ6:   Which type of topology optimisation and which software is most suitable for designing a glass bridge, and how are this type and software used for the final design?

1.5 Methodology

In this section, the methodology to answer each sub-question is given. With the answers from the sub-questions, the main research question is answered.

SQ1: What are the characteristic properties of glass, and how can it be used as a structural material in a cast glass structure?

This question is answered with a literature review that focuses on the fundamentals of glass. First, the physical, structural, and mechanical properties are given, followed by different glass types, glass manufacturing processes, annealing processes, and current building regulations and design methods.

SQ2: What are the fundamental principles of additive manufacturing, and how can it be used for glass structures?

A literature review is performed to investigate different mould types and manufacturing techniques. Additionally, a detailed explanation of additive manufacturing is given and how it can be used for casting glass.

SQ3: What are the fundamental principles of topology optimisation, and how can it be used for glass structures?

This question investigates the fundamentals of topology optimisation. In the literature review, the concept of structural optimisation is given, followed by the classification of different topology optimisation approaches and objective functions.

SQ4: What are the structural design principles of the new pedestrian bridge made from cast glass?

From the literature study follows the most appropriate bridge topology. Second, the current regulations are provided and discussed. Third, multiple pedestrian and bicycle bridges are examined on design and material use. The result from this question is the approach used to design the bridge. After production, the bridge must be transported and placed on location. During this process, it is essential to consider the limitations the surrounding area gives. The bridge has a significant weight and size, which impacts the transportation and construction method.

SQ5: How does the weather affect the bridge, and how should this be incorporated in the bridge design?

A bridge is exposed to weather effects such as solar radiation, precipitation, and wind. These effects can cause thermal expansion or shrinkage, the bridge becoming slippery and horizontal forces. These effects are modelled to see their behaviour. When necessary, the weather effects are implemented during the design phase.

SQ6: Which type of topology optimisation and which software is most suitable for designing a glass bridge, and how are this type and software used for the final design?

The type of TO methodology and objective function used is addressed to answer this question. Various available software packages are studied. For each package, the advantages and limitations are considered. This results in the most suitable TO optimisation software for cast glass. The shape of the arches, the boundary conditions, the support conditions, and how this influences the design is explored. These variant studies show which topology and boundary conditions are most suitable for the final bridge design. A roadmap is given that provides a feasible method to design a cast glass structure. This roadmap is used during the case study.

1.6 Structure

Part 2, chapter 2 until 6, gives the framework in which an overview of the relevant information needed is given for designing a glass topology optimised bridge. This includes the fundamentals of glass, additive manufacturing, topology optimisation, and bridge design. The last chapter of part 2 summarizes the constraints and starting points used in part 3. In part 3, chapter 7 until 9, a comparison is made between different topology optimisation tools. With the most suitable tool, a design is made for the glass bridge, multiple variant studies were done to arrive at the bridge's final design. In chapter 9, the design for the case study is elaborated further. In part 4, chapter 10 until 12, the conclusion, discussion, and recommendations for further research are given.

Part 2

Framework

The framework gives an overview of the relevant information needed when designing a cast glass topology optimised bridge. The fundamentals of glass, additive manufacturing, topology optimisation, and bridge design are explained. Based on these fundamentals and various cases, a list with design constraints and starting points is made that are considered during the glass bridge design.

2. Building with glass

Glass has had increasing popularity over the last few decades. The reduced manufacturing costs due to the new mass-production techniques developed throughout the 20th century resulted in the increased use of glass. The development of the float glass process in the 1950s resulted in flat sheets of glass with a high quality (Freiman, 2007). Glass is an incredibly durable and fully recyclable material that can be transparent. This makes it very suitable to use in the building industry.

This chapter includes a summary of different glass types, physical properties, structural behaviour, and other properties of glass. Additionally, manufacturing processes are explained that could be used to produce 3D objects. This includes the production method, glass treatment, design considerations and safety, and reference projects. Lastly, a conclusion about the production of 3D elements with the different manufacturing processes is given.

2.1 Different glass types

2.1.1 Commercially used glass types

The commercially used glass types are soda-lime, borosilicate, lead silicate, aluminosilicate, fused silica and 96% silica. The chemical compositions and characteristics differ for these glass types (Oikonomopoulou, Bristogianni, Barou, Veer, & Nijsse, 2018). Table 2.1 gives an overview of the glass types and their characteristics and typical application.

Table 2.1 Glass types with their characteristics and typical applications. From (Oikonomopoulou et al., 2018).

Glass type	Characteristics	Typical applications
Soda-lime (window glass)	Durable. Least expensive type of glass. Poor thermal resistance. Poor resistance to strong alkalis (e.g., wet cement)	Windowpanes Bottles Façade glass
Borosilicate	Good thermal shock and chemical resistance. More expensive than soda-lime and lead glass.	Laboratory glassware Household ovenware Lightbulbs Telescope mirrors
Lead silicate	Second least expensive type of glass. Softer glass compared to other types. Simple to process while cold. Poor thermal properties. Good electrical insulating properties.	Artistic ware Neon-sign tubes TV screens (CRT) Absorption of X-rays (when PbO % is high)
Aluminosilicate	Excellent thermal shock and chemical resistance. High manufacturing cost.	Mobile phone screens Fibreglass High-temperature thermometers Combustion tubes
Fused silica	Biggest thermal shock and chemical resistance. High melting point. Challenging to work with. High production cost.	Outer windows on space vehicles Telescope mirrors
96% silica	Excellent thermal shock and chemical resistance. The meticulous manufacturing process and high production cost.	Furnace sight glasses Outer windows on space vehicles

2.1.2 Physical properties

Glass does not go through phase changes. By heating the glass, only the viscosity changes. At a low temperature, glass can be considered a solid material, and when heating the glass, the behaviour of the glass becomes viscous. In Figure 2.1, the relation for soda-lime glass is given between temperature and viscosity. When producing new glass from raw materials, the ingredients must be heated until the mean melting point. The softening point is the temperature where the glass flows under its self-weight. The viscosity of the glass at softening point is around $10^{7.65}$ poise. The corresponding temperature should be used during kiln casting. The annealing point (glass transition temperature) lies in the transformation range. The strain point is the lowest temperature in this range. The transformation range is where glass moves from viscous to solid. (Oikonomopoulou, 2019). Because the viscosity decreases significantly during cooling, the glass molecules do not have enough time to rearrange themselves to form a crystal structure. When glass is cooled slow enough, the glass can form crystal structures. When this happens, the glass becomes translucent (Haldimann, Luible, & Overend, 2008).
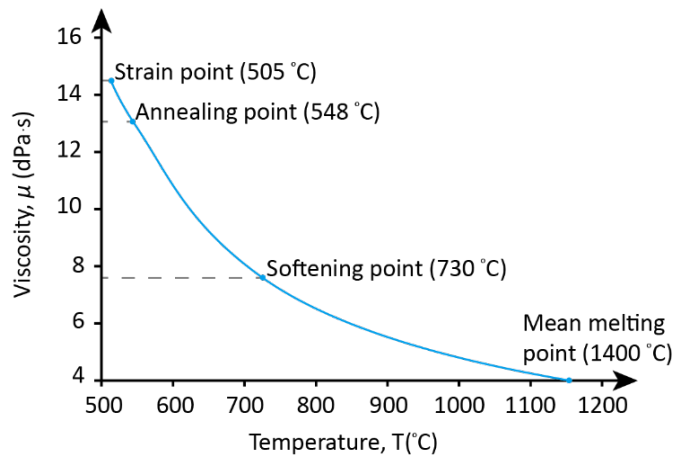
Figure 2.1 Relation between viscosity and temperature, based on (Rubem et al., 2012).

Only approximations can be given for the material properties of glass. For each glass type, there are several different glass compositions. All these compositions have slightly different physical properties. In Table 2.2, the approximate physical properties are given for the different glass types.

Table 2.2 Approximate physical properties of different glass types. From (Institution of Structural Engineers, 2014; Oikonomopoulou et al., 2018).

Glass type	Unit	Soda-lime	Borosilicate	Lead silicate	Aluminosilicate	Fused silica	96% silica
Approximate Composition	%	73% SiO_2 17% Na_2O 5% CaO 4% MgO 1% Al_2O_3	80% SiO_2 13% B_2O_3 4% Na_2O 2.3% Al_2O_3 0.1% K_2O	63% SiO_2 21% PbO 7.6% Na_2O 6% $K2O$ 0.3% CaO 0.2% MgO 0.2% B_2O_3 0.6% Al_2O_3	57% SiO_2 20.5% Al_2 12% MgO 1% Na_2O 5.5% CaO	99.5% SiO_2	96% SiO_2 3% $B2O_3$
Mean melting point at 10 Pa. s	ºC	1350-1400	1450-1550	1200-1300	1500-1600	>>2000	>>2000
Softening point	ºC	730	780	626	915	1667	1500
Annealing point	ºC	548	525	435	715	1140	910
Strain point	ºC	505	480	395	670	1070	820
Density	kg/m³	2460	2230	2850	2530	2200	2180
Coefficient of expansion 0 ºC - 300 ºC	10^{-6}/ºC	8.5	3.4	9.1	4.2	0.55	0.8
Young's modulus	GPa	69	63	62	87	69	67
Poisson's ratio	-	0.23	0.2				

Glass types used in structures

Soda-lime glass is the cheapest and most used type of glass on the market. Due to the higher thermal expansion coefficient and the longer annealing time, this type of glass is less suitable for casting. The expansion coefficient and longer annealing time are less critical for float-glass since float-glass is produced with a small thickness. Borosilicate glass has a good thermal shock performance due to the lower thermal expansion coefficient. During production, lower temperatures are needed to produce an element. Additionally, this glass type anneals faster in comparison to soda-lime glass. Lead silicate has a high thermal expansion coefficient, high density and is relatively soft compared to other types of glass. This makes it very suitable to use for optical elements and crystal glass for tableware since it is easy to form the glass in the desired shape. Aluminosilicate glass has a smaller expansion coefficient and has a high chemical resistance. However, it is harder to fabricate elements from this type of glass. Fused silica and 96% silica have a very high mean melting point, softening point, and annealing point. The temperatures needed during the production process of these glass types make the formation of the glass elements more expensive and more challenging compared to the other glass types.

It can be concluded that soda-lime glass is most favourable when using glass in the building industry in the form of float-glass since it is the cheapest and most readily available. The best material used for casting is borosilicate glass since it has an excellent thermal shock performance and shorter annealing time.

2.2 Structural behaviour & Properties of glass

Glass is a brittle material with a low capacity for tensile stresses and a high capacity for compressive stresses. Glass has an amorphous (non-crystalline) molecular and isotropic structure. (Wurm & Peat, 2007)

2.2.1 Structural properties of glass

When comparing glass with the behaviour of steel and concrete, the main difference that can be found is that steel starts to yield when loaded in tension until a certain stress. The yield strength is a well-known material property of steel and can be used during design. Glass and unreinforced concrete, on the other hand, do not yield. Because of the strong covalent bonds, the theoretical yield strength of glass is estimated to be close to 8 GPa. This strength is approximately thirty times higher than the yield strength of steel. But due to geometric surface flaws such as scratches, inclusions, bubbles, and inhomogeneities, the tensile strength is a hundredth times smaller than the expected theoretical strength of glass (Lehman, n.d.; Wurm & Peat, 2007). A prediction could be made for the strength of glass by looking at it on a microscopic level, which is a very costly and time-consuming process. Therefore, experimental data is known that predicts the failure of a glass piece. A comparison of the stress-strain diagram of glass and steel can be found in Figure 2.2.
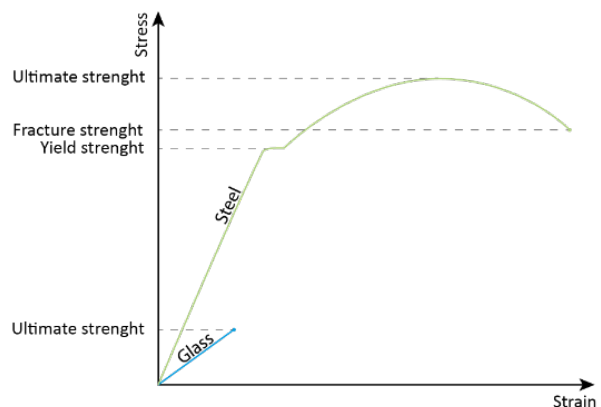
Figure 2.2 Stress-strain diagram of steel and glass.

2.2.2 Probability distribution

No distribution aligns with the probability failure distribution of glass. The Weibull probability density function is mainly applied with a high coefficient for the variation of strength. However, a single Weibull distribution is not enough to predict the failure stress. Veer and Rodichev (2011) showed that multiple Weibull distributions are a better approximation for the failure stress of glass.

2.2.3 Structural application of glass

Glass can still be used for load-bearing components such as beams, columns, walls, or floors. This is because it presents a compressive load-bearing capacity higher than concrete and many types of structural steel and due to its increased safety by laminating and tempering the glass elements (Oikonomopoulou, 2019).

The tensile strength of glass is influenced by the pane size, the type of glass, the pane age, the air moisture content of the surrounding medium, and the load duration. The surface quality has a substantial correlation with the tensile and bending strength. A large and old pane has a lower strength due to the higher possibility of critical defects (Wurm & Peat, 2007). Due to the high compressive capacity, local tensile stresses occur near supports and irregular geometries. These stresses can lead to local failure. Because of this phenomenon, glass's compressive strength is about 5 GPa, and under permanent load, this value is even lower and is estimated to be 170 MPa (Wurm & Peat, 2007). The design strength of glass can be calculated according to NEN 2608:2014. In this calculation, a distinction is made between annealed glass and pre-tensioned glass. The following values are advised to use in the analysis of a glass structure: a compressive strength of 200 MPa, a tensile strength of 20 MPa for annealed glass (6 MPa for long term loads), a tensile strength of 40 MPa for heat-strengthened glass, and a tensile strength of 80 MPa for fully tempered glass (Oikonomopoulou, 2020).

2.2.4 Thermal shock resistance

For glass that is exposed to temperature differences, the thermal shock resistance must be considered. The thermal shock resistance is the temperature difference an element can withstand without breaking. For basic annealed soda-lime glass, this is 40 $^{\circ}$C, and for borosilicate glass, this is more than double the temperature for soda-lime. This difference is mainly due to the difference in thermal expansion coefficient between the materials. For annealed soda-lime glass, the expansion coefficient is equal to 8.5 x 10^{-6} K^{-1} compared to borosilicate with an expansion coefficient of 3.4 x 10^{-6} K^{-1} (Wurm & Peat, 2007).

2.3 Glass manufacturing processes

Standard production processes for glass are: floating, drawing, casting, blowing, pressing and extraction (Haldimann et al., 2008). Glass used in the building industry is primarily flat and sometimes corrugated, extruded, or cast. With float glass, 3D printed glass, and cast glass, it is possible to produce a three-dimensional object, which could be used in the building industry. With float glass, this can be done by cutting out and laminating different layers. With 3D printed glass, a three-dimensional object is formed via material extrusion, and with casting glass, a three-dimensional element can be created by hot-pouring and kiln casting. The focus of the following three sections is on these three methods.

2.3.1 Float glass

The development of the float glass process in the 1950s resulted in flat sheets of glass with high quality and lower manufacturing cost (Freiman, 2007). Since then, float glass became the most used form of flat glass in the building industry.

2.3.1.1 *Production process*

A schematic overview of the production process can be found in Figure 2.3. In the production process, the raw materials and recycled glass are heated in the melting furnace to about 1500 ^{o}C. The molten material is poured onto a tin bath to produce a flat ribbon with uniform thickness (Institution of Structural Engineers, 2014). The thickness of the glass can be varied between 2 and 25 mm by adjusting the top rollers. After leaving the float bath, the glass enters the annealing lehr. In this step, the glass is gradually cooled down from 600 ^{o}C to 100°C over a length of up to 150 meters. When the glass leaves the annealing lehr, the glass is automatically inspected for visual defects. Where necessary, these defects are removed during the cutting process. The standard size of the panes is 3.21 x 6 meter. However, in recent projects, elements with dimensions up to 4 x 20 meter were used (Oikonomopoulou, 2019). The standard thickness of float glass is 2, 3, 4, 5, 6, 8, 10, 12, 15, 19, and 25 mm. Glass with a thickness between 4-15 is primarily used in the building industry. Thicker glass is hardly fabricated because of the longer cooling and annealing process and the problems that arise during cutting (Oikonomopoulou, 2019).
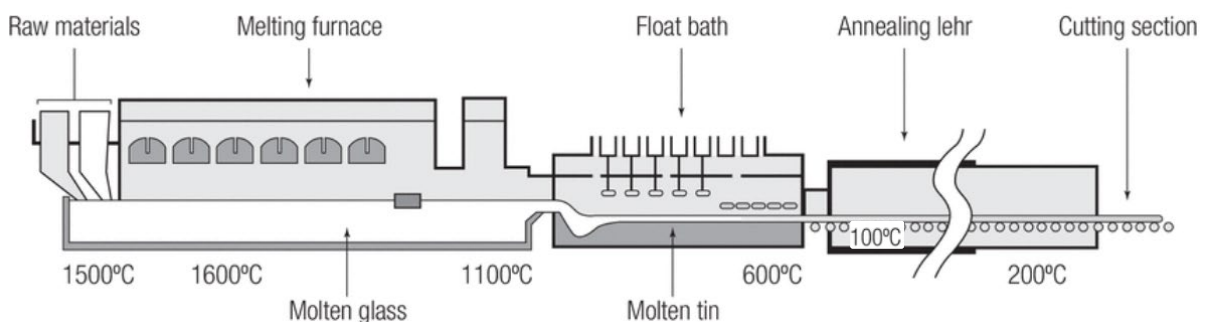
Figure 2.3 Float glass process. From (Institution of Structural Engineers, 2014).

2.3.1.2 *Annealing and Glass treating*

Annealing is the primary treatment of glass. Glass transitions from liquid to solid glass at different speeds and at different moments. Because of this, permanent stresses occur in the glass due to unequal behaviour. The stresses are reduced during annealing in the annealing lehr. The main processes to further strengthen the glass is thermal tempering, chemically toughening, and lamination. Thermal tempering of glass can be subdivided into heat strengthened glass and toughened glass. The production of heat-strengthened glass starts with annealed glass being reheated until roughly 620 ^{o}C and is then cooled rapidly with jets of air. As a result, the surface becomes compressed. Toughened glass is produced in a similar process as heat strengthened glass. The most crucial difference is that the cooling process is even faster than the cooling process for heat-strengthening. During cooling, the surface solidifies first. Second, the interlayer cools down and shrinks. This results in a central layer in tension and a surface in compression. The thermally tempered glass performs better to thermal shock than annealed glass.

Due to the internal stresses in the heat-strengthened and toughened glass, the glass behaves differently than annealed glass during fracture. The thermal tempering of glass has a significant impact on the redundancy of the structure. Annealed glass fractures in relatively large shards, this type of glass has the highest redundancy compared to heat-strengthened and toughened glass. The heat-strengthened glass fractures in smaller fragments compared to annealed glass. This is due to the residual stresses present in the element. This type of strengthening gives a relatively good structural performance compared to basic annealed glass, and the pieces are still large enough to bear a part of the load after failure. The fully tempered glass (safety glass) fractures into tiny shards of about 1 cm^2 because this type of treatment leaves high residual stresses in the element. Due to these high residual stresses, the strength of this glass type is relatively high. However, after failure, the glass fragments perform poorly under a load. The fracture patterns of glass with different treatments are shown in Figure 2.4. (Haldimann et al., 2008)
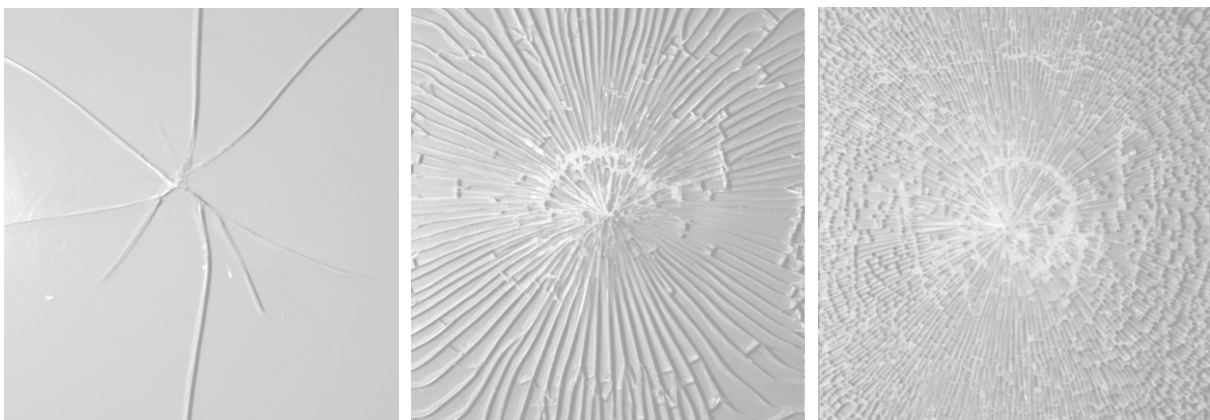
Figure 2.4 Fracture pattern for annealed glass (displayed on the left), heat-strengthened glass (shown in the middle), and fully tempered glass (shown on the right). From (Haldimann et al., 2008).

During the chemically toughening of glass, the composition of the outer layer is modified. The glass is altered by dipping it into an electrolysis bath. In this bath, the sodium ions from the outer layer are replaced with potassium ions. The outer layer is under compression because potassium ions are 30% bigger. The chemically strengthened glass performs better to thermal shock than annealed glass. (Institution of Structural Engineers, 2014)

Multiple glass layers can be combined by lamination. During this process, two or more sheets of glass are bonded with a viscoelastic interlayer. After the layer is placed, the pieces are heated, pressed, and bonded. With this process, the overall thickness is increased, which increases mechanical resistance. Additionally, the glass has an increased capacity against the impact of objects because the interlayer can absorb the energy. Furthermore, the risk of shards flying around is reduced because the interlayer's will held the shattered glass together (Institution of Structural Engineers, 2014).

To calculate the effective thickness of a laminated element, a coupling factor needs to be used. The coupling factor describes the degree of coupling between the layered glass plates. When determining the coupling factor, a distinction is made between the ultimate limit state for the stress check and the serviceability limit state for strain calculation.

2.3.1.3 Design considerations and safety

It is be expected that damage occurs due to intentional or unintentional behaviour from users. The glass layers can be thermally tempered and laminated to increase safety and obtain a higher redundancy. If one of the layers of a laminated element breaks, the other layers can still carry some load. Additionally, it can prevent the element from collapsing, which could otherwise have catastrophic consequences. By adding a sacrificial layer on top of a component, the component's safety can also be increased. This layer protects the structural glass from users damages, such as dropping something on the element. A sandblasted pattern or a ceramic fritted pattern could be added to the top surface to increase the slip resistance of the glass (Clayton, n.d.).

Float glass should be stacked horizontally to produce a transparent component. When stacking the glass vertically, the different layers are visible. Additionally, the maximum pane thickness should be considered. Since the production of panes thicker than 15 mm is only done by a limited number of manufacturers, it is advised to use glass panes with a maximum thickness of 15 mm. The maximum number of layers is estimated to be ten layers. Extra layers result in an even more challenging lamination process. When writing this thesis, the only building regulations for glass are the country-specific code, NEN 2608. NEN 2608 gives requirements and determination methods for flat glass. The code can be applied to test glass loaded with static loads and impact loads. In the future, an additional Eurocode EN 2020 'Eurocode 10: Design of glass structures' will contain the building regulations for glass structures.

2.3.1.4 Reference projects

An important aspect when producing a large 3D element from float glass is the connection of the multiple layers. In this report, four examples are given of float glass used in a three-dimensional way. First, an overview is shown in Table 2.3, followed by a more detailed description.

Table 2.3 Overview of laminated float glass 3D elements with their characteristic properties.

Project	Unit	Laminata	layered glass	Stacked column	All-glass bridge
Location		Leerdam	Gersthofen	TU Eindhoven	Glasstec 2008
		The Netherlands	Germany	Eindhoven	Düsseldorf
Dimensions	m	Varying thickness: 0.2 – 2	-	0.1x0.1x0.25	Length: 7
Geometry		Wall	Disk	Four-sided Column	Bridge
Adhesive		Silicone-based sealant	SentryGlass	Epoxy adhesive Ad821	-
Number of layers		Different per wall	18	20	6-8
Thickness of layers	mm	10	15	12	4
Total weight	kg	-	3600	-	-
Type of glass		Soda-lime	Soda-lime	Soda-lime	Soda-lime

The glass walls

The Laminata house was built in 2001 in Leerdam, the Netherlands. The building is built up out of a concrete slab, laminated glass walls and a plywood roof. The walls are composed out of 10,000 individually cut glass panes of 1 cm, see Figure 2.5. The glass panes are vertically stacked and glued together with a silicone-based sealant. This specially developed sealant is UV-resistant and flexible enough to accommodate expansion and contraction due to temperature differences. The wall thickness varies from 20 centimetres up to 2 metres (Richards & Gilbert, 2006).

Figure 2.5 Laminata house in Leerdam, the Netherlands. From (Luuk Kramer).

18-layer laminated element

For the glasstec 2018 convention, Sedak produced the world's thickest laminated glass element made from 18 layers of safety glass with a total thickness of 30 centimetres and a weight of 3.6 tons (see Figure 2.6). Each glass pane is 15 mm thick and has a strength of at least 160 MPa. The layers are bonded together with a SentryGlas interlayer. (Sedak, 2018)

Figure 2.6 Laminated glass element. From (Sedak).

Stacked column

Heugten (2013) researched the possibility of making a loadbearing structure made from stacked glass at Eindhoven University of Technology (see Figure 2.7). Steel is the most favourable intermediary material from experimental research into intermediary materials (between glass and test machine). For the interlayer (between glass layers), epoxy adhesive Delo AD821 is the most favourable. The tested setup was comprised out of twenty glass panels and the above-mentioned intermediary material and interlayers. The initial crack stress was found to be -108,1 N/mm^2, and the ultimate failure stress -190,3 N/mm^2. When looking at a stacked glass column, the flatness and thickness have to be considered. To minimize the flatness and thickness, it is not advised to use toughened glass because roller waves are introduced during the toughening process, resulting in an uneven surface. Additionally, glass should be used from the centre of large panes since the variation is most significant at the edges of the panes.

Figure 2.7 Stacked glass columns. Left: Experimental tested column, Right: Artistic impression. From (Heugten, 2013).

All-glass bridge

For the glasstec convention of 2008 in Düsseldorf, Seele produced a bridge made from cold-bent glass, see Figure 2.8. The bridge is build up out of three components: the floor and two balustrades. The base consists of eight panes with a thickness of 4 mm and has a curvature with a radius of 16 meters. The railings consist of six panes of 4 mm thick and have a curvature with a radius of 16 meters. The total length of the bridge is 7 meter. The combination of laminating the glass and bending the glass resulted in a rigid structure. (Engelsmann Peters, 2008)

Figure 2.8 Seele all-glass bridge. From (Engelsmann Peters, 2008).

2.3.1.5 *Achieving 3D glass structure*

When designing a bridge with float glass, it is more difficult to produce different shapes and sizes. Large 2D glass elements can buckle relatively quickly due to the disproportional length-thickness ratio. Consequently, the glass fails on tensile stresses, which means the compressive capacity is not fully utilised (Oikonomopoulou, 2019). A waterjet cutter cuts out each layer into the desired shape to produce three-dimensional structural elements from float glass. This process has a considerable amount of glass waste, which is simple to reuse. The layers are combined by lamination to produce a three-dimensional object. More attention should be given to the accuracy during lamination since it is challenging to laminate many elements together with a small margin of error (Heugten, 2013).

Since the thickness of each pane is limited by the production process, the annealing time is not an issue for this element. This means topology optimisation is not needed to reduce the annealing time. Nevertheless, optimisation is still required to reduce the total weight of the structure. During optimisation, it is not needed to restrict the maximum change in cross-section. Due to the lamination of different elements, the redundancy of the component is increased. When one piece breaks, the other parts can still transfer some load. Float-glass is the least expensive production method of glass. Because of the lower melting point of soda-lime glass, it requires less energy to be produced. A summary of making a 3D element with the lamination of float glass is given in Table 2.4.

Table 2.4 Advantages and disadvantages of producing a 3D element with float glass.

	Advantages	Disadvantages
Float glass	• No topology optimisation necessary to reduce annealing time • Annealing time is not an issue • No mould necessary • The least expensive production method of glass • High redundancy due to lamination of layers • No constraints for the abrupt change in cross-sections	• Topology optimisation necessary to reduce weight • High production cost due to cutting and lamination • Laminating of multiple layers is challenging • Lots of glass waste is generated during cutting (can be reused relatively easy) • Layering visible

It can be concluded that float glass can be used to produce a 3D element. However, during the design and construction phase, multiple aspects need to be considered. The aspects of the design phase are:

- Panes thicker than 15 mm are only produced by a limited number of manufacturers and are more complex and expensive to produce. Because of this, glass panes are used with a maximum thickness of 15 mm.
- The maximum number of layers is estimated at 10. More layers result in a more challenging lamination process.
- Soda-lime glass is used since it is the most used material in this process.
- The top layer should not have holes since this is the place where people walk.

During design and construction, these aspects are:

- A sacrificial layer needs to be added. This layer is the first line of defence for damages.
- The flatness and thickness of the glass have to be considered, either by choosing the most suitable intermediary layer or by using glass from the centre of large panes.
- When using toughened glass, the glass should first be cut and then toughened. More attention should be given during the toughening process towards an uneven surface.

- Float glass should be stacked horizontally to ensure transparency in the vertical direction. When stacking the glass vertically, the different layers are visible.
- The intermediary layer should be UV-resistant.

2.3.2   3D printed glass

The use of a 3D printer to produce a glass object is relatively new. There are various ways to 3D print glass, such as material extrusion and binder jetting.

2.3.2.1 *Production process*

Klein et al. (2015) introduced a method to print optically transparent glass via material extrusion. The design space for the 3D printing system, as shown in Figure 2.9, is 250 x 250 x 300 mm. The glass is melted before it is added to the upper chamber (the crucible). For soda-lime glass, the upper room is set at a temperature of approximately 1040 ^{o}C. The glass flows through the nozzle into the annealing chamber that is heated at a temperature of 480 ^{o}C, which is a little below the annealing temperature. However, the heat radiation of the glass from the upper chamber results in a temperature of 500-570 ^{o}C. This process ensures that the glass is still hot enough to attach to the next layer. The temperature,

Figure 2.9 Overview of the 3D printing system. Numbered elements: (1) crucible, (2) heating elements, (3) nozzle, (4) thermocouple, (5) removable feed access lid, (6) stepper motors, (7) printer frame, (8) print annealer, (9) ceramic print plate, (10) z-drive train, (11) ceramic viewing window, and (12) insulating skirt. From (Klein et al., 2015)

viscosity, flow rate, layer height, and supply rate can be changed to match the design. After finishing the printing, the element is cooled down gradually to reduce the formation of internal stresses.

The glass flows through the nozzle due to gravitational forces. The printing process is stopped by cooling the nozzle tip with compressed air. The process is reinitiated by heating the nozzle tip with a propane torch. After completing the element, the nozzle and crucible can be emptied by increasing the temperature to 1165 ^{o}C. A picture of the nozzle tip can be seen in Figure 2.10.

Figure 2.10 Nozzle tip. From (MIT Media Lab).

In a later version, the material extrusion process was upscaled so it could produce building components. The upscaled process included an integrated digital thermal control system and a function to control the flow, spatial accuracy, and precision via a 4-axis motion control system. Additionally, the production rate is faster, and glass can be deposited up to 30 kg in a continuous way (MIT Media Lab, n.d.). During the challenging glass conference of 2020, Chikara Inamura, a member of the group developing this technology, added that the maximum production rate is 7.5 kg per hour. The maximum dimensions of an element can be 300 x 300 x 300 mm. An element of 10 kg needs 8 hours of annealing (Inamura, 2020).

A second method to produce glass objects is sintering. Sintering is the fusion of particles under melting temperature. The printing is mainly done on a powder bed via binder jetting. The particles are bonded temporarily with the binding agent before the sintering. During sintering, the glass element undergoes thermal treatment. The glass objects made with sintering are fragile and opaque due to the incomplete conversion of the particles (Klein et al., 2015).

2.3.2.2 Annealing

After finishing the printed element, the annealing chamber is set to a temperature of 480 °C. This can be the chamber where the part is printed in or a separate annealing kiln to increase production. The cooling cycle that is used during annealing is given in Table 2.5.

Table 2.5 Annealing cycle for 3D printed elements. From (Klein et al., 2015).

T(°C)	Cooling rate (°C/h)	Dwell time (h)
480	-	1
400	25	-
150	50	-
80	50	-
20	120	-

2.3.2.3 Design considerations and safety

The maximum compressive strength of the 3D printed glass is equal to 150 MPa (Inamura, 2020). The ultimate tensile strength is unknown. The layering in the element probably results in a lower flexural capacity. Because the component is produced in a continuous process, the redundancy of the element is probably low. Experiments should be carried out to check the residual strength after the failure of a component. The maximum dimensions of a 3D printed part are 300 x 300 x 300 mm. Production of a large structure needs to be done by printing multiple smaller 3D parts. The redundancy of such a structure is higher since other non-fractured elements could take over the load.

2.3.2.4 Reference projects

Underneath are two projects that show what kind of elements can be produced via material extrusion. The first items made via material extrusion are the glass vases and the second items are the glass columns.

Glass vases

Various vases were made from soda-lime glass with the first version of material extrusion (see Figure 2.11). These vases show what kind of appearance the 3D printed element has when produced via material extrusion. Because of the surface textures, the light refracts and scatters in a complex manner. The vase is purely for decoration and is not suitable to function as a load-bearing element.

Figure 2.11 3D printed glass vase. From (MIT Media Lab).

Glass column

With the second upscaled extrusion process, several columns were made, see Figure 2.12. These columns are 3-meter-tall and consist out of 15 segments. The columns are prestressed and free-standing and carry their own weight and the weight of the build-in installation (MIT Media Lab, n.d.).
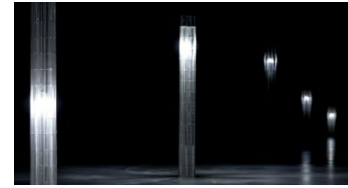
Figure 2.12 3D printed columns. From (MIT Media Lab).

2.3.2.5 *Achieving 3D glass structure*

With the 3D printing production process, it is relatively easy to produce a three-dimensional element. The production method is still in early development, which reflects on the size of the elements that can be made (300 x 300 x 300 mm). No mould is necessary to produce a part, and less glass is wasted. However, additional supports need to be designed and printed to sustain the element's shape during printing. Due to the complex shapes and the layering, an intriguing light refraction pattern can be obtained. The layering is also a disadvantage since it reduces the transparency of the object. No structural application is developed yet with these elements (only the self-supporting glass columns). Compared to cast glass and float glass, the structural capacity of the pieces will be lower due to the layering. The advantages and disadvantages of producing a 3D element with 3D printing are given in Table 2.6.

Table 2.6 Advantages and disadvantages of producing a 3D element with 3D printing.

	Advantages	Disadvantages
3D printed glass	• No mould necessary • Light refracts and scatters in a complex, intriguing manner • Less glass wasted • Possible to generate complex forms	• Lower strength compared to float and cast glass due to layering of the glass • Production method still in early development • No structural applications yet • Currently, only small elements are produced • Layering visible • Additional supports need to be designed and printed to sustain the shape of the element during printing.

It can be concluded that 3D printing of glass is a viable option to produce a 3D element. However, since this type of production is still in early development and it is only possible to make small elements, it is unsuitable to use this production method to produce large glass elements.

2.3.3 Cast glass

Cast glass can be produced in any shape and size. However, the annealing time is a limiting factor that must be considered when making the object. By optimising the element on shape and size, a structure can be created that uses the compressive strength of the glass in an optimal manner. Over the past few years, a giant leap was made in the development of manufacturing techniques. When producing cast glass, it is necessary to make a mould. A mould can be created with various techniques. These techniques can be subdivided into subtractive manufacturing, formative manufacturing, and additive manufacturing (Pereira, Kennedy, & Potgieter, 2019).

Glass elements can be produced via primary casting where raw ingredients are used or secondary casting where existing glass is re-molten and shaped into a new piece, see Figure 2.13 (Oikonomopoulou, 2019). For secondary casting, one type of glass should be used. Mixing different glass types can result in internal stresses (Cummings, 2001). Hot-pouring (melt-quenching) is the main process used for primary casting, and kiln casting is the main process used for secondary casting. The most crucial difference between these two production methods is that for primary casting, the raw materials are molten, then the glass is poured into the mould outside the oven, and finally, the glass is placed in a furnace for annealing. For the secondary casting, the glass is remolten, poured and annealed in the same furnace (Oikonomopoulou et al., 2018). Glass can be cast into disposable moulds such as silica plaster, alumina-silica fibre, and sand or permanent moulds such as steel and graphite (Oikonomopoulou, 2019).

Figure 2.13 Left: primary casting. Right: secondary casting. From (Oikonomopoulou, 2019).

2.3.3.2 *Moulds*

In this section, first, different manufacturing techniques for moulds are discussed. Secondly, different mould types are given, followed by a detailed explanation of additive manufacturing of sand moulds.

Manufacturing techniques

A machine removes material by machining, drilling, or grinding material from a solid piece to produce the desired shape with subtractive manufacturing. This can, for example, be done with a CNC milling machine. A disadvantage of subtractive manufacturing is the material wasted in the process. Also, with three-axis milling, it is not possible to produce an undercut. With five-axis milling, undercuts are possible. However, parts must often be split into separate pieces (Jipa et al., 2016). With formative manufacturing, the liquid material is injected or poured into a mould and then cooled down. Additive manufacturing, better known as 3D printing, produces shapes with a high level of design freedom. At the start of a new printing process, the workspace is empty. By extruding or melting material layer by layer, a new object is formed. According to Dillenburger and Hansmeyer (2013), additive manufacturing is very suitable for producing large-scale 3D printed elements without increasing costs and geometric constraints.

Mould types

Moulds used for casting glass can be subdivided into four main categories. These are the disposable mould, open metal mould, press metal mould and adjustable metal mould. In Figure 2.14, an overview is given of the different mould types. The type of mould that should be used depends on the reusability, desired precision of the casted element, the geometry, and the number of components needed (Oikonomopoulou, 2019).
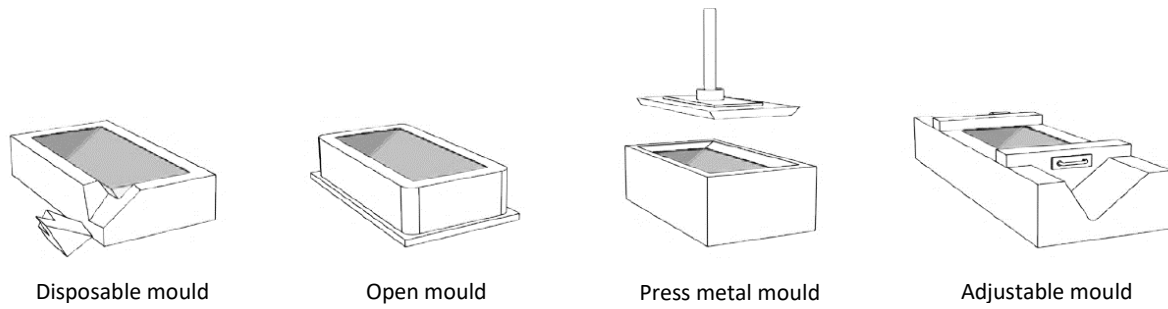
Figure 2.14 Different mould types used for cast glass. From (Oikonomopoulou, 2019).

Disposable mould

For disposable moulds, silica plaster or alumina-silica fibre is mainly used. Silica plaster moulds have lower manufacturing costs and a low/moderate accuracy. Alumina-silica fibre moulds have high accuracy and a high price. A promising option as a disposable mould for cast glass is a 3D printed sand mould which has a low manufacturing cost and a high accuracy. It is recommended to use a disposable mould when producing only one element or a small batch. In Table 2.7, the characteristics are given for each material.

Table 2.7 Characteristics for the different disposable moulds. From (Bhatia, 2019; Oikonomopoulou, 2019).

	Silica plaster	Alumina-silica fibre	Sand with inorganic binder
Production method	Investment casting/ lost wax technique	Subtractive manufacturing	Additive manufacturing
Manufacturing costs	Low	High	Low
Top temperature	900-1000 °C	≈1650 °C	500-900 °C
Glass annealing method	Mould stays in place during annealing		
Release method	Immerse in water	Water pressure	Chisel
Accuracy	Low/moderate	High	High
Finishing surface	Translucent/ rough	Translucent/ rough	Translucent/ rough
Post-processing	Grinding and polishing		
Applicability	Single component		

The use of sand moulds is a technique that has been used for centuries. Originally, sand was compacted around a premanufactured mould pattern. This pattern was then removed before casting the element. This is an efficient and economical method for large quantities, but for small amounts, the need for a mould pattern can be an issue during new product development. That is where additive manufacturing becomes essential since the need for the pattern vanishes (Hackney & Wooldridge, 2017). Additive manufacturing that produces sand moulds uses sand in combination with binder jetting/extrusion. The production of sand moulds with additive manufacturing has the advantage of being a relatively fast process compared to the original sand-casting method. Another advantage is the lack of fabrication constraints. Because of this lack of limitations, it is possible to produce components in almost any shape. The largest sand printer on the market is the VoxelJet VC4000 which can create elements with an accuracy in the range of 0.2 mm with a maximum dimension of 4 meters by 2 meters by 1 meter (Voxeljet, n.d.).

Different kinds of binders can be used when 3D printing sand: furan binders, phenolic binders, and inorganic binders (Voxeljet, n.d.). Bhatia (2019) explored the use of 3D printed sand moulds for casting glass. In total, seven experiments were carried out to analyse sand moulds with different binders and finishing layers. From these experiments followed that the inorganic and cold hardening phenolic remained intact during the casting of glass. Crystal cast was found to be a suitable coating to increase the surface quality.

It is essential that the formed sand keeps its shape during casting and has sufficient strength. A layer of epoxy can be sprayed on the outer surface to strengthen the mould. (Rippmann, Liew, Van Mele, & Block, 2018). The mould should fulfil the following criteria (Hackney & Wooldridge, 2017):

- The permeability of the sand must be high enough to allow gas to pass through it. However, a lower permeability results in a higher surface finish.
- The mould should be able to withstand high temperatures for a longer time without cracking or collapsing.
- The reusability of the sand is also essential to consider for economic and environmental reasons.

For the mould design, it is essential to ensure that the unused sand can be removed after the printing and that the coating can be applied to every surface within the mould. The division of the mould should be done such that every part is accessible. Interlocking nodes and/or screw holes are needed to connect the different parts. (Bhatia, 2019).

For the casting process, a pouring cup is needed that has a larger diameter than the nozzle. Additionally, vent pipes are necessary to avoid the possible development of air entrapments inside the element. Risers might be helpful to cope with the excess material when the mould is filled up. (Bhatia, 2019). A minimum thickness of the walls is required because the mould must withstand the forces from casting and annealing. This means that a minimum distance between the different elements is required. Bhatia (2019) compared young's modulus from glass with aluminium and steel. As a result of this comparison, a minimum thickness of a wall was set at 4 mm. In Figure 2.15, an example of a mould design is given.
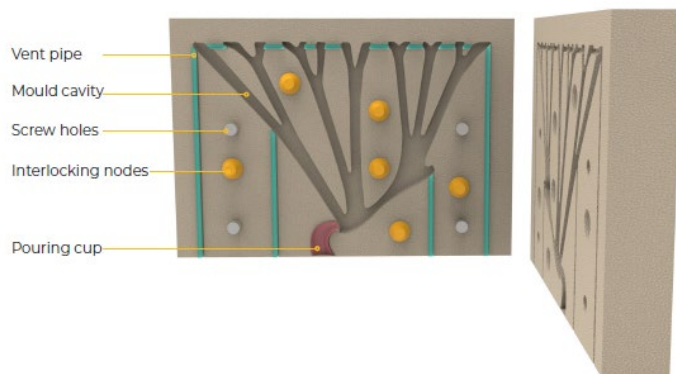
Figure 2.15 Mould design. From (Bhatia, 2019).

Permanent mould

Permanent moulds for casting glass are usually made of steel, stainless steel, or graphite. Moulds produced from steel or stainless steel can be open, pressed, or adjustable. Graphite moulds can only be open or adjustable. Adjustable moulds can be used for elements that have roughly the same shape and size, but adaptions to the length of the component need to be possible. The level of accuracy is between moderate to very high. Pressed moulds are used when a very high level of accuracy is required. The permanent moulds have an increased accuracy, robustness, surface quality, and price compared to the disposable moulds. Therefore, it is advised only to use this mould to produce elements with a large circulation. These moulds are used mainly during the hot-pouring process since

this process is significantly faster than the kiln casting, which means the moulds can be used to produce more elements in a shorter amount of time (Oikonomopoulou, 2019). In Table 2.8, the characteristics are given for each material.

Table 2.8 Characteristics for the different permanent moulds. From (Oikonomopoulou, 2019).

	Steel/Stainless steel			Graphite	
Adjustability	Adjustable	Fixed	Pressed	Adjustable	Fixed
Production method	Mulling/ cutting and welding			Milling/ grinding	
Manufacturing costs	Moderate to high			High	
Top temperature	≈ 1200 ºC / 1260 ºC			unknown	
Glass annealing method	Mould is usually removed but can also stay in place if high accuracy is required			Mould removed before annealing	
Release method	Release coating necessary				
Accuracy	Moderate/ High	High	Very High	Moderate/ High	High
Finishing surface	Glossy. Surface chills may appear if the mould is not preheated correctly			Glossy with surface chills	
Post-processing	Minimum or no post-processing required			Minimum to moderate post-processing required	
Applicability	High volume production				

Conclusion

When choosing the right mould type, it is crucial to keep in mind the kind of element that is going to be produced. To produce a kiln cast element with low circulation, high accuracy, and low cost, the sand with inorganic binder mould performs best. The level of complexness that can be reached with this type of mould with high accuracy in a relatively fast and cheap manner makes it very suitable for a one-of-a-kind topology optimised glass bridge.

2.3.3.3 Annealing

The main problem when producing a large cast glass element is the required annealing and cooling time. This time can be between minutes and months and sometimes even up to a year for huge parts. Annealing is the primary treatment of glass. During this process, the glass transforms from liquid to solid at different speeds and at different moments. Because of this, residual stresses occur in the glass due to unequal behaviour. During the solidification process of the glass, the outer surface solidifies first. When glass solidifies, it tends to shrink. Due to this uneven shrinkage, stresses develop in the element (Institution of Structural Engineers, 2014). The formation of stress is dependent on the cooling rate during annealing, the expansion coefficient of the glass, and the thickness of the element (McLellan & Shand, 1984).

In Figure 2.16, an example is given of the annealing and cooling process of a glass element. Five phases can be distinguished during this process. All steps have a different temperature change and a different duration. In zone A, the oven is heated until 5 ºC above the annealing point. This temperature is kept constant in zone B until the temperature is constant throughout the cross-section. At the annealing point, the behaviour of the glass changes from plastic to elastic. At this point, the viscosity of the glass is enough to reduce the stresses from the previous process in a short amount of time (Vogel, 1994). The annealing point is different for every type of glass. In zone C, the element is cooled until a certain

temperature below the strain point. The strain point is the lowest point at which the annealing process occurs. However, the annealing process is significantly slower at this temperature than at the annealing point (Vogel, 1994). During phase C, the temperature gradient throughout the cross-section should not differ more than 5 $^\circ$C (Sawyer, 2009). Zone D is the cooling of the next 50 $^\circ$C, and in Zone E, the final cooling occurs.
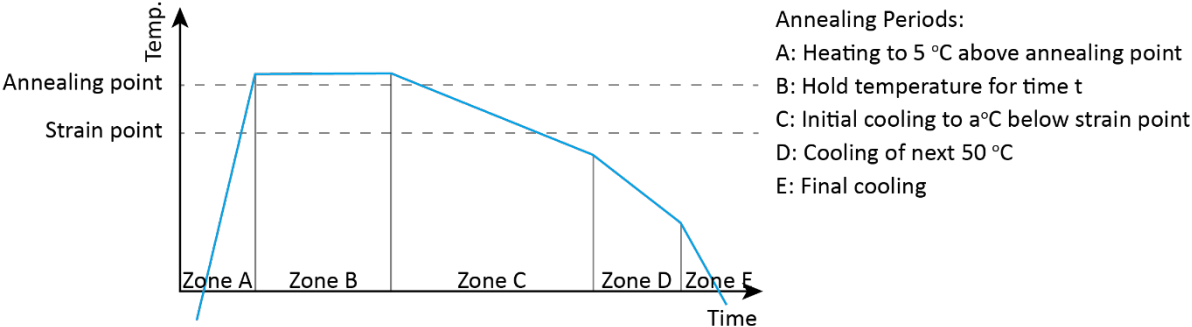
Figure 2.16 Ideal annealing schedule for ordinary ware, based on (McLellan & Shand, 1984).

Most of the time, the annealing process that is carried out is based on previous experiments and observations. This is mainly because the prediction of annealing time with a heat flow model is complicated because of the many factors that influence the process. These factors are the shape of the element, mass distribution, exposed sides, the presence of other elements in the oven, and the properties of the oven (Oikonomopoulou et al., 2018). Still, researchers tried to find a guide to predict the necessary annealing process. However, these are primarily based on unstated assumptions and are only applicable for a small number of cases (Watson, 1999).

The optimisation process should be based on a value. A chart provided by Bullseye Glass for soda-lima glass is analysed. These annealing times are based on flat slabs with uniform thickness, where the glass can cool down equally from the bottom- and topside. If this is not the case, it is advised to use an annealing cycle of a piece that is twice as thick as the thickest area (Bullseyeglass, 2009). The values given in Table 2.9 are based on corning's method that is explained in McLellan and Shand (1984). In Figure 2.17, the data from Table 2.9 is plotted. A trendline is plotted through the points to predict the behaviour of thicker glass elements. For the anneal soak time, the formula is given at equation 2.6.1, and for the total minimum annealing time, the formula is given at equation 2.6.2.
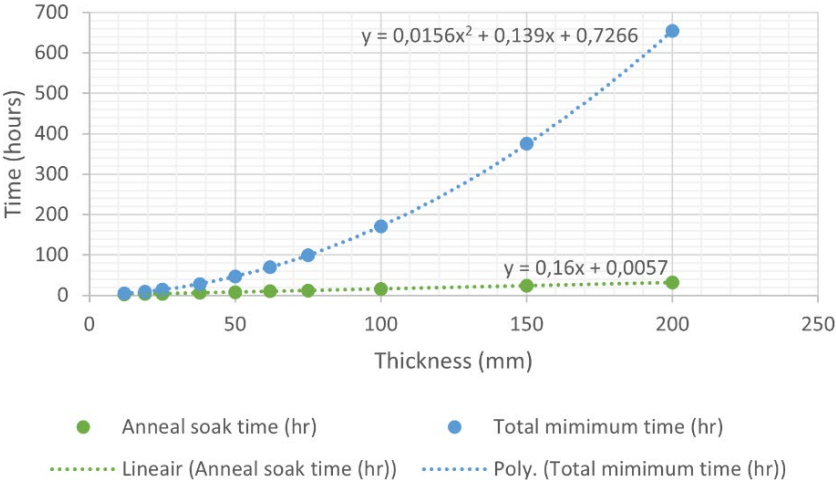
Figure 2.17 Plot of the annealing time vs thickness.

Table 2.9 Annealing time for a flat slab of soda-lime glass with uniform thickness based on Corning's method. From (Bullseyeglass, 2009).

Slab thickness	mm	12	19	25	38	50	62	75	100	150	200
Anneal soak time	hr	2	3	4	6	8	10	12	16	24	32
Total minimum time	hr	5	9	14	28	47	70	99	170	375	654

$$T_{anneal\ soak\ time} = 0.16 \cdot t + 0.0057 \qquad (2.6.1)$$
$$T_{total\ minimum\ time} = 0.0156 \cdot t^2 + 0.139 \cdot t + 0.7266 \qquad (2.6.2)$$

Where:

T Time in hours

t Thickness in mm

The formula to calculate the annealing time needs some tweaking since this formula is for a flat slab made from soda-lime glass cooled from the top and bottom sides. However, in this thesis, borosilicate glass is used during the casting of glass, the design is non-flat, and cooling does not take place from two sides. The annealing time of the bricks from the Atocha Memorial made from borosilicate glass is compared to the bricks from Crystal Houses made from soda-lime glass, see section 2.3.3.6. The annealing time of an Atocha Memorial brick is about half compared to a brick from Crystal Houses. To implement this in the formula, the annealing time is halved. Since the element is topology optimised, it must be considered that the annealing process takes longer because of the shape, mass distribution and exposed sides. To implement this in the formula, the annealing time is doubled. When implementing these differences, the equation stays the same.

2.3.3.4 *Interlayer between cast elements*

With the correct interlayer between cast glass elements, the elements can endure small displacements within the structure. It results in improved ductile behaviour, resulting in increased fracture toughness of the bridge. A soft interlayer prevents peak stresses due to the micro-asperities in adjacent elements by deforming when used. Depending on the cast glass's surface quality, an interlayer could also reduce the need for post-processing. (Oikonomopoulou, 2019)

When choosing the interlayer material, the most critical factor is the stiffness of the material. It should allow for even load distribution, adapt to micro-asperities, and avoid penetration. The hardness for rubber-like materials is expressed in the shore hardness scale.

In a study by (Aurik, Snijder, Noteboom, Nijsse, & Louter, 2018) on orthomorphic interlocking glass blocks, different experiments were done on multiple interlayers. In this study, the following criteria were defined for the interlayer:

- A shore hardness between 60 A and 80 A
- Compressive strength that is higher than 20 MPa
- Sufficient creep resistance
- Possibility to form material in the desired shape with a thickness between 3 mm and 6 mm
- Transparent or translucent
- UV-light resistant
- Water-resistant
- Operating temperature between -20°C and 50°C
- Slow-burning/ self-extinguishing/ non-flammable

The conclusions that followed from the experimental work by (Aurik et al., 2018) are summarized as follows:

- A 3 mm thick interlayer performs best when looking at the contact area, absorbing surface irregularities and stiffness.
- A polyurethane interlayer with a shore hardness between 60 A and 80 A is the best candidate. The material properties of polyurethane can be found in Table 2.10.

Table 2.10 Mean properties of polyurethane (rubber/cast) from CES Edupack 2015 (Granta Design Limited 2015).

Material	polyurethane
Compressive strength [MPa]	48
Yield strength [MPa]	>50
Poisson's ratio	0.48
Transparency	Clear
UV-resistance	Fair
Flammability	Slow burning

2.3.3.5 Design considerations and safety

Three aspects can be considered to reduce the annealing time and increase the feasibility of the structure. The first one is to reduce the mass of the structure. The second one is to design an element without corners sticking out and without sharp edges. These parts cool down much faster, causing inhomogeneous shrinkage, which as a result, causes higher residual stresses at these spots. The third one is to distribute the material equally through the element. This reduces the formation of internal stresses during annealing. However, it is still possible to change the dimensions of cross-sections. Abrupt changes should, however, be prevented, but gradually changing cross-section do not form a hazard. Fragile elements should be removed from the structure. These elements need a longer time to fill with glass during the casting process, and they are more prone to break during the removal of the mould or user phase. (Bhatia, 2019; Oikonomopoulou, 2019)

When considering the safety and redundancy of a structure, it is better to divide a structure into smaller elements. This was, for example, done for Crystal Houses, where they split the façade into small bricks. When one of the bricks from the façade cracks, the propagation of this crack is minimal, the other elements can still function as a load-bearing structure, and only a small number of bricks has to be replaced. When a large element of glass cracks, the crack propagates over the entire piece. This means the part loses most of its load-bearing capacity, and the whole element needs to be replaced.

For large, virtually monolithic pieces, other safety measures need to be implemented. As a safety measure, the large casted element can be protected by adding laminated float-glass and a sacrificial layer.

Glass casting is used to produce elements for various applications such as art pieces, radiation shields, building envelopes, and telescope mirrors.

Art project

The Denis Altar is a cast glass art piece of 1.42 x 1.42 x 0.28 metres and weighs 1400 kg (see Figure 2.18). The tricky part about this project was that the glass block and the supporting stone had to fit each other seemingly. This was done by casting a rectangular block made from Corning 7056 optical glass in a container made from metal with a non-stick refractory paper between the glass and metal. The block needed one month of annealing. The glass was reheated until softening point to

Figure 2.18 Cast component Denis Altar. From (Thierry Dannoux).

imprint the plaster mould with the same pattern as the stone. This mould was loaded with a 500 kg load. To ensure the mould being imprinted in the glass, the softening temperature was maintained for a month, followed by a cooling process of one month (Oikonomopoulou, 2019).

Envelopes

In the past few years, structures like the Atocha Memorial built in 2004 (esmadrid, 2004), Crown Fountain built in 2004 (Chicago, n.d.), The Optical House built in 2012 (Fuji, 2013), and Crystal Houses built in 2016 (Scagliola & Brakkee, 2019) used structural components made from cast glass, see Figure 2.19. The glass bricks used in these structures use the compressive strength of the glass more optimally. A substructure supported the Optical house and Crown fountain, and the Atocha memorial and Crystal houses used adhesives. This was done to ensure stiff and stable structures. The characteristics of the four building envelopes can be found in Table 2.11.

Figure 2.19 Left top: Atocha Memorial. From (esmadrid, 2004); Right top: Crown fountain. From (Matthews, 2017); Left bottom: Optical Glass House. From (Fuji, 2013); Right bottom: Crystal Houses. From (Scagliola & Brakkee, 2019).

Table 2.11 Characteristics of the four building envelopes made from cast glass. From (Oikonomopoulou, 2019).

Project	Unit	Atocha memorial	Crown fountain	Optical house	Crystal house
Location		Madrid	Chicago	Hiroshima	Amsterdam
		Spain	Illinois, USA	Japan	The Netherlands
Envelope dimensions	m	8 × 11	12.5 × 7 × 4.9	8.6 × 8.6	10 × 12
Geometry		Elliptical cylinder	Cube	Flat envelope	Flat envelope
Structural system		Adhesively bonded	Support structure	Support structure	Adhesively bonded
Number of blocks		15,600	22,500	6000	7500
Size of blocks	mm	300 × 200 × 70	127 × 254 × 51	235 × 50 × 50	210 × 210 × 65
					210 × 157.5 × 65
					210 × 105 × 65
Number of different blocks		1	1	1	3
Weight of block	kg	8.4	4.5	2.2	7.2/5.4/3.6
Total weight	t	130	50.6	13	40.5
Type of glass		Borosilicate	Low-iron soda-lime	Borosilicate	Low-iron soda-lime
Annealing time		20 h	unknown	unknown	8–38 h (size dependent)
Type of mould		Press steel mould	Open steel mould	Press steel mould	Open steel mould
Post-processing		no	Polishing in one side	no	Polishing 2 faces to ± 0.25 mm precision

The bricks for the Atocha Memorial were made from borosilicate glass. Compared to soda-lime glass, borosilicate glass has a lower thermal expansion coefficient, resulting in lower natural shrinkage during the cooling process and higher dimensional accuracy. Additionally, for the casting precision, press moulds were used to ensure high accuracy. For Crystal Houses in Amsterdam, soda-lime glass was used. Soda-lime glass has a higher thermal expansion coefficient and has a longer annealing time. A higher expansion coefficient results in reduced dimensional accuracy. When using an open steel mould, the accuracy of the elements was not high enough to directly use the component in the wall. This meant post-processing was needed. Because of the necessity for post-processing, due to the use of an open steel mould, the cheaper soda-lime glass was chosen. During post-processing, two faces of the elements were polished to a 0.25 mm precision (Oikonomopoulou, 2019).

Telescope mirrors

The biggest monolithic piece of cast glass ever made is the Giant Magellan Telescope (Oikonomopoulou et al., 2018). The telescope consists of seven segments that work together as a single mirror. Each part has a diameter of 8.4 m, the thickness varies between 0.44 and 0.89 meters, it weighs 16 t and requires an annealing time of 3 months (GMTO, 2020). In comparison, the biggest solid blank (Hooker telescope) of 2.5 m in diameter and 4 t in weight required an annealing time of 12 months, and the Hale-1 blank of 5 m
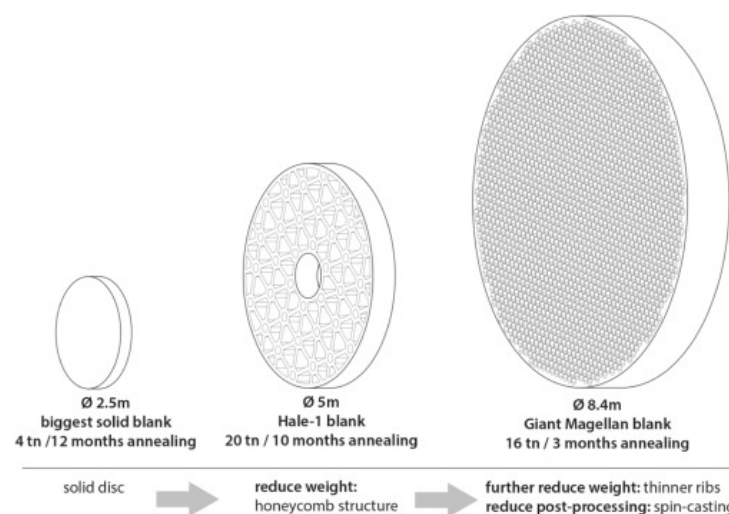
Figure 2.20 Comparison between solid cast glass elements and geometrically optimised mirrors. From (Oikonomopoulou, 2019), based on data from (Zirker, 2005).

in diameter and 20 t in weight needed an annealing time of 10 months, see Figure 2.20 (Oikonomopoulou et al., 2018). The characteristics of the three mirrors can be found in Table 2.12. A honeycomb pattern and spin casting are suitable for a giant circular mirror but are not ideal for most structural non-circular applications. A good alternative could be the use of Topology Optimisation.

Table 2.12 Characteristics of the three mirrors made from cast glass. From (Oikonomopoulou, 2019), based on data from (Zirker, 2005).

Project	Unit	Biggest solid blank	Hale-1 blank	Giant Magellan blank
Dimension	mm	Ø 2500	Ø 5080	Ø 8417
Thickness	mm	325	660 (when cast)	Max: 894 Min: 437
Geometry		Solid disc	Honeycomb disc	Honeycomb disc
Glass type		Wine bottle glass (St Gobain)	Pyrex Glass (Corning)	E6 Borosilicate Glass (Ohara Inc)
Density	g/cm³	unknown	2.23	2.18
Component weight	t	4	20 (14.5 after polishing)	16
$T_{batch\ melt}$	°C	unknown	1482	1180
Expansion coefficient	1/ °C	$9x10^{-6}$	$32.5x10^{-7}$	$28x10^{-7}$
Moult type		unknown	Steel mould with silica firebrick cores bolted with steel bolts	Base: SIC baselines lined with aluminosilicate refractory fiberboard Cores: Carborundum Carbofrax SiC
Casting method		unknown	Hot pouring Annealing within mould	Spin-(kiln) Casting Annealing within mould
Annealing time	months	~12	~10	~3
Post-processing		Grinding	Grinding and polishing (10 years)	Grinding and polishing (3 years)

Sand moulds

Jipa et al. (2016) researched topology optimisation combined with additive manufacturing to produce two concrete slabs. From their research into the mould design followed a couple of fabrication constraints. The samples should be smoothed because of the discretized nature of the sample surface after optimisation. Geometric features that are too fragile for 3D printing or are too narrow for post-processing should be filtered out. Too narrow paths are also a problem for the concrete flow during casting. Geometric features of

Figure 2.21 Post-processing of the 3D printed sand mould. From (Jipa et al., 2016).

around 20 mm were problematic for this fabrication method. Additionally, the architect wanted a specific surface quality and certain edge details and ornamentation. These adjustments only have a small impact on the optimised structure compared to other fabrication methods such as three-axis milling or five-axis milling. In the first phase of mould production, the mould was formed by binder jetting the sand. After the 3D printing was finished, the unconsolidated sand was removed. This process can be seen in Figure 2.21. As a final step, the mould was strengthened by treating the surface with epoxy resin.

As follow-up research for the two concrete slabs, Meibodi et al. (2018) researched the use of 3D-printed formwork for casting a concrete ceiling slab of 78 m² for the DFAB HOUSE, see Figure 2.22. For this slab, eleven post-tensioned elements were designed and produced with a length of 7.4 meters. The design was optimised to reduce the amount of material needed. During the optimisation, a cantilever of up to 4.5 meters had to be considered. This optimisation resulted in a weight reduction of almost 70% compared to a standard concrete slab. The thickness of the ribs varies from 60 cm in the centre to 30 cm at the edge. The thickness of the interstitial surface that is in between the ribs is only 1.5 cm. Most of the formwork was produced with binder jetting. Fused filament deposition was used to implement the building services into the slab. The formwork for the upstanding ribs, as seen in Figure 2.23, was made from laser-cut plywood.

Figure 2.22 Finished Smart Slab. From (Meibodi et al., 2018).

Figure 2.23 Installation of the Smart Slab. From (Meibodi et al., 2018).

Meibodi, Giesecke, and Dillenburger (2019) researched the use of additive manufacturing to produce two hundred aluminium connections for a space frame. Binder jetting was used to 3D print the sand moulds. The joint geometry and matching mould were generated automatically, which increased the efficiency of the design-to-production process. The amount of post-processing needed that was caused by the seepage of aluminium through the seams was high. The severity of this problem was decreased by placing the seams in a more strategic place and by adding locks that make sure the moulds stay together in the correct position. A finished aluminium connection can be seen in Figure 2.24.
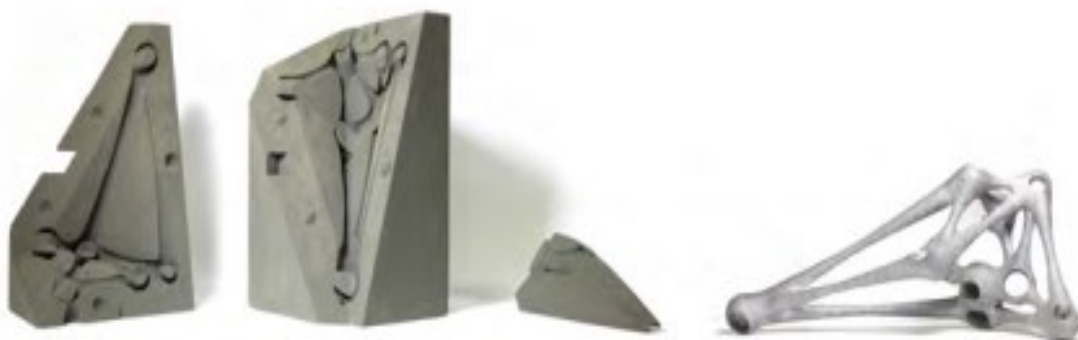
Figure 2.24 3D printed sand mould and casted aluminium connection. From (Meibodi et al., 2019).

Sand structures

Binder jetting of sand can also be used to produce elements such as the Quake Column and the Involute Wall. The quake column is designed not to have stress concentration points and resonant frequencies. This type of column is based on Incan structures. The column is made from lightweight hollow blocks that interlock with each other. During an earthquake, the column and blocks can move slightly and resettle into another position without collapsing. The involute wall is also created with binder jetting of sand. The wall is designed for acoustic dampening and thermal mass. The acoustic dampening is done by reducing the resonance, redirecting the sound waves, and increasing the absorption. Since most of the wall is shaded, it is very suitable for hot climates with considerable variation in temperature to use as thermal mass(Rael & Fratello, 2014). Pictures of these structures are given in Figure 2.25.

Figure 2.25 Left: Construction of the Quake Column, Middle: Finished Quake Column, Right: Involute wall. From (Rael & Fratello, 2014).

2.3.3.7 *Achieving 3D glass structure*

Because the glass is cast in one piece, no layering is visible, which is the case for 3D printed glass elements and laminated float glass elements. It is also easier to produce components with complex shapes and without size limitations. However, the long annealing time limits the thickness of the elements and the larger the piece, the more difficult it is to handle. During the production of a cast glass element, less glass is wasted than the production of a 3D element with float glass. The production can more easily be done with different types of glass. However, the manufacturing and post-processing of the mould can be challenging and expensive. The advantages and disadvantages are summed up in Table 2.13.

Table 2.13 Advantages and disadvantages of producing a 3D element with cast glass.

	Advantages	**Disadvantages**
Cast glass	• No layering visible • Easier to produce an element with a complex shape • No limitations on size • Less glass wasted • Production in different glass types	• Glass objects of substantial thickness present long annealing times. • Mould manufacturing is challenging, and some mould types can be expensive • Large geometries are difficult to handle

With cast glass, it is easier to produce different shapes and dimensions. The elements are secondary casted (kiln cast) with borosilicate glass. For this process, the glass is molten, poured and annealed in the same furnace. The mass of the element is decreased by using topology optimisation to reduce the annealing time. The pieces are designed without corners sticking out and sharp edges and with an equally distributed mass. The total annealing time is estimated with formula 2.3.3.

$$T_{total\ minimum\ time} = 0.0156 \cdot t^2 + 0.139 \cdot t + 0,7266 \qquad (2.3.3)$$

Where:

T Time in hours

t Thickness in mm

Several types of moulds could be used to produce the element. For the casting of the three-dimensional piece, 3D printed sand moulds are used. In this thesis, the limitations of these moulds are considered during the design phase. The maximum dimensions of printed sand moulds are 4 x 2 x 1 meter. However, multiple prints can be connected. The division of the mould should be done such that every part is accessible. This way, unconsolidated sand can be removed, and a coating can be added on every surface. However, divisions should be minimal and in strategic places. More divisions result in more postprocessing since the glass could seep through the seams. Interlocking nodes and/or screw holes are needed to connect the different parts. Additionally, a pouring cup, vent pipes, and risers should be added to the mould design. Fragile elements should be removed from the structure. The topology optimised structure should be smoothed, geometric features should be minimal 20 mm, and the minimum wall thickness of the mould should be around 4 mm.

A 3 mm thick interlayer between cast elements performs best when looking at the contact area, absorbing surface irregularities and stiffness. A polyurethane interlayer with a shore hardness between 60 A and 80 A is the best candidate.

A laminated float-glass and sacrificial layer are added to protect the cast glass structure. To connect the float-glass to the casted glass, the top surface of the element needs to be flat. The thickness of the float-glass determines the maximum size of the openings of the top surface. Additionally, the cast glass can have steel (pre-stressed) cables added to the structure to add a second load path to ensure sufficient structural capacity after the failure of the glass.

It can be concluded that cast glass can be used to produce a 3D element. However, during the design and construction phase, multiple aspects need to be considered. During the design phase, these aspects are:

- The thickness of the cross-section should be reduced to decrease the annealing time.
- Sharp edges and corners should be avoided to reduce unequal cooling and reduce the risk of too high internal stresses.
- Narrow paths should be removed.
- The material must be equally distributed and should gradually change to reduce the formation of internal stresses.
- In between cast elements, a polyurethane interlayer should be used with a thickness of 3 mm.
- The top surface should be flat or slightly curved, and the maximum hole size should be calculated according to the chosen thickness of the float glass.

- The difference between tensile and compressive strength is considerable and should be considered.
- Divisions in the mould should be minimal and in strategic places.
- The maximum dimensions of a single mould element are 4 x 2 x 1 meter.
- Interlocking nodes and/or screw holes are needed to connect the different parts of the mould.
- A pouring cup, vent pipes, and risers should be added to the mould design.
- Fragile elements should be removed from the structure, geometric features should be minimal 20 mm, and the minimum wall thickness of the mould should be 4 mm.

During production, these aspects are:
- Steel cables could be added to ensure structural capacity after failure.
- Only one type of glass should be used during secondary casting. When using multiple glass types, uneven stresses occur during the annealing process.
- Borosilicate glass is most favourable when looking at thermal expansion and annealing time.

2.4 Conclusions and recommendations glass

In this section, the design aspects and advantages and disadvantages are given for the different production methods.

Float glass

For designing a three-dimensional element from float-glass, the following aspects must be considered.
- Glass panes are used with a thickness of 15 mm.
- In total, a maximum of 10 layers is used.
- Soda-lime glass is used.
- The top layer should not have holes in it.

During construction, these aspects are:
- A sacrificial layer is added to the top glass pane.
- An intermediary layer is chosen that takes into account the flatness of an element
- The toughening of the glass when applied needs to be done after cutting.
- Float glass should be stacked horizontally
- The intermediary layer should be UV-resistant.

Cast glass

For designing a three-dimensional element from cast glass, the following aspects must be considered.
- The thickness of the cross-section should be reduced.
- Sharp edges and corners should be removed.
- Narrow paths should be removed.
- The material should be equally distributed and gradually change.
- The top surface should be flat or slightly curved.
- In between cast elements, a polyurethane interlayer should be used with a thickness of 3 mm.
- The tensile and compressive strength of the glass should be considered.
- Divisions in the mould should be minimal and in strategic places.

- The maximum dimensions of a single mould element are 4 x 2 x 1 meter.
- Nodes and screw holes are needed in the mould.
- A pouring cup, vent pipes, and risers should be added to the mould design.
- Fragile elements should be removed from the structure, geometric features should be minimal 20 mm, and the minimum wall thickness of the mould should be 4 mm.
- No holes near the supports.
- The dimensions of the top holes depend on the thickness of the added glass layers.

During production, these aspects are:
- One type of glass should be used (Borosilicate)

Advantages, disadvantages and limitations

Table 2.14 gives an overview of the advantages and disadvantages of producing a 3D element with float glass and cast glass. Since 3D printed glass still has a limited application, this production method is disregarded. In Table 2.15, an overview and limitations of the different glass manufacturing types is given.

Table 2.14 Overview of advantages and disadvantages of producing a 3D element with the different production processes.

	Advantages	Disadvantages
Float glass	- No topology optimisation necessary to reduce annealing time - Annealing time is not an issue - No mould necessary - The least expensive production method of glass - High redundancy due to lamination of layers - No constraints for the abrupt change in cross-sections	- Topology optimisation necessary to reduce weight - High production cost due to cutting and lamination - Laminating of multiple layers is challenging - Lots of glass waste is generated during cutting (Very easy to reuse this glass) - Layering visible
Cast glass	- No layering visible - Easier to produce an element with a complex shape - No limitations on size - Less glass wasted - Production in different glass types	- Glass objects of substantial thickness present long annealing times. - Mould manufacturing is challenging, and some mould types can be expensive - Large geometries are difficult to handle

Table 2.15 Overview and limitations of the different glass manufacturing types by (Oikonomopoulou, 2019).

Process	Optical	The main type of glass used	Size	Thickness
Float	Smooth Transparent	Soda-lime	Standard: 3,21 x 6 m Max: 4x 20 m	2-25 mm
Cast	Smooth Transparent	Soda-lime, Borosilicate, and Lead	Currently up to 20000 kg	n/a

3. Topology Optimisation

Structural optimisation (SO) searches for optimal material distribution in a predefined physical volume. The physical volume must support or transfer the loads applied to it. During structural optimisation, the manufacturing and user phase must be considered, for example, reducing displacement and stress while maintaining high stiffness. It is also possible to apply structural optimisation to reduce weight or volume. Structural optimisation can be categorised in size, shape, and topology optimisation (Querin et al., 2017).

In this chapter, the concept of structural optimisation is given, followed by different objective functions, and finally, the classification of different topology optimisation approaches is presented. The results of this chapter are the most suitable topology optimisation (TO) types and functions that are used during the case study. In addition, it is discussed how to improve TO to match it to the material glass.

3.1 Structural optimisation

3.1.1 Size optimisation

When using size optimisation, a designer or engineer already knows how the structure looks, but the components' size is not yet determined. In Figure 3.1, on the left, a simple supported truss is displayed. The layout of the members is already known, but the size of the cross-section of each member is still unknown. Figure 3.1 on the right displays which members should have a smaller or larger cross-section. All individual members can have any cross-section. However, they are always present at the end of the optimisation process. (Bendsoe & Sigmund, 2003)
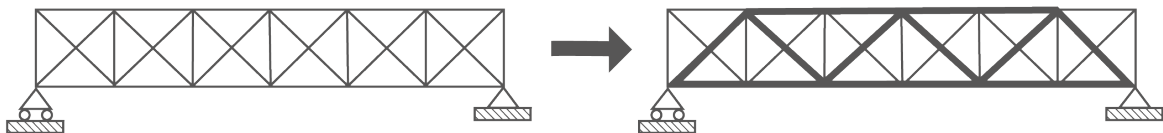
Figure 3.1 Size optimisation of a simple supported truss. Adapted from (Bendsoe & Sigmund, 2003).

3.1.2 Shape optimisation

With shape optimisation, everything is known except for the shape of parts of the structure. In Figure 3.2 (Bendsoe & Sigmund, 2003), a simply supported truss is given with six circular holes. The new shape of the optimised truss is more beneficial to the load transfer. When performing shape optimisation, the structure is adapted, but no load-bearing elements are removed.
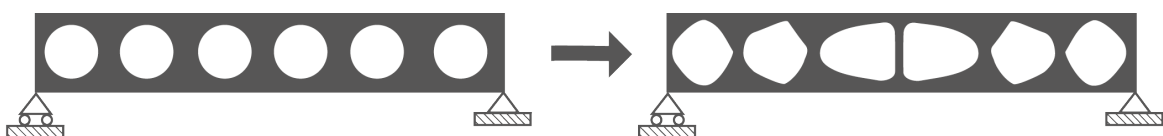
Figure 3.2 Shape optimisation of a simple supported beam. Adapted from (Bendsoe & Sigmund, 2003).

3.1.3 Topology optimisation

Topology optimisation (TO) can be used when the shape and size of the structure are not known. TO is the most general optimisation strategy of the three. When using TO, the material is added and removed where needed. The structural topology changes within the defined boundary. For a discrete structure, this means that members can be removed and resized to get an optimal structure. An example can be found in Figure 3.3A. For a continuum structure, the material is removed where not needed and added where needed, as shown in Figure 3.3B. (Bendsoe & Sigmund, 2003)
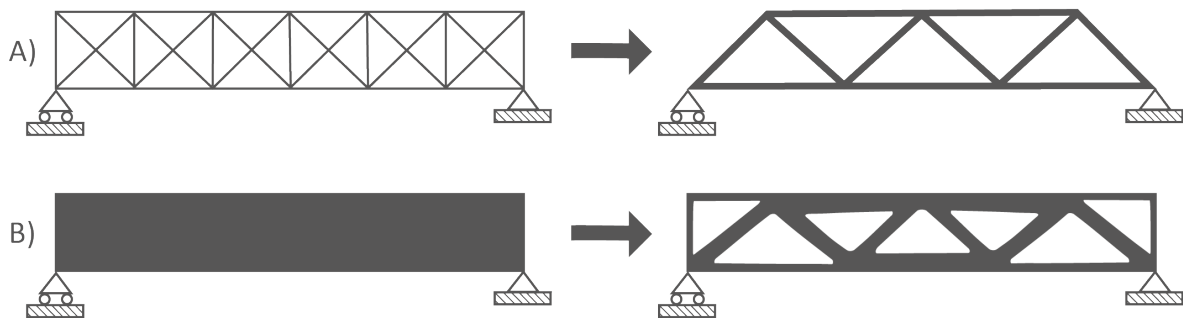
Figure 3.3 Topology optimisation of a simple supported truss and beam. Adapted from (Bendsoe & Sigmund, 2003).

3.2 Objective function

The objective function used for most TO problems is to minimise the weight or compliance of an element with stress or volume restrictions. It is crucial to keep the boundary conditions, design domain and material characteristics in mind when choosing one of the two methods (Hailu Shimels, Dereje Engida, & Fakhruldin Mohd, 2017).

3.2.1 Compliance based

With compliance-based TO, the optimal layout is based on minimising the compliance (displacement measured as strain energy) under a volume constraint. Compliance based methods primarily result in a more complex design than stress-based TO. This method cannot take stress into account, and thus post-processing is needed to make the stress acceptable within its boundaries. There are also many variations between results when using this method. The distributed material affects the optimal outcome, resulting in different layouts for different amounts of material (Hailu Shimels et al., 2017).

3.2.2 Stress based

The optimal solution for stress is based on the material used and considers the stress concentrations. This type results in a stress in each segment that is smaller than the failure stress. This way, the optimisation is always done based on the failure criterion instead of the distribution of the material. Because of this, there is almost no variation between results. Post-processing is not necessary since the loads and stresses are already considered during the TO process. This makes stress-based TO more viable from an engineering perspective for designs where stress is most important. However, stress-based TO is also challenging since it demands a high computational capacity and has issues such as the singularity phenomenon, and local nature and nonlinear behaviour of stress constraints (Hailu Shimels et al., 2017).

A distinction should be made between TO for isotropic, anisotropic, ductile, and brittle materials. Additionally, the distinction should also be made between materials with a similar compressive and tensile strength and materials with a different compressive and tensile strength. Anisotropy can be a result of intrinsic material properties or can be process-induced. When the anisotropy is a material property, a directional preference should be included in the optimisation. The process-induced anisotropy is an unfavourable weakness that follows from the fabrication process. Although much research has been done in developing anisotropic TO approaches, a successfully realized algorithm is still not employed yet. The mathematics behind this optimisation approach is very complex, which has been the main problem for implementing an efficient optimisation process. Multiple objective functions have been developed for isotropic material such as Von Mises, principal stresses, Drucker-Prager, and maximum shear stress. Von Mises is most suitable for ductile material, and the principle stress method is most suited for brittle materials (Mirzendehdel, Rankouhi, & Suresh, 2017).

3.2.2.1 *Von Mises*

When using stress-based TO, the Von Mises stress is used primarily. The Von Mises criterion states that when the material exceeds its yield strength, it fails. The Von Mises Stress is calculated by taking an average of the principle and shear stresses, as shown in equation 3.2.2. Because of this, the Von Mises yield criterion is only applicable to ductile materials (Hartsuijker & Welleman, 2009). This makes it unsuitable to use for a glass structure. Stress-based TO for glass should use a different objective function.

$$\sigma = \sqrt{\frac{1}{2}((\sigma_1 - \sigma_2)^2 + (\sigma_2 - \sigma_3)^2 + (\sigma_1 - \sigma_3)^2)} \tag{3.2.2}$$

Where σ_1, σ_2, and σ_3 are corresponding to the tensile, compressive, and shear stresses.

The Tsai-Wu criterion is an adaption of the Von Mises criterion and considers the orthotropy of materials, unidirectionality of composites, and anisotropy. (Mirzendehdel et al., 2017)

3.3 Classification of methodologies

There are many different ways a TO process can be carried out. A distinction can be made between TO approaches based on optimality and heuristic criteria (Querin et al., 2017).

3.3.1 Optimality Criteria

The first one is an indirect method called the *Optimality Criteria* method. For the first method, a set of criteria must be satisfied related to the structural behaviour. This method is particularly suitable for structures with multiple design variables and minimal constraints. The Optimality Criteria method can be subdivided into Homogenization method, Solid Isotropic Material with Penalization (SIMP), Level Set Method, and Growth Method for Truss Structures (Querin et al., 2017). All the methods are explained in the following sections.

3.3.1.1 *Homogenization method*

The homogenization method for Topological Optimisation assumes that the linear elastic structure has an infinite amount of infinite small voids. Those voids result in a porous structure. An optimal layout of the porosity must be found to find an optimal solution. The density of each element can have any value between zero and one. The elements in the structure where there is no porosity results in solid material. The elements in the structure where there is only porosity results in the removal of material. For intermediate states, a porous structure is created (Bendsøe & Kikuchi, 1988; Suzuki & Kikuchi, 1991). In Figure 3.4, the solid material is given by black boxes, the removed material by white boxes, and the intermediate material by grey boxes.
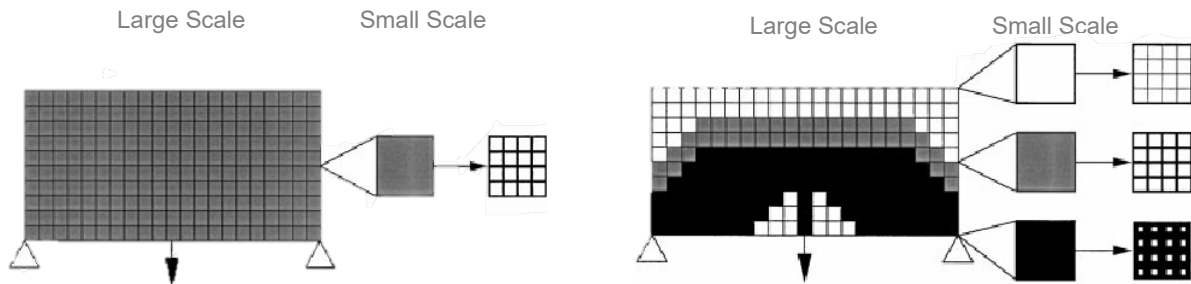
Figure 3.4 Homogenisation method. Left: initial geometry; Right: Optimised geometry. From (Belblidia & Bulman, 2002).

3.3.1.2 *Solid Isotropic Material with Penalization*

From the Homogenization method, the Solid Isotropic Material with Penalisation (SIMP) method was developed. With SIMP, every element gets an artificial element density. This density can have any value between zero and one. The actual volume of the element can be calculated by multiplying the artificial density with the volume of the component. In Figure 3.5, an example of the SIMP method is given. The white area indicates the zone where the density is equal to zero, the black area indicates the zone where the density is equal to one, and the grey area shows all intermediate values. A penalization is used to remove the grey zone, which results in a black and white solution. Most commercial TO software's use SIMP for their optimisation. A weakness of this method is the absence of clearly defined boundaries. Because of this, the designer should almost always interpret the geometry. (Querin et al., 2017)
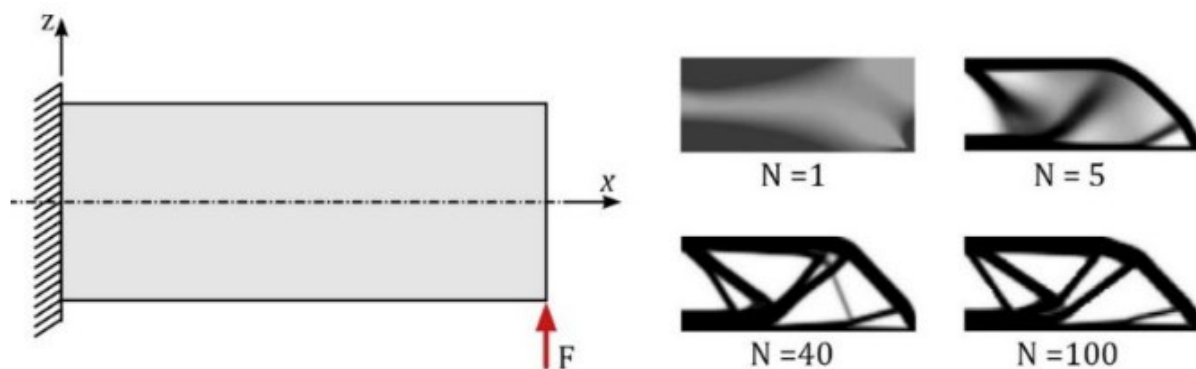
Figure 3.5 SIMP Topology optimisation of a clamped beam. From: (Leary, Merli, Torti, Mazur, & Brandt, 2014).

3.3.1.3 *Level Set Method*

The Level Set method is boundary-based. This method changes the boundaries of the design during the optimisation process, which results in an optimised design with clear edges and smooth contours. In Figure 3.6, an example of the Level Set method is given. This approach combines topology and shape optimisation. This means that new topologies are formed with the principles of shape optimisation. By adding randomly placed voids and moving the design boundaries in every iteration to a more optimum position, these randomly placed voids merge, split, or disappear. Material is added at spots where stresses are too high and removed where stresses are too low. When more voids are added at the beginning of the optimisation process, the number of iterations is less, but the result hardly changes. (Jiang & Chen, 2017; Wang, Wang, & Guo, 2003)
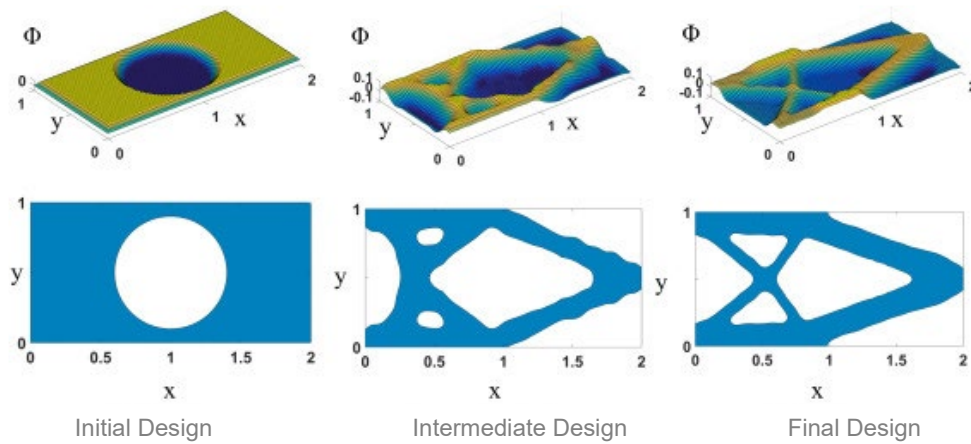
Figure 3.6 Example of the Level Set method. From (Jiang & Chen, 2017).

3.3.1.4 *Growth Method for Truss Structures*

The growth method can be used for a two-dimensional truss structure that has a single load case. The method is a combination of size, shape, and topology optimisation. During the optimisation process, the element can have size and stress constraints. At the beginning of this process, the component's geometry is elementary. In every iteration, a joint and bars are added and optimised. This process is displayed in Figure 3.7. There are two possibilities in this process. The first option is to add a joint in the centre of the largest bar. This joint is connected to the nearest joint by adding a new bar. Before going to the next iteration, the position of the joint is optimised. In this process, the bar stiffness is the variable. The second option is to separate an existing joint and connect these separate joints with a new bar. In this process, the joint separation is the variable. (Querin et al., 2017)
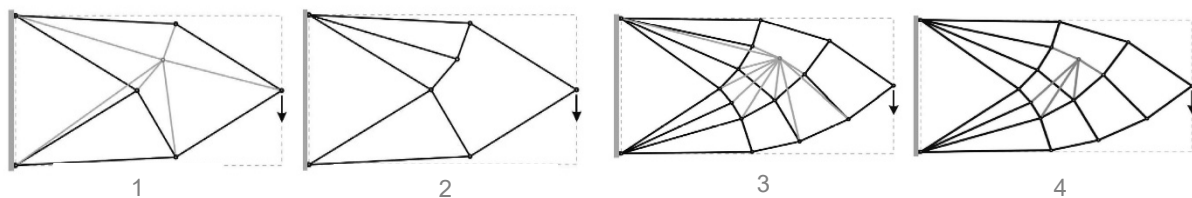
Figure 3.7 Example of the growth method for truss structures. From (Querin, Victoria, Alonso, Ansola, & Martí, 2017).

Heuristic Method

The second method is based on instinct, experience, construction processes, or based on organic systems. This method is called the *Heuristic Method* and gives feasible but not always optimal results. The following categories fall under the Heuristic method: Fully Stressed Design, Computer-Aided Optimisation (CAO), Soft Kill Option, Evolutionary Structural Optimisation (ESO), Bidirectional Evolutionary Structural Optimisation (BESO), Sequential Element Rejection and Admission (SERA), Isolines / Isosurfaces Topology Design (ITD) (Querin et al., 2017).

3.3.2.1 *Fully Stressed Design*

The Fully Stressed Design method optimises on topology and size. This method is suitable for structures that are subjected to stress and have a minimum gage constraint. During optimisation, the not fully stressed elements are reduced in gage by removing material (see Figure 3.8). However, a minimum gauge constraint can be inserted to limit the removal of material. This method assumes that only the stresses change when adding or removing material, implying that other changes are negligible or have no effect (Querin et al., 2017).
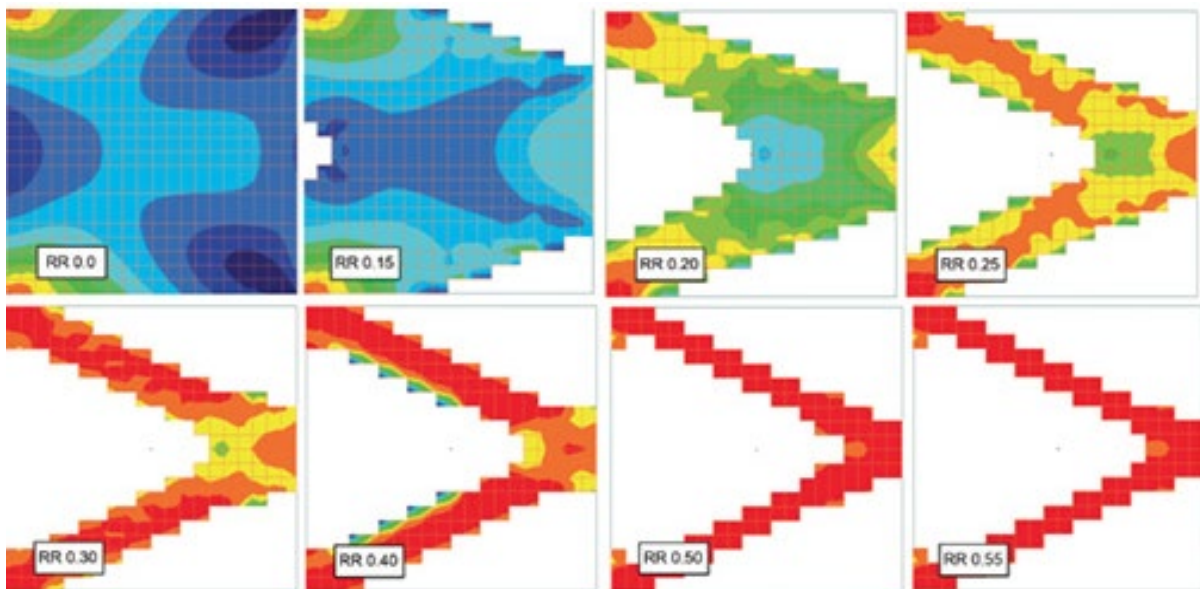
Figure 3.8 Example of the Fully Stressed Design approach for topology optimisation. From (Abbey, 2017).

3.3.2.2 *Computer-Aided Optimisation (CAO)*

During a Computer-Aided Optimisation (CAO) approach, the local stresses are reduced by adding material until the components' stresses are equal. The topology of the final design is mainly dependant on the initial design and on the parts of the element that are not fully loaded. During CAO, only the existing contours are reshaped, no new holes are added. This means that some parts of the component still have a higher capacity than necessary. Only by adding the holes manually at these spots, a more optimised structure can be obtained. (Baumgartner, Harzheim, & Mattheck, 1992)

3.3.2.3 *Soft Kill Option*

The soft kill option looks at the stress distribution and varies the young's modulus accordingly. This method is inspired by the adaptive bone mineralization process, where the bone is denser in areas with high stresses and less dense in areas with low stresses. During the optimisation process, the structure is weakened at underloaded places and strengthened at highly loaded places. This is done by changing Young's modulus according to the distribution of the stresses. During the optimisation, non-loaded parts are deleted from the structure. (Baumgartner et al., 1992)

3.3.2.4 *Evolutionary Structural Optimisation (ESO)*

The Evolutionary Structural Optimisation method looks at the not fully stressed elements and removes the inefficient material. By slowly removing the material that has the lowest stresses, an optimum design is reached. This optimisation results in a black and white solution without any intermediate (grey) elements. In Figure 3.9, the result of an Evolutionary Structural Optimisation is given. In addition to the Von Mises stress-based optimisation, a compliance optimisation approach has been developed, where elements with low strain values are removed. (Querin et al., 2017)

| Rejection Rate = 3% | Rejection Rate = 6% | Rejection Rate = 9% | Rejection Rate = 12% | Rejection Rate = 15% | Rejection Rate = 18% | Rejection Rate = 21% | Rejection Rate = 24% | Rejection Rate = 27% | Rejection Rate = 30% |
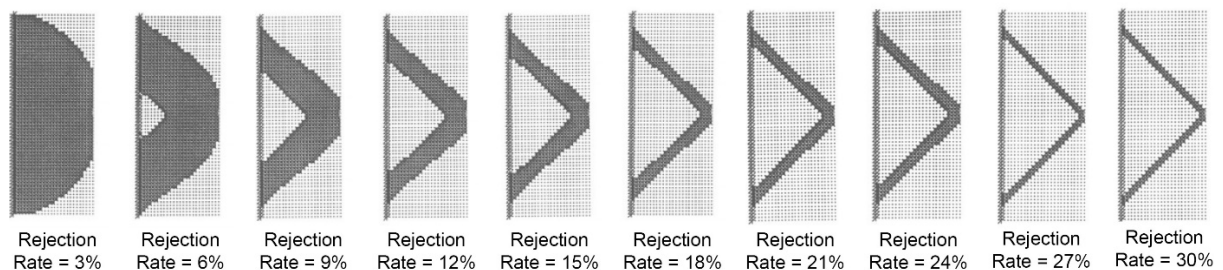
Figure 3.9 Example of an Evolutionary Structural Optimisation. From (Xie & Steven, 1997).

3.3.2.5 *Bidirectional Evolutionary Structural Optimisation (BESO)*

With the ESO method, it is not possible to reintroduce material into the design domain. As a result, the Bidirectional ESO method was developed to remove material at low stressed places and introduce material at locations where the stresses in the material are too high. The optimality of the solution with the ESO method depends on the initial design settings. With BESO, an optimum solution is always found. In Figure 3.10, an example is given where the start geometry is a single line. During the optimisation process, the same geometry was found as with the ESO method in Figure 3.9 (Xia, Xia, Huang, & Xie, 2018).
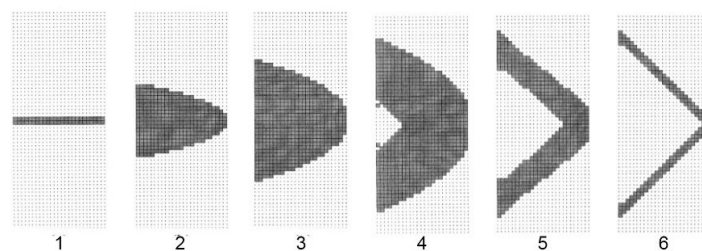
Figure 3.10 Example of a Bidirectional Evolutionary Structural Optimisation. From (Xia et al., 2018).

3.3.2.6 *Sequential Element Rejection and Admission (SERA)*

The Sequential Element Rejection and Admission method can also remove material and introduce material bidirectionally, just like the BESO method. This method can be used to optimise on stress and on compliance. During the optimisation process, a distinction is made between two material domains: the 'virtual' and 'real' domain. In the virtual domain, the stiffness of the material is almost negligible. For this method, the introduction and removal of material is done with two independent criteria. This way, the material can interchange from 'real' to 'virtual'. At the and the 'real' material represents the final design. (Querin et al., 2017)

3.3.2.7 *Isolines/Isosurfaces Topology Design (ITD)*

With the Isolines/Isosurfaces Topology Design method, first, the topology is optimised, followed by the shape of an element. The element is optimised on structural behaviour by using the isosurfaces or isolines of that specific element. Material is added or removed until the desired volume fraction is reached. (Querin et al., 2017)

3.4 Reference projects

In this section, several reference projects are addressed.

3.4.1 Millipede: Optimised concrete slab prototype A

Jipa et al. (2016) produced two optimised concrete slabs. Prototype A can be seen in Figure 3.11. For this prototype, a process was used that combined mesh subdivision and TO. The element was optimised in 2D with the plugin Millipede that can be used in combination with McNeel Rhinoceros and Grasshopper. During optimisation, the element was discretized into 135,000 nodes. In total, 500 iterations were carried out. A reduction of 80 % of the material was the goal while keeping the deformations in an acceptable range. The result of the TO process was a greyscale bitmap. A three-dimensional element was designed by vectorizing the bitmap and taking the different grey values to correspond with the thickness of the elements.

Figure 3.11 Optimised concrete slab prototype A. From (Jipa, Bernhard, Meibodi, & Dillenburger, 2016).

the elements. The result was smoothened with the Catmull-Clark and Loop subdivision to obtain the final design.

3.4.2 SIMULIA Abaqus: Optimised concrete slab prototype B

Jipa et al. (2016) developed two optimised concrete slabs. Prototype B can be seen in Figure 3.12. This prototype was optimised in 3D with SIMULIA Abaqus. During optimisation, the 1.8 x 1 x 0.15 meter element, with four simple supports at the corners, was discretized into 83,072 nodes, resulting in nodes of 3.4 cm^3. Only slight differences were observed when taking 270,336 nodes and 2,162,688 nodes. However, the optimisation with a higher number of nodes increased the computation time significantly. A reduction of 82 % of the material was the goal while keeping the stresses in an acceptable range.

Figure 3.12 Optimised concrete slab prototype B. From (Jipa et al., 2016).

3.4.3   Ameba: Jue Chair

Li (2020) developed an optimised 3D printed chair. A picture of the chair is given in Figure 3.13. An ancient Chinese wine utensil inspired the initial design. The element was optimised in 3D with the plugin Ameba used in combination with McNeel Rhinoceros and Grasshopper. The chair is supported by line supports, and loads are exerted on the seating surface, back surface, and armrests. Due to symmetry, only half of the chair had to be optimised. A non-design domain is added to make sure some parts are not optimised.

Figure 3.13 Jue Chair (Li, 2020).

3.4.4   ANSYS: Research Delft University of Technology

This section summarises the research done in previous years at Delft University of Technology on using TO and additive manufacturing for cast glass structures.

3.4.4.1 *Cast glass shell node*

Damen (2019) researched the possibility of using TO to design a cast glass node for a grid shell. The optimisation process focussed on optimising production, structural behaviour, and assembly of the node. In Figure 3.14, an overview is given of the optimisation approach with the matching software. The connections were optimised using the software program ANSYS. This program uses minimum compliance to optimise material use. The cross-section of each element was set to have a thickness ranging from 15 to 50 mm to ensure the casting and cooling process to be successful.

Figure 3.14 Topology optimisation approach of the optimised node with used software.

Afterwards, it became clear that bigger elements should be used to make sure the node can be assembled more easily. By optimising the node on maximum cross-section, the annealing time was assumed to be reduced by two-thirds compared to the initial geometry. In Figure 3.15, the cast glass optimised shell node is given.

Damen (2019) highlighted that TO also has a weakness. TO gives a highly optimised shape for a specific boundary condition. When the conditions change, the optimal result also changes. Removing less

Figure 3.15 Topology optimised cast glass shell node. From (Damen, 2019).

43

material is not the most efficient option since this leads to over-dimensioning for a specific load case. By taking different load cases, the optimisation process can be done separately. In the end, the results can be combined. However, this does not result in the most optimal multi-objective shape. Another option is to have a load case that is always dominant. This way, the optimal result does not change when the conditions change.

As a follow-up research Damen (2019) recommended looking into the use of stress-based TO algorithms. Additionally, a method should be developed that considers the difference between the tensile and compressive capacity of the materials to use the glass more efficiently.

3.4.4.2 Cast glass column

Bhatia (2019) investigated additive manufacturing to produce topology optimised glass columns for the Kolumba Museum in Cologne. To optimise the column, the program ANSYS was used. The mass of the column was reduced to 4404.4 kg in comparison to the 17146 kg un-optimised column. The column was split into two separate columns to further reduce the overall thickness and the annealing time. The splitting of the column was also done because the student license restricted further
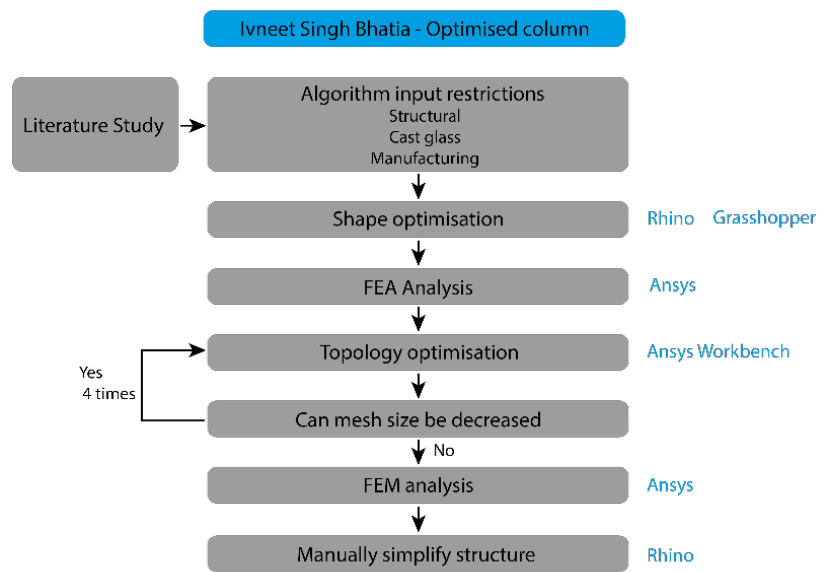
Figure 3.16 Topology optimisation approach of the optimised column with used software.

optimisation. In Figure 3.16, an overview is given of the optimisation approach with the matching software. In Figure 3.17, the optimised columns are shown.

The research additionally explored the use of 3D printed sand moulds. In total, seven experiments were carried out to analyse sand moulds with different binders and finishing layers. In the first three experiments, moulds with furan binder were tested. First, by hot pouring glass into the mould, second by observing the behaviour of the mould at different temperatures, and third a crystal cast layer was formed around the mould before kiln casting. These experiments found that the furan binder vaporises when exposed to high temperatures, disintegrating the mould. During experiments four and five, moulds with three binder systems were tested: inorganic, high heat strength, and cold hardening phenolic. The high heat strength binder disintegrated at high temperatures. Fortunately, the inorganic and cold hardening phenolic remained intact at temperatures of 500 to 900 degrees. Moulds with these two binders remained intact during the casting of glass. However, the surface finish was very rough. The main goal for experiment
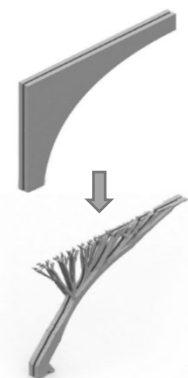
Figure 3.17 Topology optimised cast glass column. From (Bhatia, 2019).

six and seven was to find a suitable coating that can be used on the mould. Crystal cast performed the best in these experiments since it results in the best optical quality. However, it is still necessary to post-process the glass afterwards.

Bhatia (2019) proposed further research into various coatings to find one that creates a smooth and transparent finish. Additionally, a parametric tool could be made that can be used during mould designing. Finally, the pouring of glass inside the mould should be studied to prevent air bubbles and spillage.

3.4.4.3 *Cast glass slab*

Stefanaki (2020) investigated TO as a design tool and its potential and limitations when producing a large cast glass slab using a 3D printed mould. With ANSYS, a mass reduction of 55.2% was obtained with a cross-section thickness ranging between 100 and 180 mm. In Figure 3.18, an overview is given of the optimisation approach with the matching software. The render of the final design is shown in Figure 3.19.

Stefanaki (2020) recommends doing further development of the integration of additional constraints during the optimisation process. Such as aesthetic criteria. Several licence limitations were faced during optimisation.

Figure 3.19 Topology optimised cast glass slab. From (Stefanaki, 2020).
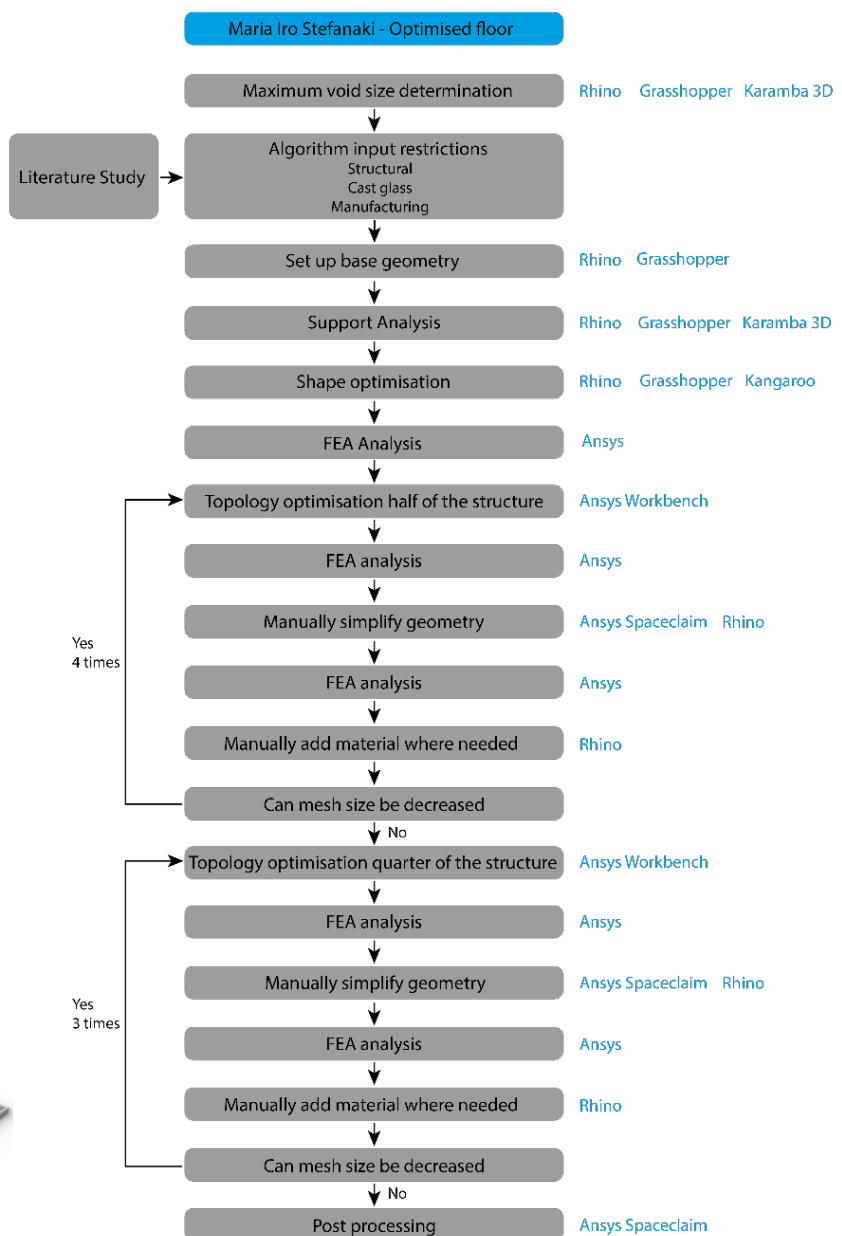
Figure 3.18 Topology optimisation approach of the optimised slab with used software.

Because of these limitations, the slab was split before optimisation. When optimizing the entire slab before splitting, fascinating asymmetrical results could be obtained by using different boundary conditions.

Cast glass shell

Naous (2020) investigated how a cast compressive free-form glass structure can be designed using TO. It shows how TO for shell structures can offer a solution for large glass structures. A compression shell is very suitable for materials that have low tensile and high compressive strength. During the design phase, a mass reduction of 43% was achieved. This was done with the use of the ANSYS topology optimisation tool. In Figure 3.20, an overview is given of the optimisation approach with the matching software. In Figure 3.21, a render is shown of the final design.
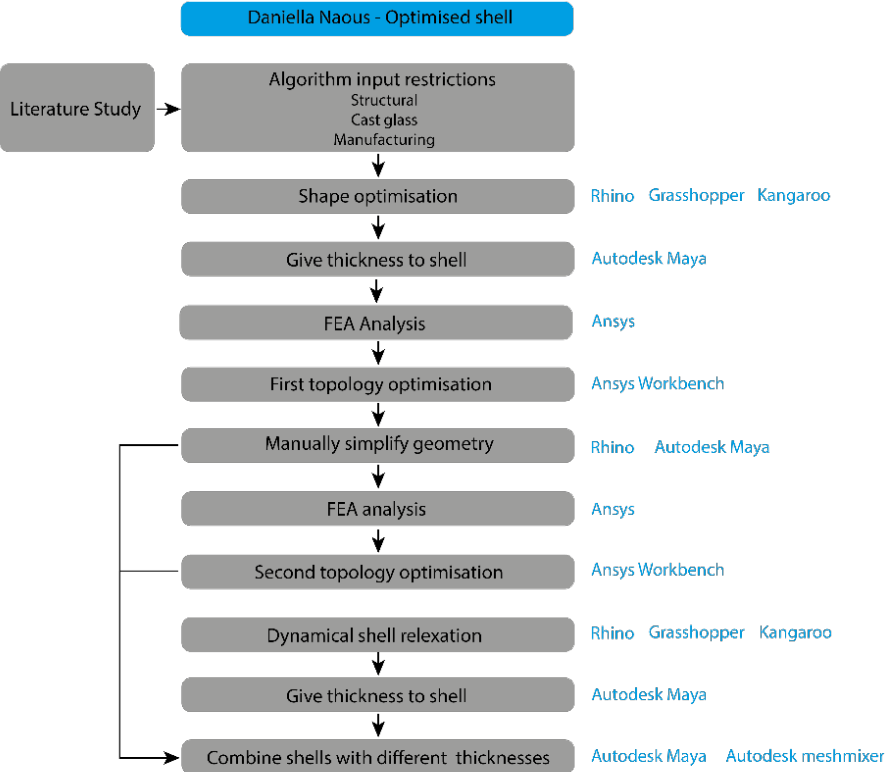
Figure 3.20 Topology optimisation approach of the optimised shell with used software.

Naous (2020) explains that compliance-based TO needs much post-processing. Recommendations are made to further investigate and compare different TO approaches, such as the Drucker-Prager method. Another
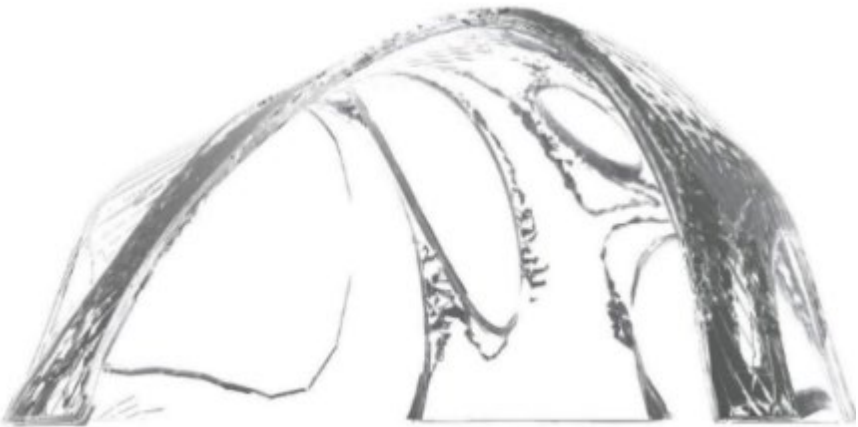
Figure 3.21 Topologically optimised cast glass shell. From (Naous, 2020).

suggestion is to compare and explore various software packages. It was concluded that developing a new TO algorithm focussing on materials such as glass should be a PhD research or separate MSc thesis.

Conclusion previous research at TU Delft

Various structures have been researched in the past years that used TO combined with cast glass and additive manufacturing. It can be concluded that it is a promising combination. Still, a couple of obstacles must be overcome. More research should be done into other optimisation approaches that are not compliance-based or use the Von Mises Stress. Additionally, research should be done on mould design, choosing a suitable coating during casting, integrating additional constraints during the optimisation process, and comparing various software packages.

3.4.5   Fusion 360: JPL's Interplanetary lander

Generative design technology was used by NASA's Jet Propulsion Lab (JPL) to design a new concept space lander. The total weight of a space lander had to be as low as possible. A weight reduction of the structural part meant that the scientific instruments, radiation protection, or extra batteries and expendables could take up more of the total weight. To reduce the structural weight of the rover JPL and Autodesk
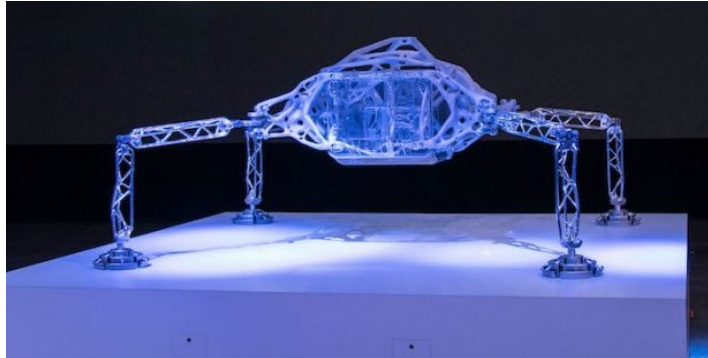
Figure 3.22 JPL's interplanetary space lander. From (Collins, 2018).

teamed up in a multi-year collaborative research project. The application 'generative design' was used during this research. With generative design technology, multiple design strategies are considered, producing various solutions instead of other software programs that only optimise one element on weight or stiffness. The body and legs of the lander were optimised. The final mass of the new design was reduced by 35% while improving the overall performance (Collins, 2018). In Figure 3.22, a picture is given of the final product.

3.4.6   Fusion 360: Vertico 3D printed concrete bridge

The Vertico bridge is a 4-meter-long, 3D printed, post-tensioned, topology optimised concrete bridge. In Figure 3.23, a picture is given of the final product. During the design phase of the bridge, the optimisation was displacement driven and was done in 2D. Optimisation programmes for post-tensioned concrete structures are not yet developed for 3D structures. Because 3D printing was

Figure 3.23 Vertico bridge. From (Vantyghem, De Corte, Shakour, & Amir, 2020).

used, printing constraints and limitations had to be added to the optimisation expression. Because of the symmetry of the beam, only half of the structure had to be modelled and optimised. The optimised 2D design was transformed to 3D with the help of the program Fusion 360. The design was modelled and analysed in a 3D finite element program. During the analyses, three load cases were considered. These were self-weight, self-weight + post-tensioning, and self-weight + post-tensioning force + live load. (Vantyghem et al., 2020)

3.4.7 Karamba: The glass swing

The glass swing is a vector active structure with steel nodes and bundled extruded glass columns. In Figure 3.24, a picture is given of the final product. The structure was optimised in 2D with the add-on Karamba. This add-on can be used in combination with McNeel Rhinoceros and Grasshopper. Karamba uses the BESO method during optimisation. The use of this software made it possible to only use a single model. The structure was optimised for when the vertical and horizontal loads were exerted at the same time. The optimised result from Karamba was interpreted by engineering judgement into a buildable structural. (A. H. Snijder, van der Linden, Goulas, Louter, & Nijsse, 2020)
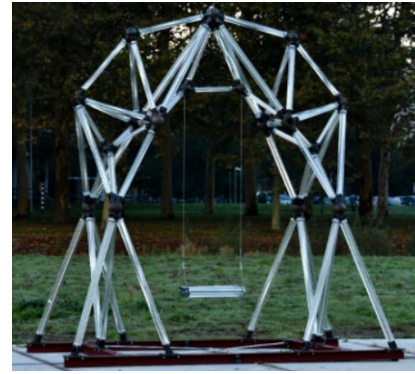
Figure 3.24 The Glass Swing. Photo: José Galan.

3.4.8 OptiStruct: Arup's steel node

Galjaard et al. (2015) produced an optimised steel node that is part of a tensegrity structure. The optimised node can be seen in Figure 3.25. The node was created with Direct Metal Laser Sintering. During this process, each layer of powder is selectively fused by a laser. For the TO process, OptiStruct was used, and for the pre- and post-processing, other software packages were needed. The initial design space was set up in a parametric way in McNeel Rhinoceros/Grasshopper. This way, the process could be used for all nodes. During optimisation, the stress limit was set at 80% of the maximum tensile strength. The optimisation goal was to reduce the structural weight while keeping the Von Mises stress in an acceptable range. The final design of the optimised node was 75 % lighter than the original node and was half the height. This reduction had a significant impact on the entire structure, which could be reduced by 40%.
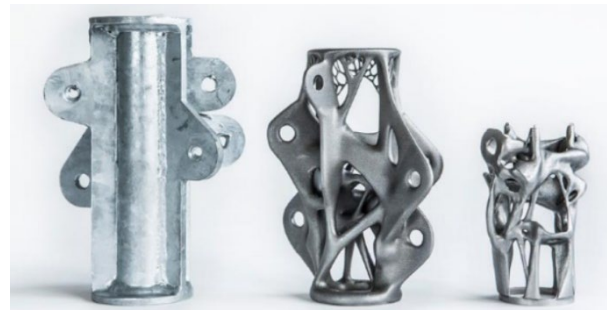
Figure 3.25 Arup's optimised steel nodes. From (Galjaard, Hofman, Perry, & Ren, 2015).

3.4.9 The Castilla-La Mancha bridge

The Castilla-La Mancha bridge is a 3D printed bridge with a span of 12 meters and a width of 1.75 meters (see Figure 3.26). The bridge consists out of eight segments that have a maximum footprint of 2 by 2 meter. The structure is the first 3D printed bridge ever built. The design of the bridge was optimised with a generative algorithm on material distribution. The printing of the bridge took two months. The construction of the bridge was completed in 2016. The bridge was printed using fused concrete powder and reinforced with polypropylene. (Buchanan & Gardner, 2019)

Figure 3.26 The Castilla-La Mancha bridge located in Madrid. From (IAAC, 2017).

3.5 Conclusions and recommendations for topology optimisation

In this section, the conclusions and recommendations are given about the topology optimisation approach.

3.5.1 Objective function

The objective function that is most suited for optimising a cast glass bridge is a method that can optimise a component with material that has unequal behaviour in tension and compression. However, such an approach is not yet successfully implemented for glass. Because of this, it is decided to use compliance-based optimisation. The stresses have to be checked at the end of each optimisation process. If there is still capacity left in the structure, an additional optimisation round could be added.

3.5.2 Methodology

The most implemented optimisation methodology is the SIMP method. The Level Set method and BESO method are also commonly used methodologies. These methods are very suitable to use during optimisation due to the possibility of being used with a compliance-based objective function, the option to optimise a continuum structure, and the ease the black and white solution can be interpreted.

4. Bridge design

In this section, first, the most promising bridge topology is explained. Second, the current regulations are given. Third, multiple pedestrian and bicycle bridges are examined on design and material use.

4.1 Bridge topology

When designing a bridge made from cast glass, it is essential to consider how the forces are transferred within the bridge. Materials such as unreinforced concrete, masonry, natural stone, and glass are excellent in sustaining compressive forces. Because of the low tensile strength of these materials, bridges must be designed such that no high tensile stresses occur. Bridges can be divided into seven different types. Each type is given in Figure 4.1. The members in compression are indicated with yellow, and the members in tension in blue. As shown in the figure, the only type of bridge entirely in compression is the arch bridge.

Since ancient times arch bridges have been built. This shape was used because it made it easy to build with locally sourced materials, resulting in strong and rigid bridges. The disadvantages of arch bridges are the long construction time and a large amount of material needed. An arch-shaped bridge constructed with masonry and natural stone is given in Figure 4.2.

Figure 4.2 Arch shaped bridge, Bagijnhofbrug located in Delft.
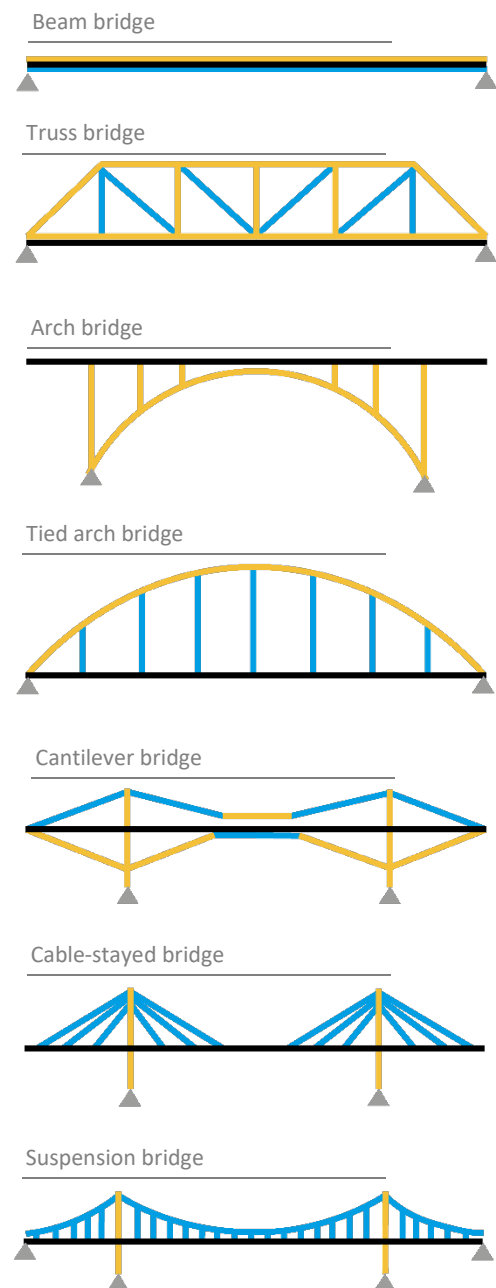
Figure 4.1 Types of bridges with in blue the members in tension and in yellow the members in compression.

Arch bridges can be grouped into parabola shaped and circular shaped arch bridges. A look should be given to the line of thrust to obtain the ideal arch shape. The line of thrust concept can be best explained by looking at a cable structure. In a cable structure, no compression forces and bending moments occur, only axial forces. The inverted shape of the cable is the best shape for an arch that is only in compression. This shape is also called the line of thrust. Figure 4.3 gives the cable shape and arch shape (line of thrust) for four load cases.
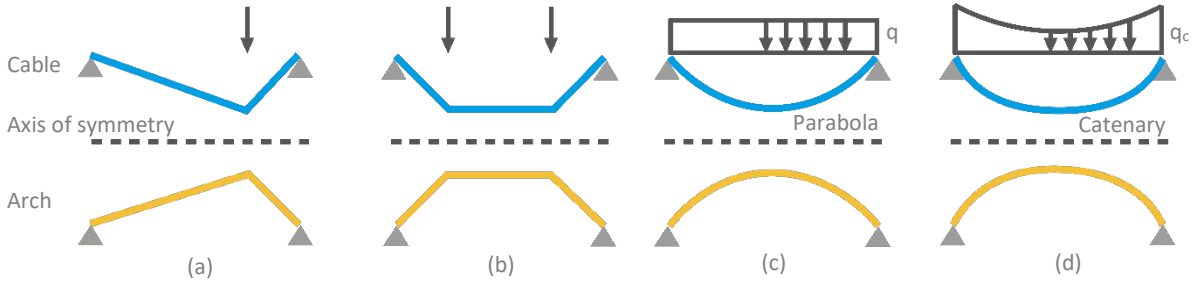
Figure 4.3 The ideal arch shape is obtained by inverting the shape of the cable for the specific load configuration. Based on Aurik (2017).

To obtain an entire structure in compression, the line of thrust should lie between 1/3 and 2/3 of the total thickness of the cross-section of the arch. If the line of thrust falls outside this area, only a part of the cross-section is in compression. In Figure 4.4, an example is given for an eccentric line of thrust.
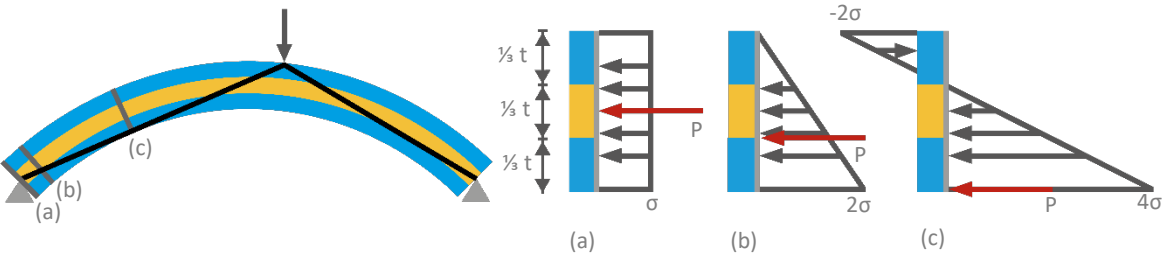
Figure 4.4 Example of the stress distribution of an eccentric line of thrust. Based on Hoogenboom (2014).

4.2 Designing a pedestrian bridge and Regulations

When designing a pedestrian bridge, the most critical aspect is the accessibility of the bridge. This can be translated into a good connection with the footpath, a gentle ramp, minor height differences and no obstacles. Smooth large surfaces should be avoided to prevent vandalism such as graffiti. The bridge's width should be minimally 1.5 meters and preferably more than 1.8 meters (Berg, 2015). In Figure 4.5, an overview is given of the spatial needs for different pedestrians. Additionally, an opening should be added of 3.1-meters-wide and 1-meter-high for maintenance to the waterway. (Gemeente Delft, 2019)
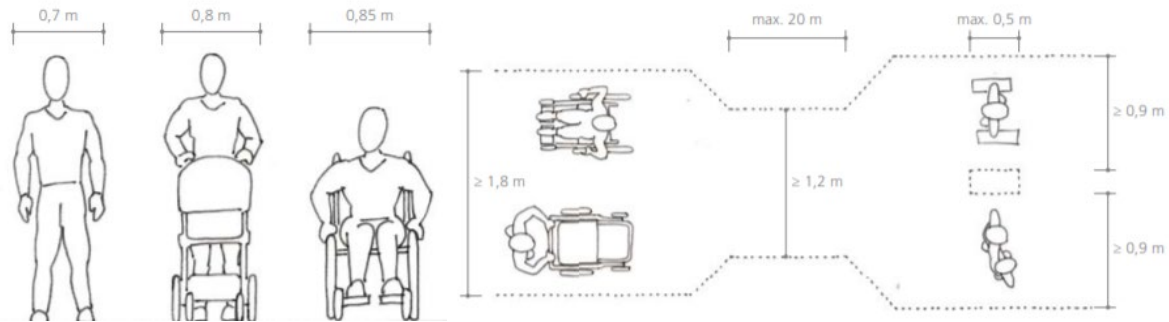
Figure 4.5 Spatial needs for the different pedestrians. From (Berg, 2015).

For safety reasons, a railing needs to be added to the bridge. For bridges with a drop larger than 1 meter, a railing is required with a minimum height of 1 meter. Because some cyclists use the bridge, the chance of falling off a bike over the railing should be considered. A railing of 1.2 or 1.3 meters is on the safer side.

The transportation and construction of the bridge is a limiting factor in the bridge design. The maximum dimensions a flatbed trailer can carry are 13.6-meters-long, 2.48-meters-wide, and 2.5-meters-high. The maximum payload capacity is 31,900 kg (DSV Global Transport and Logistics, n.d.). There are numerous different cranes on the market. The maximum load capacity, maximum hoist height, and maximum radius need to be considered when choosing a crane. The cranes need to hoist the bridge parts from the closest road to inside the park. This distance is approximately 40 meters. To ensure the bridge element can be safely lifted from the nearest road and make sure it is not necessary to rent the most expensive crane, the maximum weight of a single component is set at 3,000 kg.

4.3 Loads on the bridge

For the design of the bridge, the Eurocodes and the Dutch National Annex is used. The permanent load, traffic load, wind load, and temperature load is considered. The design life of the bridge is 50 years, and a consequence class of 3 is assumed. This consequence class is chosen because a cast glass bridge is a new type of structure, bringing many uncertainties. Furthermore, the collapse of such a bridge would harm the development of cast glass structures in the future. The bridge is not accessible for maintenance vehicles and emergency services. A barrier is added to prevent vehicles from passing the bridge.

The horizontal force caused by people walking over the bridge should be considered and is 10% of the total distributed load. According to NEN-EN 1991-2+C1:2015, a second traffic load case should be considered for local effects. Additional to the distributed vertical and horizontal load case, another load case should be considered with a point load. This point load of 10 kN should be applied on a surface of 0.1 by 0.1 meter. The dynamic load caused by people and by wind is negligible due to the small size of the bridge and its high dead weight compared to its slenderness.

The load combinations used during the validation of the topology optimised structure are given in Table 4.1. The loads that belong to the different load cases used during structural calculation can be found in Table 4.2. In Appendix B, more information is given about the loads, partial factors and load combinations.

Table 4.1 Load combinations.

	Permanent	Traffic	Wind	Temperature
L.C. 1	**1.40**	1.5 · 0.4	1.65 · 0.3	1.65 · 0.3
L.C. 2	1.25	**1.5 · 1.0**	1.65 · 0.3	1.65 · 0.3
L.C. 3	1.25	1.5 · 0.4	**1.65 · 1.0**	1.65 · 0.3
L.C. 4	1.25	1.5 · 0.4	1.65 · 0.3	**1.65 · 1.0**

Table 4.2 Load cases used during structural verification of the bridge.

	Without factor	L.C.1	L.C.2	L.C.3	L.C.4
$g_{,soda\ lime}$	$2460\ kg/m^3$	$\bm{3444\ kg/m^3}$	$3075\ kg/m^3$	$3075\ kg/m^3$	$3075\ kg/m^3$
$g_{,borosilicate}$	$2230\ kg/m^3$	$\bm{3122\ kg/m^3}$	$2788\ kg/m^3$	$2788\ kg/m^3$	$2788\ kg/m^3$
$q_{f,vertical}$	$5\ kN/m^2$	$3\ kN/m^2$	$\bm{7.5\ kN/m^2}$	$3\ kN/m^2$	$3\ kN/m^2$
$q_{f,parallel}$	$0.5\ kN/m^2$	$0.3\ kN/m^2$	$\bm{0.75\ kN/m^2}$	$0.3\ kN/m^2$	$0.3\ kN/m^2$
$Q_{fv;vertical}$	$10\ kN$	$6\ kN$	$\bm{15\ kN}$	$6\ kN$	$6\ kN$
$q_{wind,vertical}$	$\pm0.52\ kN/m^2$	$\pm0.26\ kN/m^2$	$\pm0.26\ kN/m^2$	$\pm\bm{0.86\ kN/m^2}$	$\pm0.26\ kN/m^2$
$q_{wind,perpendicular}$	$1.28\ kN/m^2$	$0.63\ kN/m^2$	$0.63\ kN/m^2$	$\bm{2.11\ kN/m^2}$	$0.63\ kN/m^2$
$q_{wind,parallel}$	$0.51\ kN/m^2$	$0.25\ kN/m^2$	$0.25\ kN/m^2$	$\bm{0.84\ kN/m^2}$	$0.25\ kN/m^2$
ΔT_n	$27\ ℃$	$13.37\ ℃$	$13.37\ ℃$	$13.37\ ℃$	$\bm{44.55\ ℃}$
ΔT_m	$9\ ℃$	$4.46\ ℃$	$4.46\ ℃$	$4.46\ ℃$	$\bm{14.85\ ℃}$

Since the foundation is not infinitely stiff, the bridge may undergo unequal settlement. The bridge should be able to withstand an unequal vertical settlement of up to 10 mm.

4.4 Reference projects

In this section, several reference projects are discussed. These projects are all pedestrian/bicycle bridges made with an unconventional material or constructed irregularly. In sections 3.4.6 and 3.4.9, two optimised 3D-printed concrete bridges were already discussed.

4.4.1 The glass truss bridge

An example of a recently developed bridge is the 14-meters-long and 2-meters-width glass truss bridge. The bridge is located at the entrance of the green village. The green village is a lab for sustainable innovation and is located at the TU Delft campus. For this bridge, a combination is made between the use of glass and the use of steel. This bridge has struts built up out of bundled extruded glass and nodes made of cast glass components. A picture of the bridge can be found in Figure 4.6 (A.H. Snijder et al., 2018).

Figure 4.6 Glass truss bridge located in Delft.

4.4.2 Symbio bridge

Another innovative bridge is the 39-meters-long and 10-meters-wide Symbio bridge that is part of a new hiking and biking connection. The bridge is located in Delft between the Science park Technopolis and leisure area Ackerdijkse Bos. The bridge has an unusually shaped steel load-bearing structure and a bridge deck made of fibreglass (Starink, 2016). A picture of the bridge can be found in Figure 4.7.

Figure 4.7 Symbio Bridge located in Delft.

4.4.3 MX3D bridge

The MX3D bridge is a 10-meters-long and 2.5-meters-wide steel bridge (see Figure 4.8). The bridge is built using the Wire and Arc additive manufacturing directed energy deposition process. With this production process, the object is entirely made from weld material. A six-axis robotic welding arm was used during manufacturing. (Buchanan & Gardner, 2019)

Figure 4.8 MX3D bridge located in Amsterdam. From (Buchanan & Gardner,

4.4.4 Catharina bridge leiden

The Catharina bridge is the longest and most slender bridge in the Netherlands. The 36-meters-long and 6-meters-wide bridge is made from ultra-high-performance concrete (UHPC). The use of UHPC resulted in a bridge deck of only 275 mm thick in the middle. (Tektoniek, 2016)

Figure 4.9 Catharina bridge located in Leiden. From (Tektoniek, 2016).

4.4.5 Glass bridge China

In May 2021, a glass-bottomed bridge located in Longjing city in China was heavily damaged due to strong winds. Several glass panels shattered, leaving nothing but the railing and load-bearing structure in place. Guidelines including technical standards and recommendations are missing for these types of structures in China. This probably results in an ill-designed bridge subjected to too high wind forces and higher rotations than expected. Additionally, from the pictures in Figure 4.10, it seems like the wrong glass panels were used and that they were wrongly connected to the steel frame. This resulted in less space for large rotations. (Albeck-Ripka, 2021)

Figure 4.10 Glass bottomed bridge located in China. Before and after the collapse. From (abc.net.au, 2021).

4.5 Conclusion bridge design

The design life of the bridge is 50 years with consequence class 3. The bridge deck and railing should be designed for the loads stated in Appendix B.2.1. A barrier is added to prevent vehicles from passing the bridge, and a sacrificial layer is added to the floor to prevent damages to the loadbearing structure.

An opening should be added of 3.1-meters-wide and 1-meter-high to be able to perform maintenance to the waterway. The maximum dimensions of a single casted element are 13.6-meters-long, 2.48-meters-wide, and 2.5-meters-high with a maximum weight of 3,000 kg.

5. Case Study

5.1 Location in Delft

Delft is well known for its canals and bridges. With a total of 75 bridges distributed throughout the historic city centre and approximately 431 bridges scattered throughout the city, a large variety of bridges can be found (Smit, 2020).

The combination of Delft being a touristic destination, the presence of many waterway channels, and recent activities in the development of structural glass makes it a very suitable location for a new bridge entirely made of glass. It is decided to design a bridge for pedestrians. At this early stage of using topology optimised structures combined with glass, many experiments have to be done before the bridge becomes safe to build. Therefore, the bridge should not be too big to make it feasible to produce and test. The site within Delft should fulfil the following criteria:

- There should be a necessity of placing or replacing a bridge.
- The bridge should fit within the surroundings.
- The bridge is only accessible for pedestrians.

5.1.1 Possible Locations

A list is made with the possible zones in Delft where the bridge could be placed from these criteria. In Figure 5.1, the map of Delft is given with these zones.

5.1.1.1 *Zone 1*

The Wilhelminapark, located 1.4 km from the central station, was constructed from 1930-40 to a design by O. de Vries. The park has meandering water features, vistas, and sloping lawns. It is a pity that the park does not have a unique collection of plants, art expression, and information about its history. In addition, the poor condition of the area makes it almost impossible for people to have a pleasant walk through the park. This resulted in an appeal to the municipality in which the residents asked to solve this problem (Toetenel, 2020). A glass bridge could be part of the revival of the park. Additionally, the natural surroundings would be an excellent backdrop for the bridge.
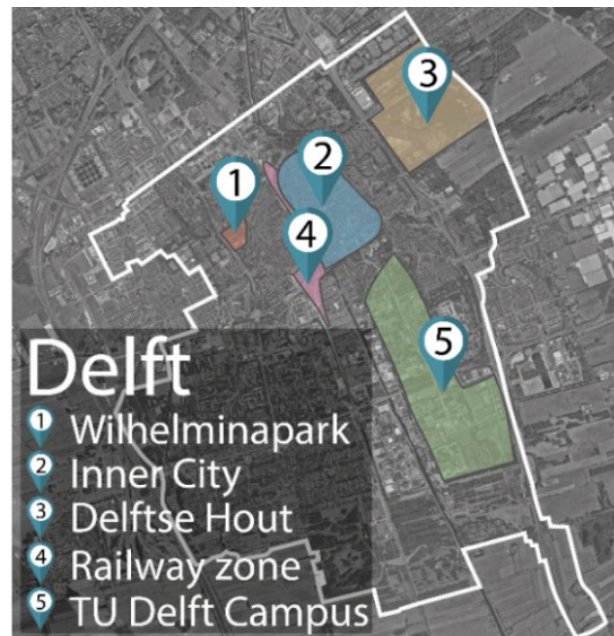
Figure 5.1 Map of Delft with zones for the possible bridge location. From (Google, n.d.).

5.1.1.2 *Zone 2*

The inner city of Delft has a total of 75 bridges. The beautiful canals, courtyards, facades, and monumental buildings take you centuries back in time. The historical backdrop is very suited for a glass bridge. It would give a nice contrast between old and new. This can also be a disadvantage since people want to keep the historic part of the inner city as it is.

5.1.1.3 *Zone 3*

The Delftse Hout is located at the northern edge of Delft. There are 400 hectares of recreation and nature area that primarily consist of a lake and forest. The most visited place is the 20 hectares lake (Delft, 2020). One of the branches of this lake would be a suitable location for the glass bridge. A disadvantage of this location is the distance to the civilised world.

5.1.1.4 *Zone 4*

In 1988 the Dutch Railways unfolded its plans to double the track capacity in Delft. A study of alternatives resulted in designing and constructing a four-track railway tunnel. Many buildings had to be demolished to make room for the construction site. After completing the tunnel, underground station, and city hall, a large area next to the inner city came available for redevelopment. The redevelopment consists of constructing houses, offices, and public spaces such as a new city park (Spoorzone, n.d.). A glass bridge would fit in nicely in this developing area, for example, in the city park or across one of the new canals.

5.1.1.5 *Zone 5*

Delft University of Technology is the oldest and largest public technical university in the Netherlands. TU Delft is a modern university with a rich tradition. The green village located on campus is a playground where all kinds of innovative research is done. The glass truss bridge mentioned earlier is one of the entrances to the green village. Another glass bridge would fit nicely in the research climate that prevails on campus.

5.1.2 Final location

The Wilhelminapark is chosen as the location for the new bridge. The site, the natural surroundings, the accessibility, and the need to improve the condition of the area makes the park very suitable. In this park, two arch bridges are present that were built between 1930-40. The bridges do not satisfy the safety requirements. The bridge located on the east side of the park is demolished to make place for a new optimised cast glass bridge. The bridge
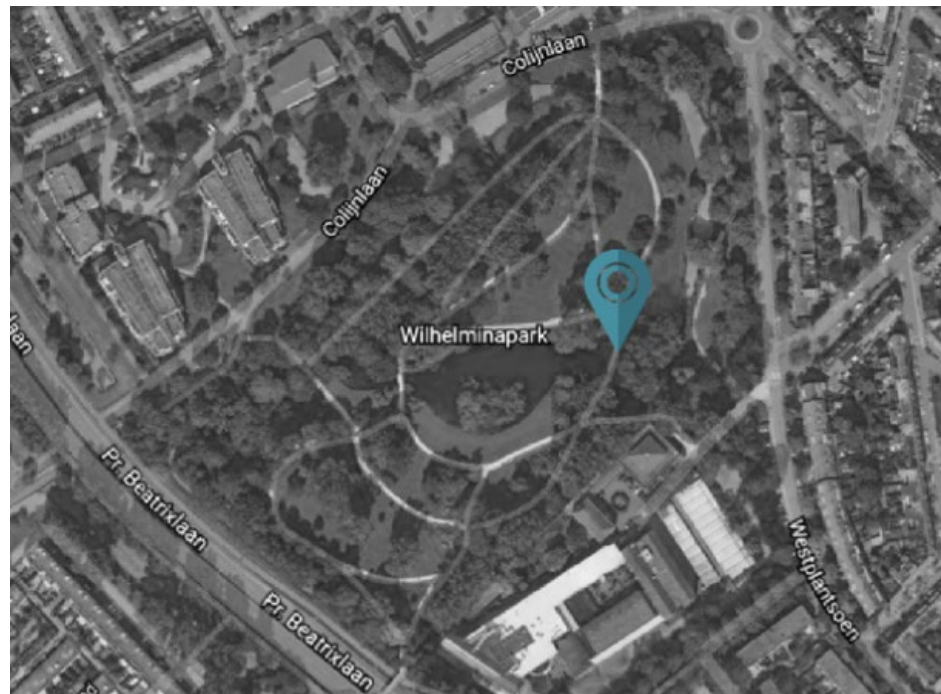
Figure 5.2 Wilhelmina Park with the final location. From (Google, n.d.).

location is indicated with the blue pin in Figure 5.2. A front and side view of the current bridge is given in Figure 5.3.

56

Figure 5.3 Left: Front view of the current bridge. Right: Side view of the current bridge.

5.2 Dimensions of the current bridge

The current bridge has an approximate length of 10 meters and a width of 2 meters at midpoint. When moving towards the sides of the bridge, the footpath widens to 2.5 meters. The bridge spans across a water canal that has a width of 6 meters. In Figure 5.4, an overview is given with the dimensions of the current bridge. The enlarged version can be found in appendix A.
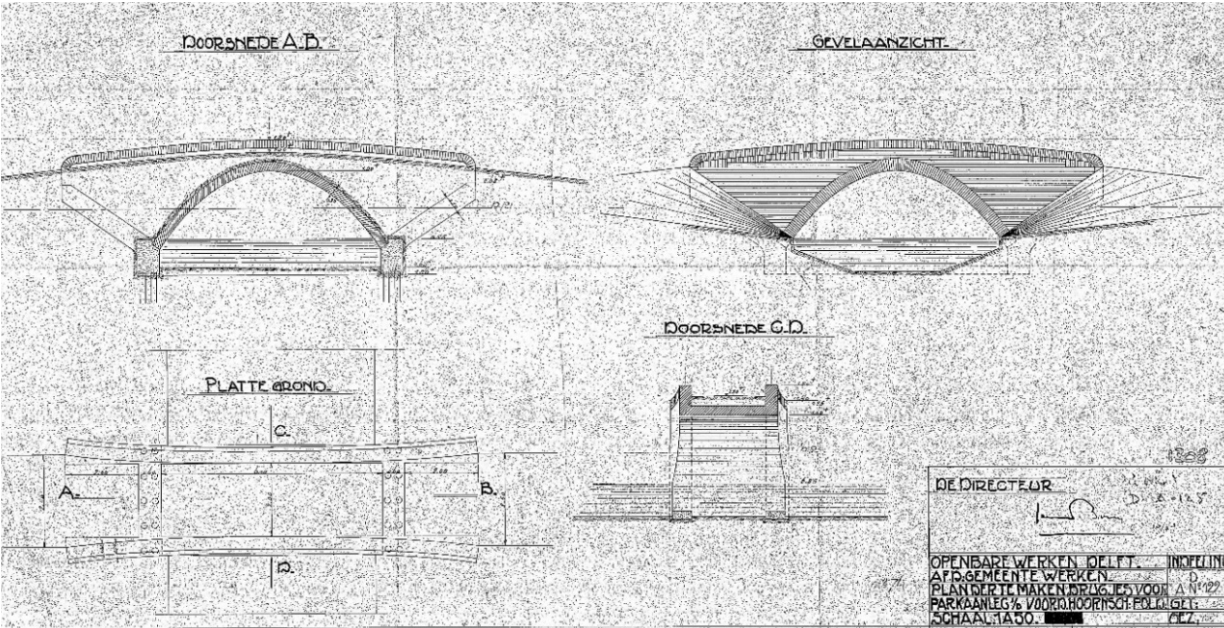
Figure 5.4 Original drawings of the current bridge. The enlarged version can be found in Appendix A. (Gemeente Delft, 2020)

5.3 Conclusions current bridge design

The new bridge should fulfil some basic requirements: the bridge spans over a water canal with a width of 6 meters, the bridge deck has a minimum width of 2 meters, and the maximum height difference between the footpath at the sides of the bridge and the middle of the bridge should not succeed the current height difference of 0.75 meters.

6. Constraints and starting points

Input restrictions have been determined during the literature research to obtain a producible design that is structurally safe. A summary of the constraints and starting points followed from chapters 2, 3, 4, and 5 is given in this chapter.

6.1 Structural

Glass is a brittle material with a low tensile strength compared to its compressive strength. The tensile and compressive stresses should be below the allowable stress. A distinction is made between the float glass top layer made from fully tempered soda lime float glass and the cast glass support structure made from borosilicate glass. The maximum flexural strength for both elements is calculated in Appendix B. The flexural strength for the float glass top layer is equal to $63.5 \ N/mm^2$ and the flexural strength for the cast glass support structure is equal to $4.5 \ N/mm^2$. The constraints on the maximum deflection are also given in Appendix B.

The permanent load, traffic load (only pedestrians), wind load, and temperature load are considered. The bridge is not accessible for vehicles. The design life of the bridge is 50 years with consequence class 3. The information about the loads and load combination factors can be found in Appendix B. The loads that belong to the different load cases used during structural calculation can be found in Table 6.1. The bridge should be able to withstand an unequal vertical settlement of up to 10 mm.

Table 6.1 Load cases.

	Without factor	L.C.1	L.C.2	L.C.3	L.C.4
$g_{,soda \ lime}$	$2460 \ kg/m^3$	$3444 \ kg/m^3$	$3075 \ kg/m^3$	$3075 \ kg/m^3$	$3075 \ kg/m^3$
$g_{,borosilicate}$	$2230 \ kg/m^3$	$3122 \ kg/m^3$	$2788 \ kg/m^3$	$2788 \ kg/m^3$	$2788 \ kg/m^3$
$q_{f,vertical}$	$5 \ kN/m^2$	$3 \ kN/m^2$	$7.5 \ kN/m^2$	$3 \ kN/m^2$	$3 \ kN/m^2$
$q_{f,parallel}$	$0.5 \ kN/m^2$	$0.3 \ kN/m^2$	$0.75 \ kN/m^2$	$0.3 \ kN/m^2$	$0.3 \ kN/m^2$
$Q_{fv;vertical}$	$10 \ kN$	$6 \ kN$	$15 \ kN$	$6 \ kN$	$6 \ kN$
$q_{wind,vertical}$	$\pm0.52 \ kN/m^2$	$\pm0.26 \ kN/m^2$	$\pm0.26 \ kN/m^2$	$\pm0.86 \ kN/m^2$	$\pm0.26 \ kN/m^2$
$q_{wind,perpendicular}$	$1.28 \ kN/m^2$	$0.63 \ kN/m^2$	$0.63 \ kN/m^2$	$2.11 \ kN/m^2$	$0.63 \ kN/m^2$
$q_{wind,parallel}$	$0.51 \ kN/m^2$	$0.25 \ kN/m^2$	$0.25 \ kN/m^2$	$0.84 \ kN/m^2$	$0.25 \ kN/m^2$
ΔT_n	27 ℃	13.37 ℃	13.37 ℃	13.37 ℃	44.55 ℃
ΔT_m	9 ℃	4.46 ℃	4.46 ℃	4.46 ℃	14.85 ℃

6.2 Cast glass

A maximum cross-sectional thickness should be added as a design constraint. With the topology optimisation tool in Ansys, a maximum member size for connecting members can be set. The thickness of the member where multiple members merge can still be slightly higher. The approximate annealing time can be calculated with: $T_{total \ minimum \ time} = 0.0156 \cdot t^2 + 0.139 \cdot t + 0.7266$

The maximum acceptable annealing time is set at one month to reduce the bridge's manufacturing cost. When implementing the constraint of one month in the formula, a maximum thickness of 210 mm is obtained. Additionally, sharp edges, sharp corners, and narrow paths should be removed. Geometric features should be at least 20 mm. The material must be equally distributed, and cross-sections should gradually change.

6.3 Manufacturing

The minimum wall thickness of the mould should be 4 mm. Divisions in the mould should be minimal and in strategic places to avoid seems. The maximum dimensions of a single mould element are 4 x 2 x 1 meter. Interlocking nodes, screw holes, a pouring cup, vent pipes, and risers should be added to the mould design.

6.4 Bridge design

The bridge should span over a water canal that has a width of 6 meters. The bridge deck has a minimum width of 2 meters. The current bridge has a footpath that is 0.75 meters higher at the midpoint of the bridge than at both ends. The new bridge should not succeed the current height difference. An opening should be added of 3.1-meters-wide and 1-meter-high for maintenance to the waterway.

6.5 Transportation and construction

The maximum dimensions of a single cast element must be below 13.6-meters-long, 2.48-meters-wide, and 2.5-meters-high and should not succeed a maximum weight of 3000 kg.

6.6 Conclusion constraints and starting points.

A summary of the constraints and starting points is given in Table 6.2.

Table 6.2 Overview of constraints followed from literature research.

Input values / Constraints	
Structural	
Design life	$50\ years$
Consequence class	3
Maximum flexural strength float glass	$63.5\ N/mm^2$
Maximum flexural strength cast glass	$4.5\ N/mm^2$
Loads (without safety factors)	Traffic case 1: $q_{fk;vertical} = 5\ kN/m^2$ $q_{fk;horizontal} = 0.5\ kN/m^2$ Traffic case 2: $Q_{fvd;vertical} = 10\ kN$ Wind: $q_{wind,horizontal,perpendicual} = 1.28\ kN/m^2$ $q_{wind,horizontal,parallel} = 0.51\ kN/m^2$ $q_{wind,vertical} = \pm 0.52\ kN/m^2$ Temperature: $\Delta T_n = 27\ ℃$ $\Delta T_m = 9\ ℃$
Maximum unequal settlement	$10\ mm$
Cast glass	
Cross sectional constraint	$210\ mm$
Minimum dimensions geometric features	$20\ mm$
Other Constraints	Remove sharp edges, corners, narrow paths, and equally distribute the material
Manufacturing	
Minimum wall thickness mould	$3 - 4\ mm$
Maximum dimension of a mould element	$4\ by\ 2\ by\ 1\ meter$
Other constraints	Minimum mould divisions. Interlocking nodes, screw holes, a pouring cup, vent pipes, and risers should be added.
Bridge design	
Minimum span water canal	$6.0\ meters$
Minimum width bridge deck	$2.0\ meters$
Maximum height difference footpath	$0.75\ meters$
Opening for maintenance to the waterway	$3.1\ meters$ wide $and\ 1\ meter$ high.
Transportation and construction	
Maximum dimension of a cast element	$13.6\ meters$ long, $2.48\ meters$ wide, and $2.5\ meters$ high
Maximum weight of a cast element	$3,000\ kg$

Part 3

Designing a glass bridge

To come a step closer to answering the main question, '*How can a virtually monolithic glass pedestrian bridge be designed and constructed feasibly by using topology optimisation while considering external influences?*' background information was needed on glass, additive manufacturing, topology optimisation, and bridge design. The outcome of the literature research is used during the next phase of this research: the software research and the designing of the bridge.

In this chapter, a comparison is made between different Grasshopper plugins and software packages. First, an overview is given of most topology optimisation (TO) tools. From this, a selection is made of different tools that are further explored. Finally, a recommendation is made that considers the advantages and limitations of the different packages.

7.1 Research methodology

Multiple software packages and plugins were researched to find the most suitable software for designing a cast glass bridge. Based on multiple criteria, a selection was made on which software package and which plugins were tested. The outcome of these tests is displayed in a Trade-off Matrix, from this matrix follows which software performs best.

7.2 Available software

In Table 7.1, an overview is given of different TO software. For every software, when known, the methodology, objective function, and some essential features are given.

Table 7.1 Overview of topology optimisation software.

Software	Methodology	Objective function	Features	Projects
ⅅⅆ SIMULIA Abaqus **ATOM**		Design Responses (Volume, mass, strain, compliance, displacement) Manufacturing Restrictions Symmetry Restrictions Material Sizing Restrictions	Linear and Nonlinear Structural Optimisation / Weighted sum of objectives / Geometric restrictions can be added for additional constraints / Pre- and Post-processing can be done in the software / Design space is recommended to set out in more suited modelling software / Can be combined with Tosca Structure for structural optimisation.	Optimised concrete slab case B (Jipa et al., 2016)
AMEBA	BESO	Compliance based Stress based (Von Mises)	Plug-in for Grasshopper / Cloud Computing / Integrated re-meshing function / Integrated mesh smoothing/ 2D and 3D optimisation.	Jue Chair
Ansys	SIMP Level Set	Compliance based	Material properties, optimisation goals and constraints can be controlled in detail / FEA software is implemented / Geometry modelling and post-processing can be done in ANSYS Spaceclaim / Can be combined with Tosca Structure for structural optimisation.	Glass cast node, column, slab, and shell
Autodesk Fusion 360	SIMP Level Set	Compliance based Stress based	A combination of different Autodesk programs / Cloud Computing / FEA software is included / TO tool uses SIMP / Generative design tool uses Level Set / The software gives multiple outcomes / Can also consider criteria such as cost and production time / Post-processing can be done with AUTODESK ReCap.	JPL's Interplanetary lander and Vertico 3D printed concrete bridge

Karamba 3D	BESO	Compliance based Stress based (Von Mises)	Plug-in for Grasshopper / Can validate structural performance / Different method for beams and shells / If design domain is parametrically defined, then it is possible to explore many different design variations / 2D optimisations	The glass swing
MILLIPEDE	Homogenization SIMP	Compliance based	Plug-in for Grasshopper / Structural analysis for linear elastic structures / Can be used in combination with Galapagos	Optimised concrete slab case A
Altair OPTISTRUCT	SIMP Level Set	Extrusion constraints Pattern repetition Symmetry constraints	Linear and nonlinear analysis / includes a fail-safe topology, multi-material topology, and multi-model optimisation / Also has an easy-to-use generative design platform.	Arup's steel node
PEREGRINE		Layout optimisation	Plug-in for Grasshopper / Layout optimisation technology (not TO) / Suited for problems with significant design freedom / Takes second or minutes instead of hours or days.	
TOPOS	SIMP	Compliance based	Plug-in for Grasshopper / gives faster results in comparison to other TO plugins / principal stresses can be plotted only directly after optimisation (not for re-meshed model)	

During short research into Autodesk Fusion 360, it was found that it is necessary to have cloud credits for generative design. The generative design function, cloud computing function, and included FEA software are useful software features. Due to not having a complete Fusion 360 licence, it is decided not to investigate this software further. The software packages Simulia Abaqus, Ansys, and Altair are all market-leading in finite element modelling. Since they have similar functionalities, only one of these software packages is explored. A full version of Ansys was available. This resulted in the decision to research this package further. Ameba, Karamba 3D, Millipede, Peregrine and tOpos are plug-ins for McNeel Rhinoceros/Grasshopper. When using these programs, it is possible to design the bridge parametrically in a single model.

It is decided that the software package Ansys and Grasshopper's plug-ins, including Ameba, Karamba 3D, Millipede, Peregrine, and tOpos are researched.

7.3 Software research

There are various requirements the software must have. It is favourable when all these requirements can be fulfilled by one software package. The software must use a suitable type of objective function and methodology. Additionally, it needs to have the possibility of optimising in 3D, set out the design space, have a pre and post-process function, and needs to be able to validate the structural performance.

Ameba, Karamba 3D, Millipede, Peregrine and tOpos are plug-ins for McNeel Rhinoceros/Grasshopper. When using these programs, it is possible to design the bridge parametrically in a single model. From the comparison between Grasshopper plugins, Ameba showed to be the most suitable for cast glass. While testing the software, it was found that this plugin is suitable for initial design but cannot compete with more advanced software packages. TO tools in Grasshopper are relatively fast, but when using the plugins to design a cast glass structure, the tools give an unfeasible solution with too large or too small cross-sections. In Table 7.2, the Trade-off Matrix is shown that gives an overview of the functions of the explored optimisation software's. Ansys was found to be more suitable to design the cast glass bridge in, since it has the possibility of implementing a cross-sectional constraint. Further explanation on why the plugins for McNeel Rhinoceros/Grasshopper appeared to be less suitable can be found in Appendix C.

Table 7.2 Trade-off Matrix between topology optimisation software.

	Ameba	Karamba 3D	Millipede	Peregrine	tOpos	Ansys
Licence	orange	orange	orange	orange	green	orange
Setting up design space	green	green	green	green	green	green
Cross-sectional constraints	red	red	red	orange	red	green
2D optimisation	green	green	green	green	green	green
3D optimisation	green	red	green	green	green	green
Post-processing	green	red	orange	orange	orange	orange
Support conditions	orange	green	orange	orange	orange	green
Type of load	orange	orange	green	orange	orange	green
Load cases	orange	orange	orange	orange	orange	green
Computation time	orange	orange	orange	green	orange	green
Structural analysis	red	green	orange	green	orange	green
Cloud computing	green	red	red	red	red	red
Easy parameter study	red	red	red	green	red	orange
Suitable for glass	orange	red	red	red	red	green

7.4 Ansys

The finite element analysis and TO are carried out in Ansys Workbench 2019 R3 mechanical, with the implemented application Ansys Spaceclaim as pre- and post-processor. This software has all the essential capabilities that are necessary for the design of a cast glass bridge.

7.4.1 Meshing

The mesh size and shape is critical to obtain an acceptable result. In the case of using the Level Set Method, all elements should have a tetrahedral shape. When using an extrusion constraint, the elements should have a hexahedral shape. The cross-sectional constraint on the minimum member size requires a mesh density that is 4 times finer than its size, and its maximum member size requires a mesh density that is 4.4 times finer than its size.

7.4.2 Connections

Connections can be modelled in two ways, via contact faces and joints. For each connection, various types can be distinguished.

The FEM calculation is done before performing TO allows for only linear contacts, such as 'bonded' or 'no separation' contacts. The option exists to use non-linear contacts together with topology optimisation in the beta version of Ansys. All contact types can be found in Table 7.3.

Table 7.3 Contact types with characteristics.

	Faces can separate	Sliding
Bonded	No	No
No Separation	No	Yes, $\mu = 0$
Frictionless	Yes	Yes, $\mu = 0$
Frictional	Yes	Yes, if $F_{sliding} > F_{friction}$
Rough	Yes	No, infinite μ

7.4.2.2 *Joints*

Before TO, only fixed joints can be used. The different joint types and their characteristics can be found in Table 7.4.

Table 7.4 Degrees of freedom in joint types.

Joint type	ux	uy	uz	φx	φy	φz
Fixed						
Revolute						✓
Cylindrical			✓			✓
Translational	✓					
Slot	✓			✓	✓	✓
Universal				✓		✓
Spherical				✓	✓	✓
Planar	✓	✓	✓			✓
General	Selection	Selection	Selection	Selection	Selection	Selection
Point on curve	✓					

7.4.3 Support type

In Table 7.5, the different support types are given with a short explanation of when to use the support type.

Table 7.5 Support types.

Fixed support	All degrees of freedom are fixed. The model is not able to move.
Displacement	The selected degrees of freedom can move
Remote displacement	The selected degrees of freedom can move in respect of a remote point
Frictionless support	Constrained in normal directions, used for symmetry conditions when the area is flat
Compression only support	Constraint for compression in the normal direction. This type is used when pins or bolts are used in the structural model but not modelled.
Cylindrical support	Can be constraint in axial, radial or tangential direction.
Elastic support	Used for modelling the elastic behaviour of the ground.

7.4.4 Loads

Thermal loads cannot be used as input for TO. This option is only available in the beta version. Since borosilicate is used for the cast glass structure, the expansion and the shrinkage is relatively small. The supports take up these changes due to temperature fluctuation. The temperature distribution over the topology optimised model is challenging to predict and requires further research. This research is outside the scope of this thesis.

This chapter gives an overview of the steps performed during the design process, including which constraint is used in each step. Second, the 2D shape of the bridge is determined, followed by the 3D shape of the bridge. Third, the different design options of the top layer are presented. Fourth the connection design is further explained. This chapter is finalized with a conclusion on the overall design of the 3D topology optimised bridge.

A TO method that can implement all constraints is yet to be developed. When designing a topology optimised bridge, it is essential to know the constraints that have to be implemented.

8.1 Design process

The design process of a topology optimised glass bridge up to the final post-processing is illustrated in Figure 8.1. The entire process consists out of 16 steps. In Table 8.1, the constraints from the literature research are recapped. Additionally, the step is given for when each constraint is applied.
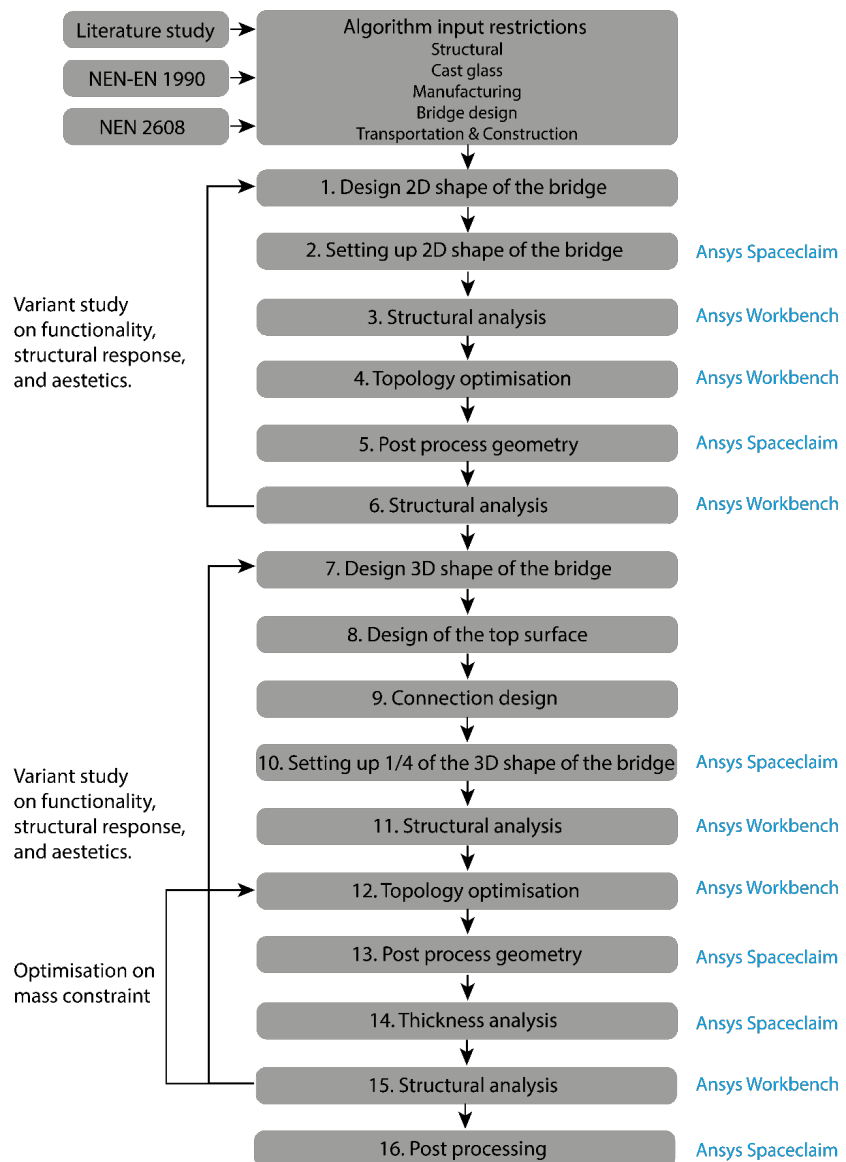
Figure 8.1 Design process cast glass bridge.

Table 8.1 Overview of constraints followed from literature research and in which step of the design process they are applied.

	Input values / Constraints	Step
Structural		
Design life	50 *years*	
Consequence class	3	15
Maximum flexural strength fully tempered float glass	63.5 N/mm^2	8
Maximum flexural strength cast glass	4.5 N/mm^2	3,6,11,15
Loads (without safety factors)	Traffic case 1: $q_{fk;vertical} = 5\ kN/m^2$ $\qquad\qquad\quad q_{fk;horizontal} = 0.5\ kN/m^2$ Traffic case 2: $Q_{fvd;vertical} = 10\ kN$ Wind: $\qquad q_{wind,horizontal,perpendicual} = 1.28\ kN/m^2$ $\qquad\qquad q_{wind,horizontal,parallel} = 0.51\ kN/m^2$ $\qquad\qquad q_{wind,vertical} = \pm0.52\ kN/m^2$ Temperature: $\Delta\boldsymbol{T_n} = 27\ ℃$ $\qquad\qquad\quad \Delta\boldsymbol{T_m} = 9\ ℃$	3,6,11,15
Maximum unequal settlement	10 *mm*	15
Cast glass		
Cross sectional constraint	210 *mm*	12,14
Minimum dimensions geometric features	20 *mm*	16
Other Constraints	Remove sharp edges, corners, narrow paths Distribute material equally	16
Bridge design		
Minimum span water canal	6.0 *meters*	1,7
Minimum width bridge deck	2.0 *meters*	7
Maximum height difference footpath	0.75 *meters*	1,7
Opening for maintenance to the waterway	3.1 *meter* wide *and* 1 *meter* high	1,7
Transportation and construction		
Maximum dimension of a cast element	13.6 *meters* long, 2.48 *meters* wide, and 2.5 *meters* high	7
Maximum weight of a cast element	3000 *kg*	7

8.2 Outline of the glass bridge

There are multiple ways to design the bridge. The first challenge is the overall shape of the bridge. In the first variant study, multiple 2D shapes are optimised to determine which shape is most suited for the bridge's final design. The second challenge is the 3D shape of the bridge and how the bridge is split into multiple segments.

8.2.1 The 2D shape of the bridge

The design of the bridge should be inside the grey area indicated in Figure 8.2. These values followed from the constraints and starting points given in the previous section. A variant study is performed into the shape of the opening for boats and the shape of the top arch. In this section, seven variants are compared on deformation, principal stresses, and functionality. One of the examples is worked out in Figure 8.3. The meshing is done with the Hex dominant method with a free face mesh type of Quad and Tri shapes with a quadratic element order and a maximum element size of 50
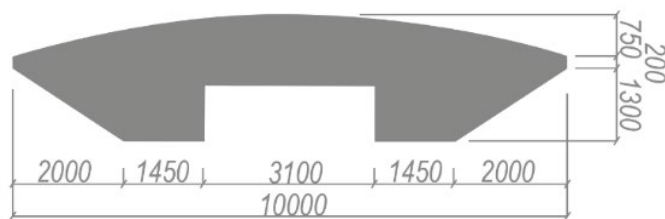
Figure 8.2 Design space of the bridge (dimensions in mm).

66

mm. The 2D shape is fixed on 2 sides with on top a force of 10 kN/m^2. The topology is optimised with a density-based function with a mass constraint dependent on the initial volume. The density-based objective function was chosen because of the fast results. However, it needs more manual post-processing compared to the Level Set method. For design 4, shown in Figure 8.3, the mass constraint was set at 35% to arrive at an end volume of around 0.35 m^3. This constraint was found by trial and error. The geometry was simplified by rebuilding it in Ansys Spaceclaim.
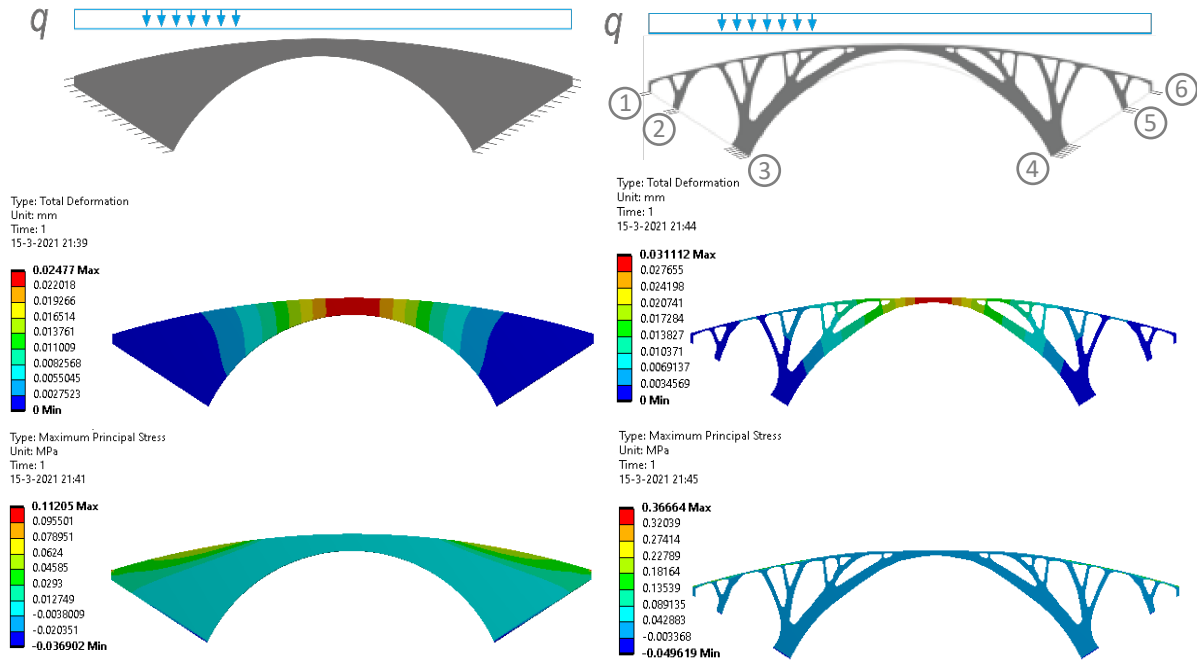
Figure 8.3 An example of 2D optimisation. Left: unoptimised shape with total deflection and principal stresses. Right: optimised shape with reaction forces, deflections, and principal stresses. The reaction forces are given in Table 8.2.

The variant study was done with fixed supports. The bending moments and the support reactions of the optimised bridge are given in Table 8.2. In the following sections, the structure is designed as a simply supported structure.

Table 8.2 Support reactions optimised structure. The support reactions are given from left to right, as indicated in Figure 8.3.

	Support 1	Support 2	Support 3	Support 4	Support 5	Support 6
Fx [kN]	0	0.2	4	-4	-0.2	0
Fz [kN]	0.25	1.5	8	8	1.5	0.25
My [kNm]	-0.07	-0.56	-2.39	2.39	0.56	0.07

The second column of Table 8.3 shows six designs with each a different opening. In the last two columns, values are given about the structural performance for each design. It is decided to change the mass constraint for every design option to obtain a similar end volume. Via this method, the

maximum deformation and principal stresses can be compared for equal amounts of material. The largest deformation and principal stresses are found in design option 5 and 6. Both designs have a relatively high horizontal support force, and both function worse during asymmetric loading than design 1 to 4. In design 1, 2, and 3, columns are placed in the waterway. Something should be added to protect the columns to prevent a collision by a boat. In design 4, no columns are placed in the waterway, thus no protection is needed. Comparing design 4 on deformation and principal stresses with design 1 to 3 shows that deformation and principal stresses are the same order of magnitude. This, together with the better functioning during asymmetric loading, is why the decision was made to develop design 4 further.

Table 8.3 Overview of results of the 2D variant study.

		Start volume [m³]	End volume [m³]	Deformation [mm]	Max principal stress [MPa]
Design 1		1.44	0.33	0.03	**0.20**
Design 2		1.19	0.35	**0.01**	0.24
Design 3		1.20	0.35	**0.01**	0.24
Design 4		0.92	0.37	0.03	0.36
Design 5		0.56	0.36	0.13	0.46
Design 6		0.43	0.32	0.23	0.80

The shape of the arch in design 4 was copied from the existing bridge. When using a material with low tensile strength, an arch shape can be beneficial to use to minimise tensile stresses. Additionally, the shape has a higher resistance against vertical deformation. However, a flat surface is easier to walk on and results in less complex connection details. An additional variant is proposed with a flat top surface, see Figure 8.4. In Table 8.4, the most important values can be found for the design with the flat surface.

In comparison with design 4, design 4.1 has twice the deformation and a similar maximum tensile stress. The deformation is acceptable but might become a problem during asymmetric loading.
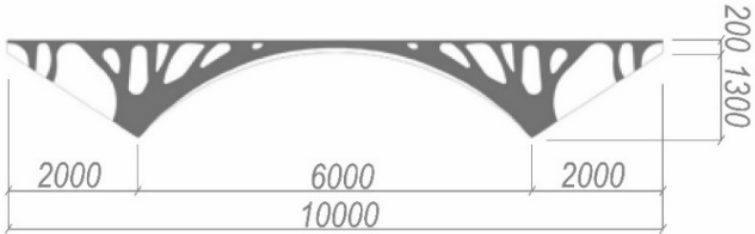
Figure 8.4 Design 4.1 with a flat surface (Dimensions in mm).

Table 8.4 Results of the 2D variant study for design 4.1.

		Initial volume [m³]	End volume [m³]	Deformation [mm]	Max principal stress [MPa]
Design 4.1		0.699	0.389	0.07	0.33

8.2.2 The 3D shape of the bridge

The first and most straightforward option to design a bridge is using a single laminated float glass sheet that spans the waterway. However, this design results in a thick and heavy structure. The goal is to design a bridge with a relatively low weight and with manageable pieces. The bridge is divided into multiple pieces to meet this restriction. Different options are compared in this section. The dimensions of the bridge can be found in Figure 8.5.
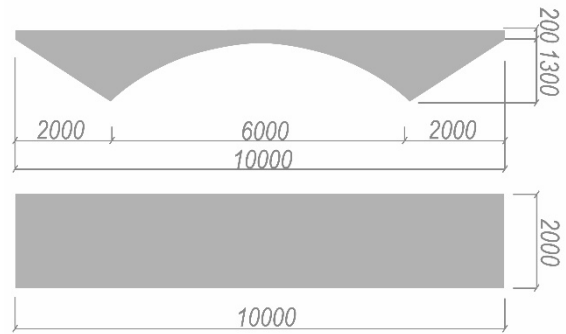
Figure 8.5 Dimension's bridge (dimensions in mm).

8.2.2.1 *Option 1*

An option is to design rib supports for the laminated float glass top layer to increase the structural capacity and reduce the bridge's weight. These ribs could be made from laminated float glass or cast glass, depending on the topology of the ribs. The top layer, in this case, would have to transfer the horizontal traffic and wind loads. The structural scheme of this option can be found in Figure 8.6.
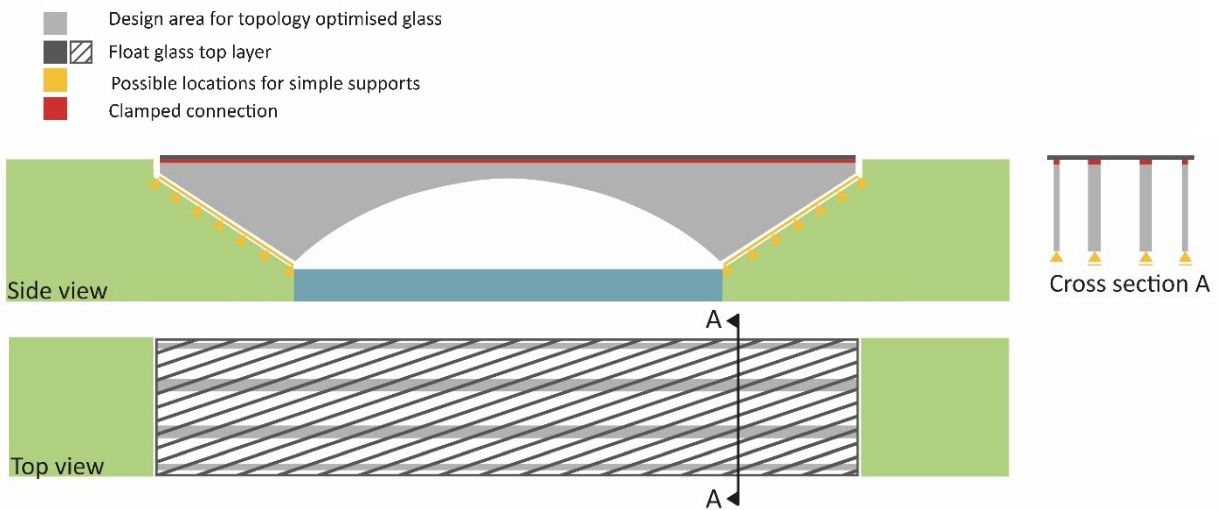
Figure 8.6 Design option 1, float glass top layer with supporting ribs.

Because the bridge is built up out of multiple separate elements, it responds well to local failure since other elements remain intact. When the entire top surface breaks, which is very unlikely, the lack of horizontal support results in the bridge's collapse. It is not advised to use the top layer to stabilize the structure since it would prevent sufficient robustness and not allow for an easy replacement of parts of the bridge. Additionally, it is essential to consider the production method of the glass. When producing a bridge with elements, as indicated in Figure 8.6, it would be easier to produce all the elements from laminated float glass instead of cast glass. Therefore, it is decided to not further research option 1.

When performing TO, the choice can be made to exclude or include certain surfaces from the optimisation process. Instead of transferring the horizontal loads in the top float glass layer, it can be decided to implement this functionality in the cast glass part of the structure. This prevents some of the problems related to option 1. The first option is to exclude the top face of the cast element during optimisation. This results in an unoptimised solid cast glass top layer. The second option is to include the top face of the cast element in the TO process. This results in holes in the top surface in places with low stress. The largest hole is decisive for the thickness of the float glass top surface. The third option is to design a support for the float glass top layer. This can be in the form of a point supported top surface or a line supported top surface. During TO, the location of these point or line supports are excluded. The structural scheme of this option can be found in Figure 8.7 with cross-section A.1 and A.2, depending on the 2D/3D optimisation strategy. To ensure the maximum weight of an element is not exceeded, the bridge is split into 4 elements in the longitudinal direction.
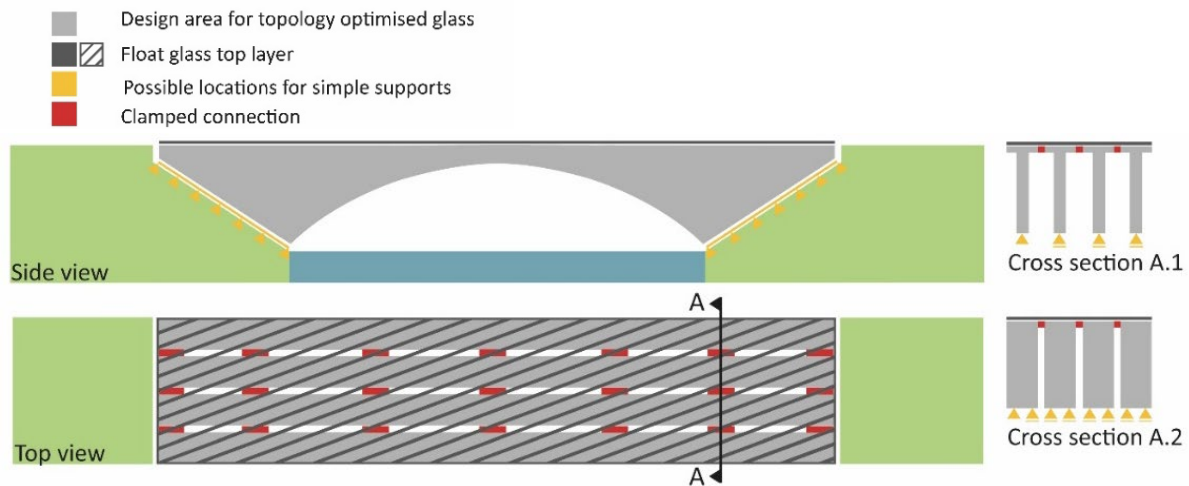
Figure 8.7 Design option 2, cast glass split in the longitudinal direction.

When producing a bridge with elements, as indicated in Figure 8.7 with cross-section A.1, it is important to consider the production method of the glass. In this case, it would be simpler to produce all the elements from laminated float glass compared to using cross-section A.2. To fully utilize the potential of cast glass in combination with sand moulds, option A.2 would be most favourable.

When looking towards the topology of the top surface of the cast glass, there are three options. For the first option, only a sacrificial layer is needed to protect the cast structure. However, for this to work, the top surface of the cast glass should be very flat with high accuracy, or a very thick intermediary layer should be used. The second option will not fully utilize the float glass capacity since it covers the solid parts of the top layer. In the third option, the total capacity of the float glass is used since the maximum allowed distance between supports is implemented in the TO.

There are two sub-options for this option; the point supported top surface and line supported top surface. A point supported top surface results in high peak stresses in the float glass top layer. The float glass has to be supported on many points to make this peak stress acceptable. This is not the case with a line supported top surface. Only the line supported top surface is developed further.

The third option is to split the bridge in the transversal direction. A distinction is made between a bridge split into two parts (see Figure 8.8) and a bridge split into three parts (see Figure 8.9). Both options are split into multiple segments and reconnected with hinges. The elements are connected over the entire width of the bridge. Like the process described for option 2, the top layer can be excluded during the topology optimisation process, the top layer can be included during the topology optimisation process, or the top surface can be designed to support the float glass top layer.

When splitting the bridge into two elements, the weight of a single element may exceed the maximum weight set for an element. The bridge should be divided into more segments to make sure this does not happen. If these elements fail, it will most likely result in the failure of the entire bridge, apart from the failure of the float glass top layer. Additionally, since hinges connect the elements, it is simpler to build in tolerances, deal with uneven settlements, and allow for expansion and shrinkage.

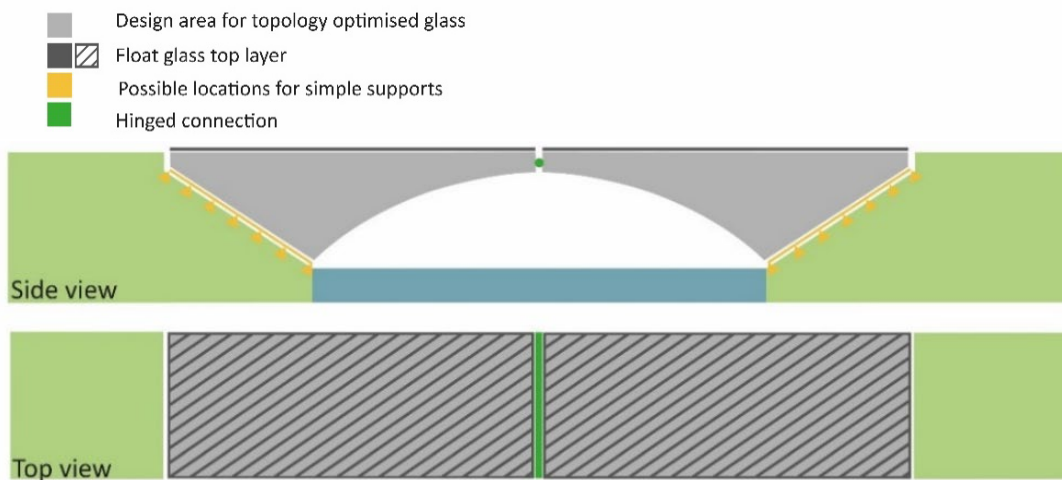*Figure 8.8 Design option 3.1, cast glass split once in the transversal direction.*
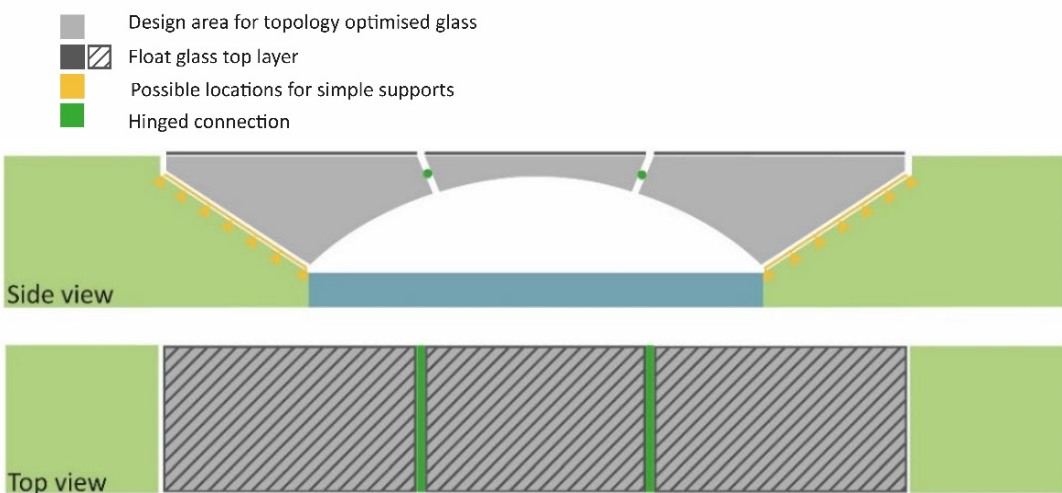
Figure 8.9 Design option 3.2, cast glass split twice in the transversal direction.

8.2.2.4 *Option 4*

For this option, it was decided to fuse option 2 and option 3.2. Option 2 results in a relatively dense cast glass top surface since it is split into 4 elements. Additionally, it responds worse during uneven settlement. The fabrication process is also challenging since a long oven is necessary. Option 3.2 results in the outer elements being too heavy for construction. For option 4, the structure is divided into 5 elements, as shown in Figure 8.10.

Figure 8.10 Design option 4, cast glass split twice in transversal direction, and outer pieces are split in the longitudinal direction.

8.2.2.5 *Conclusion*

In Table 8.5, the Trade-off Matrix is given of the different design options. Option 4 performs best. After the topology optimisation of design 4, it was found that the design had to be refined on supports and connections. This was done to ensure proper structural behaviour during the unequal settlement of the supports and for increased performance during asymmetric loading. During the first refinement, the clamped connections were removed, and the simple supports' location was changed. The structural scheme of the first refinement can be found in Figure 8.11. From the structural calculations done after optimisation on design option 4, refinement 1, followed that when the outer support settles 5 mm more than the inner support, the bridge does not stay connected to the outer supports. When it is the other way around, where the inner support settles 5 mm more than the outer support, the stresses in the cast element would be too high. The structural scheme of the final refinement can be found in Figure 8.12. The outer support areas are removed from the possible support locations in this refinement.

Table 8.5 Trade-off Matrix for the different design options.

	Option 1	Option 2.1	Option 2.2	Option 3.1	Option 3.2	Option 4
Logical to produce parts in cast glass						
How will it respond towards uneven settlement?						
Would it be easy to build in enough tolerance?						
Resistance to asymmetric loads						
Robustness of the bridge						
Fabrication process						
Construction process						
Easy to replace float glass						
Easy to replace cast glass						

72
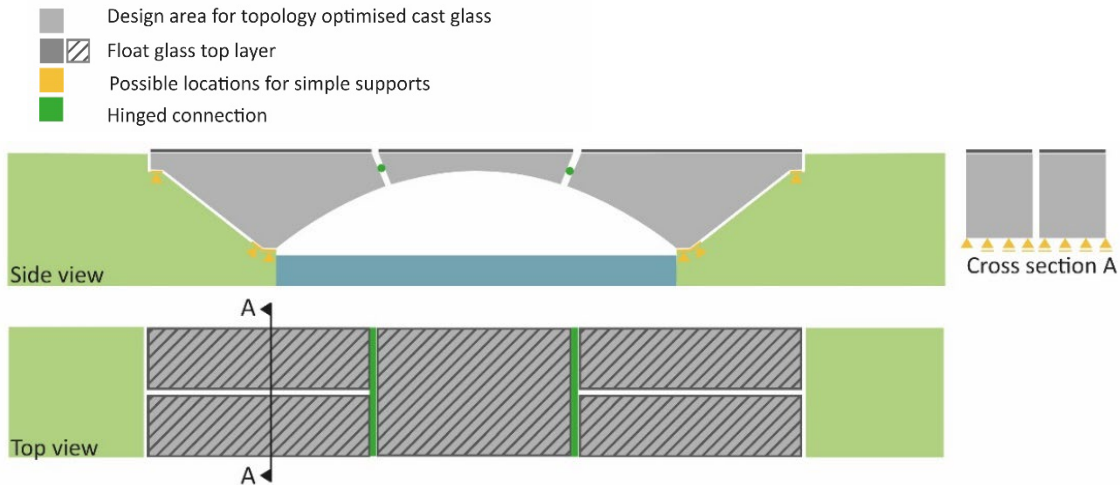
Figure 8.11 Design option 4, refinement 1, cast glass split twice in transversal direction and outer pieces are split in the longitudinal direction.

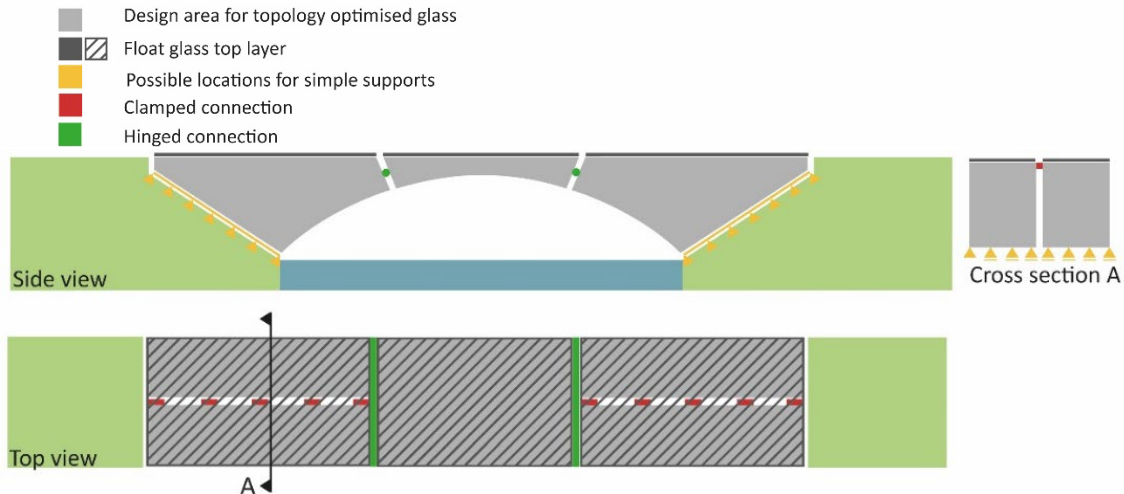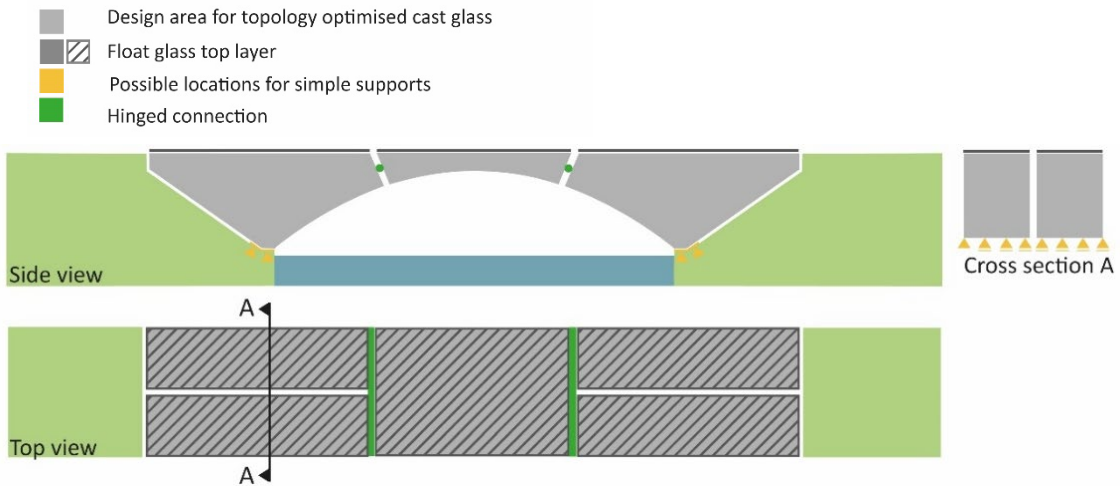*Figure 8.12 Design option 4, refinement 2, cast glass split twice in transversal direction and outer pieces are split in the longitudinal direction.*

8.3 Design of the cast glass top surface

There are three different support types for the top float glass layer and how this support can be implemented in the topology optimisation process. The first one is to exclude the top face of the cast glass element during the topology optimisation process, the second option is to include the top face in the topology optimisation process, and the

Figure 8.13 three options for the design of the top surface of the cast glass element.

third option is to design a support for the top surface and exclude this support area during topology optimisation. These three options can be found in Figure 8.13, where the surfaces in green are excluded during the topology optimisation, and the faces in grey are included.

73

8.3.1 Exclusion of top surface

The first option is to exclude the top surface during topology optimisation. A result with this exclusion can be found in Figure 8.14. For this option, only a sacrificial layer is needed to protect the cast structure. However, for this to work, the top surface of the cast glass should be flat with high accuracy, or a thick intermediary layer should be used.

Optimisation type: Level Set
Excluded: Top surface
Mesh type: Tetrahedral
Element order: Quadratic
Maximum mesh element size: 50 mm
Mesh elements: 69187
Maximum thickness member: 200 mm
Percent to retain: 30%
Optimisation time: 4 h 38 m
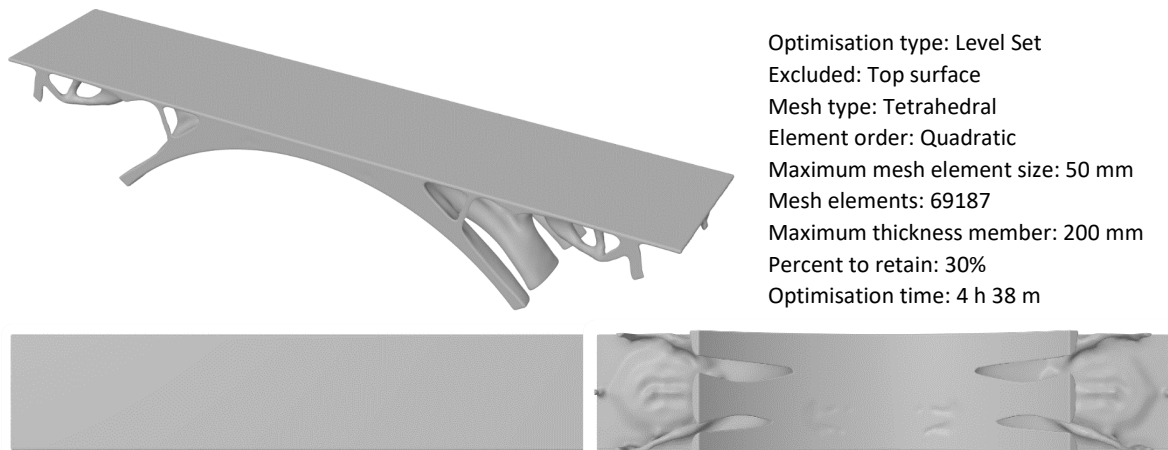
Figure 8.14 3D optimised bridge of design 4 with the exclusion of top surface.

8.3.2 Inclusion top surface

The second option is to include the top surface in the topology optimisation process. This results in holes in the top layer. The largest hole determines the thickness of the top surface. In Figure 8.15, the result is given of the topology optimisation process. The top surface is included in the optimisation process. Because of this, holes can appear on the top surface. This option will not fully utilize the capacity of the float glass since it also covers the solid parts of the top layer. Unfortunately, there is no option to implement a maximum or minimum span of these holes. In the example given in Figure 8.15, only four openings appear in the optimised shape. Additionally, on both ends, a rounded shape is found. A different solution is desired, which achieves a top surface with less casted glass and a more optimal use of the float glass.

Optimisation type: Level Set
Excluded: None
Mesh type: Tetrahedral
Element order: Quadratic
Maximum mesh element size: 50 mm
Mesh elements: 69187
Maximum thickness member: 200 mm
Percent to retain: 30%
Optimisation time: 2 h 24 m

Figure 8.15 3D optimised bridge of design 4 without exclusion of surfaces.

In the third option, the total capacity of the float glass is used since the maximum allowed distance between supports is implemented in the topology optimisation. There are two sub-options for this option; the point supported top surface and line supported top surface. A point supported top surface results in high peak stresses in the float glass top layer. The float glass must be supported on many points or have an increased thickness, to ensure these peak stresses are acceptable. This is not the case with a line supported top surface. Figure 8.16 shows a design that has an implemented grid pattern on the top surface.

Optimisation type: Level set
Excluded: Top surface
Mesh type: Tetrahedral
Element order: Quadratic
Maximum mesh element size: 40 mm
Mesh elements: 481484
Maximum thickness member: 180 mm
Percent to retain: 30-35%
Optimisation time: 12 h 3 m
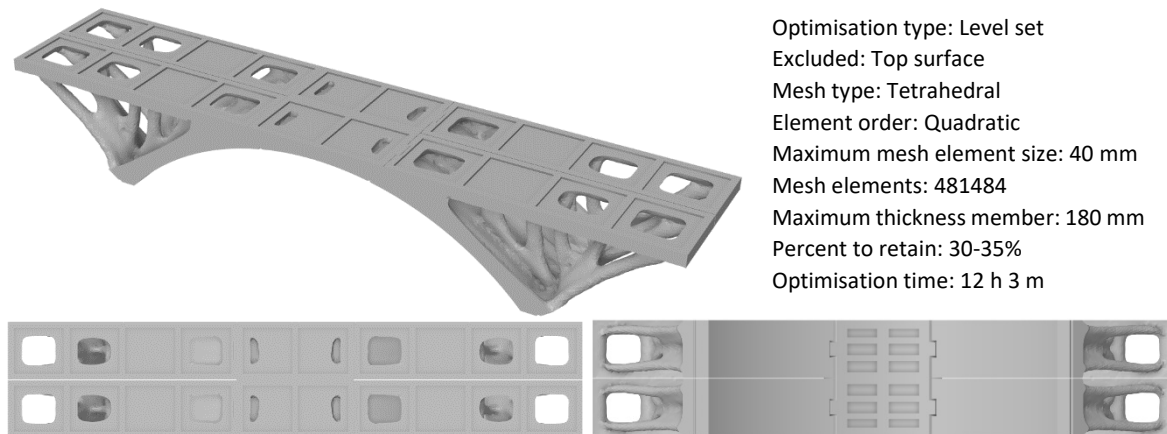
Figure 8.16 3D optimised bridge of design 4.1 with the designed top surface.

The top layer consists of multiple layers of fully tempered float glass, with an additional sacrificial layer. When stacking glass on glass, high peak stresses could occur because of the geometrical imperfections of the glass. An interlayer should be used that is resilient enough to counteract the geometrical imperfections to overcome this problem. SGX (SentryGlass XTRA) is used as interlayer material between the glass panes. This type of interlayer has a good optical quality, open edge performance, post breakage performance, and resistance against delamination. According to NEN 2608:2014, the 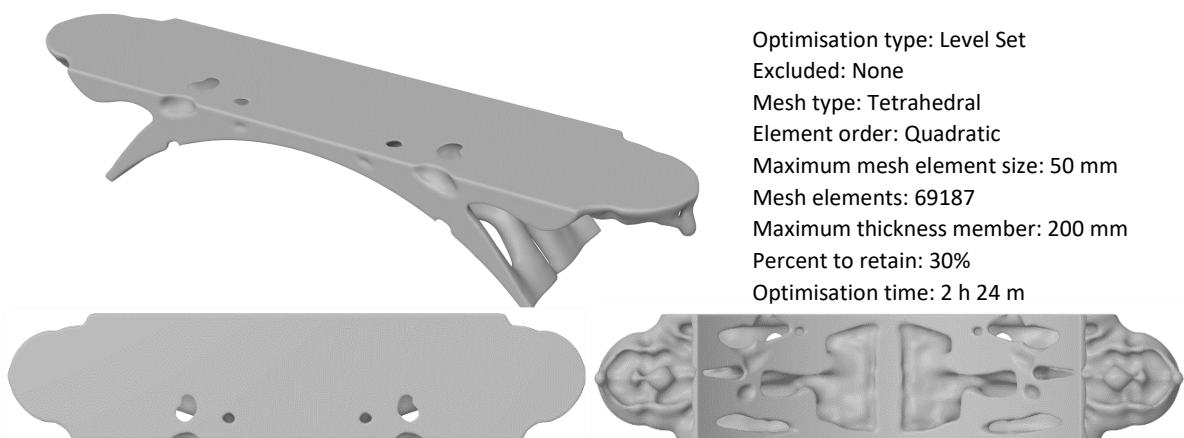temperature should be taken at 17 °C during loading. Since the datasheet does not provide this value, the young's modulus for 20 °C is used. The values given in Table 8.6 are for SGX at a temperature of 20 °C for a load duration of 50 years (Curbell Plastics, 2021). A thickness of 1.52 mm is taken for these interlayers to prevent failure due to geometrical imperfections.

The structural check is done in SJ MEPLA. The material properties for the fully tempered float glass top layer made from soda-lime glass and the SGX interlayer are given in Table 8.6. The top surface is supported by a grid structure of 1 by 1 meter. This results in four glass panes of 4 by 1 meter and one glass pane of 2 by 2 meter. This is simplified as a 1- by 1-meter surface with a maximum mesh size of 25 mm. The pane is schematized as two edges with simple supports (orange in Figure 8.17) and two edges as simple supports with additional horizontal constraints (red in Figure 8.17). Only deadweight, traffic load, and wind load are considered since the software cannot consider a temperature difference between the top and bottom pane. Further research into temperature differences should be done. This is beyond the scope of this thesis.
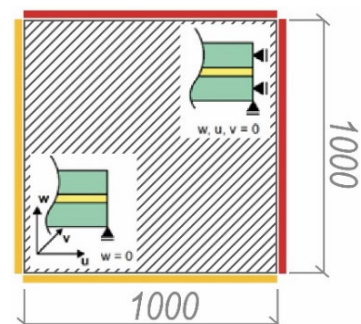
Figure 8.17 Structural scheme of the float glass top layer.

Table 8.6 Material properties SJ MEPLA.

	Unit	Soda-lime glass	SGX interlayer
Young's modulus	MPa	69000	14.9
Shear modulus	MPa	-	5.0
Poisson's ratio	-	0.23	0.48
Thermal expansion coefficient	$10^{-6}\ K^{-1}$	8.5	100
Mass density	kg/m^3	2460	950
Tensile strength	MPa	63.5	42.9

The glass is built up out of 2 tempered panes of 15 mm thick with an SGX interlayer of 1.52. In addition, a sacrificial layer is added on top with a thickness of 6 mm. For a four-sided line supported float glass top pane, the maximum allowable deflection is equal to $u_{dia,max} = 21.8\ mm$ as calculated in Appendix B.1.3. The maximum observed deflection, as shown in Table 8.7, is $1.65\ mm$ which is far below the acceptable deflection.

Table 8.7 Loads in SLS with the maximum deflection calculated in SJ MEPLA.

	Input			Results
	Deadweight	Traffic	Wind	Deflection
L.C.1	$g_{k;toplayer} = 0.89\ kN/m^2$	$q_{fk;ver} = 5\ kN/m^2$ $q_{fk;hor} = 0.5\ kN/m^2$	$q_{wind,ver} = \pm0.52\ kN/m^2$ $q_{wind,hor} = 0.51\ kN/m^2$	$0.33\ mm$
L.C.2	$g_{k;toplayer} = 0.89\ kN/m^2$	$Q_{fvd;ver} = 10\ kN$	$q_{wind,ver} = \pm0.52\ kN/m^2$ $q_{wind,hor} = 0.51\ kN/m^2$	$1.65\ mm$

The maximum flexural strength fully tempered float glass can withstand is equal to $f_{mt;u;d} = 63.5\ MPa$. In total, 5 load cases were tested, as shown in Table 8.8. Load case 4 gives the highest maximum tensile stress, which is equal to $45.5\ MPa$. It is assumed that with a rest capacity of $18\ MPa$ the glass will have enough capacity to take up the temperature load.

Table 8.8 Loads in ULS with the maximum tensile stresses calculated in SJ MEPLA.

	Input			Results
	Deadweight	Traffic	Wind	Maximum tensile stress
L.C.1	$g_{d;toplayer} = 1.11kN/m^2$	$q_{fd;ver} = 7.5\ kN/m^2$ $q_{fd;hor} = 0.75\ kN/m^2$	$q_{wind;ver} = \pm0.26\ kN/m^2$ $q_{wind;hor} = 0.25\ kN/m^2$	$3.55 MPa$
L.C.2	$g_{d;toplayer} = 1.11kN/m^2$	$q_{fd;ver} = 3\ kN/m^2$ $q_{fd;hor} = 0.3\ kN/m^2$	$q_{wind;ver} = \pm0.86\ kN/m^2$ $q_{wind;hor} = 0.84\ kN/m^2$	$1.99\ MPa$
L.C.3	$g_{d;toplayer} = 1.24kN/m^2$	$Q_{fvd;ver} = 6\ kN$	$q_{wind;ver} = \pm0.26\ kN/m^2$ $q_{wind;hor} = 0.25\ kN/m^2$	$18.46\ MPa$
L.C.4	$g_{d;toplayer} = 1.11kN/m^2$	$Q_{fvd;ver} = 15\ kN$	$q_{wind;ver} = \pm0.26\ kN/m^2$ $q_{wind;hor} = 0.25\ kN/m^2$	$45.5\ MPa$
L.C.5	$g_{d;toplayer} = 1.11kN/m^2$	$Q_{fvd;ver} = 6\ kN$	$q_{wind;ver} = \pm0.86\ kN/m^2$ $q_{wind;hor} = 0.84\ kN/m^2$	$18.65\ MPa$

8.4 Connections

The connections of a glass bridge are a critical aspect of the design. The connections have to be designed so that the deformation and maximum principal stresses are in an acceptable range. Additionally, the connections should be designed for a safe and easy assembly. Connections are designed that use little extra material to keep the bridge as transparent as possible. The cast glass pieces are locked in place by weight and friction, with, between the elements, an interlayer that can tolerate deviations formed during the casting and annealing.

From (Oikonomopoulou, 2019) the most important design criteria are taken to design the connections of this bridge. An interlocking design should fulfil the following criteria:
- Restriction of movement in the transverse and longitudinal direction.
- It is optimised on shear performance.
- The interlocking system should ensure the self-alignment of the elements.

8.4.1 Keystone connection

The middle part of the structure functions as a keystone that locks the four other parts in position by gravity. The connection between the keystone and outer parts is hinged. This is done to make sure the structure can account for settlement. The maximum horizontal and vertical displacement of the support is 10 mm. The expected behaviour can be seen in Figure 8.18. From multiple structural calculations in Ansys followed that the most detrimental case is during unequal settlement that is 10 mm in the horizontal direction and 10 mm in the vertical direction.
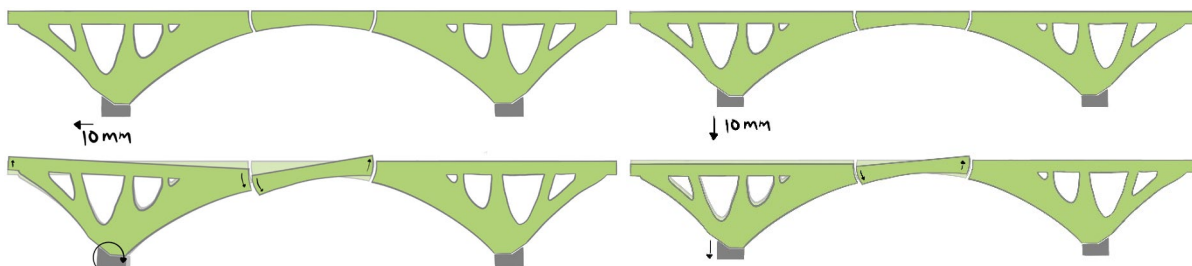
Figure 8.18 Magnified behaviour during unequal settlement. With on the left horizontal settlement and on the right vertical settlement.

As can be seen from the behaviour in Figure 8.18, the keystone rotates more than the outer parts. This could result in a height difference between the elements. This difference should be small to ensure the bridge is comfortable to walk on. As a starting point, the maximum height difference is taken as 5 mm. In total, four iterations were done to come to the result. In these iterations, the radius of the connection was varied. In Figure 8.19, the setup of the structural analysis is given. A symmetrically distributed load is exerted on the top surface. It was found that during settlement, an asymmetric load does not give a result that deviates noticeably from the symmetric load. The left side is supported by a remote displacement that is moved 10 mm in the horizontal direction, 10 mm in the vertical direction, and 0 mm in plane and can rotate around the in plane axis. An additional constraint is added such that the outer elements cannot move in plane. The results are given in Figure 8.20 and Table 8.9. For the final design, a radius of 275 mm is chosen.
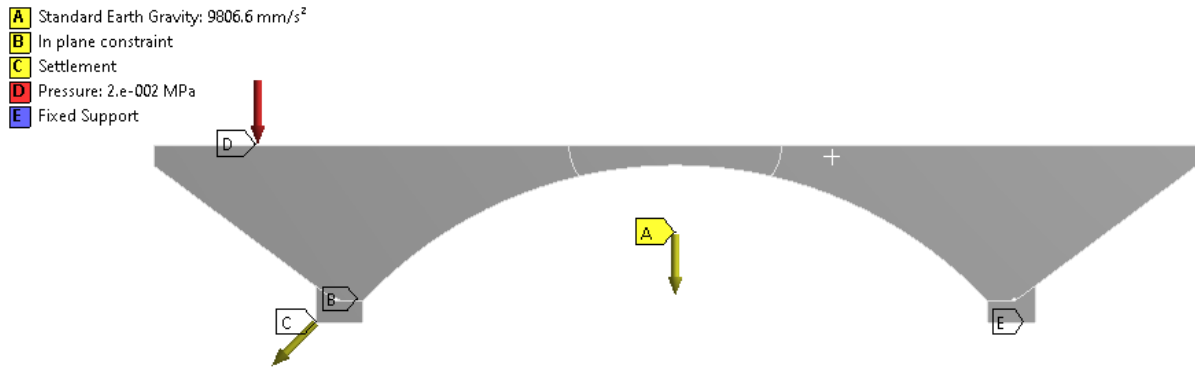
Figure 8.19 Set up structural analysis cast-cast connection.

Table 8.9 Summary of results from structural analysis of the connection between the keystone and the outer parts.

	Unit	Design 1	Design 2	Design 3	Design 4
Radius	mm	500	400	300	275
Maximum principal stress	MPa	0.9	1.40	2.27	2.35
Maximum deformation	mm	+ 13.8 - 41.1	+ 8.7 - 35.4	+ 5.8 - 31.9	+ 4.9 - 30.8
Maximum height difference between parts	mm	- 17 + 14	- 10 + 8	- 6 + 6	- 5 + 5
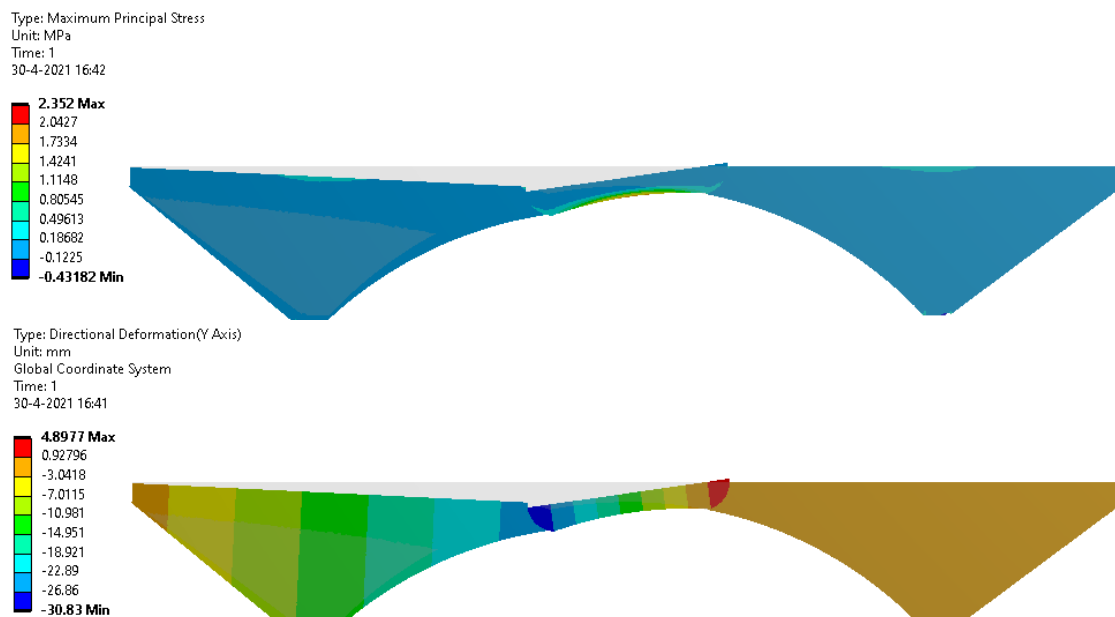
Figure 8.20 Overview of maximum principal stress and directional deformation of design 4.

The keystone should have a system that guides it to the correct position to ensure that assembly is simple. Two possible geometries are researched, a monoclastic and a synclastic surface shape. When using a synclastic connection, the surface has a dome shape. This shape increases the computational time during structural calculations and results in a more complex post-processing process of the casted element. For the final design, the monoclastic surface is used. Four protrusions are added to the keystone, and one notch is added to every outer element. This way, the pieces fit together like a puzzle. The detail is given in Figure 8.21. For the connection between the keystone and outer parts, a polyurethane interlayer is used with a thickness of 3 mm.
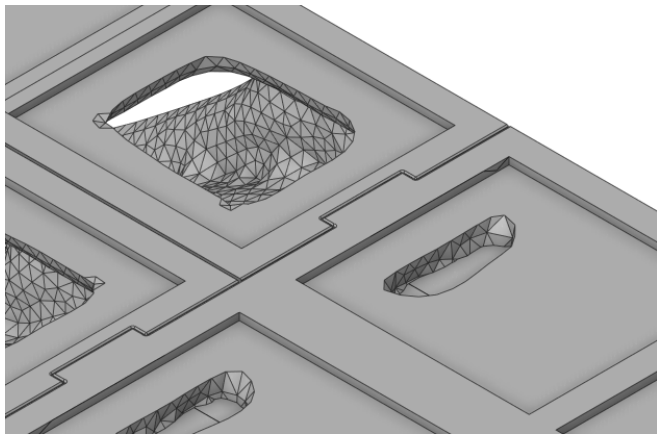
3D view connection
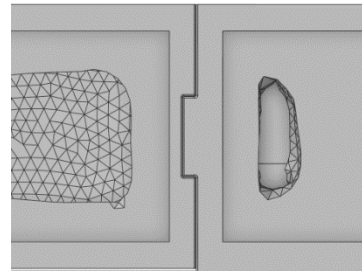
Top view connection
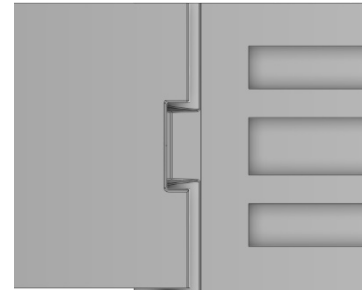
Bottom view connection
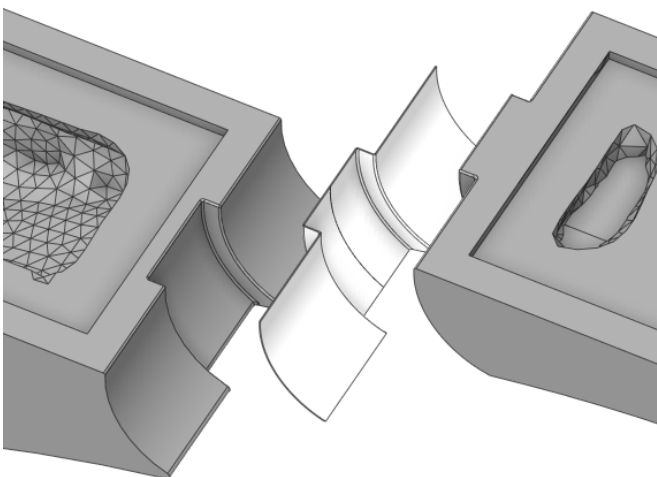
3D view exploded connection
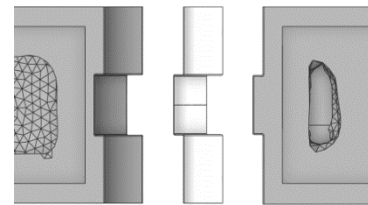
Top view exploded connection
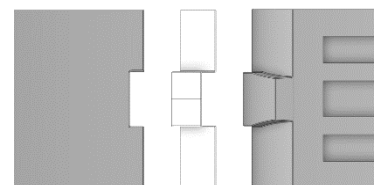
Bottom view exploded connection

Figure 8.21 Connection between keystone and outer element.

8.4.2 Support connection

The connection between the outer element and the foundation is given in Figure 8.22. A simplified version of the foundation is given. However, the connection between the cast glass and concrete functions in a similar way. For the connection between the outer parts and foundation, a polyurethane interlayer is used with a thickness of 3 mm. In the corner of the element, the material is removed to prevent peak stresses.

3D view connection

Side view connection

3D view exploded connection

Side view exploded connection
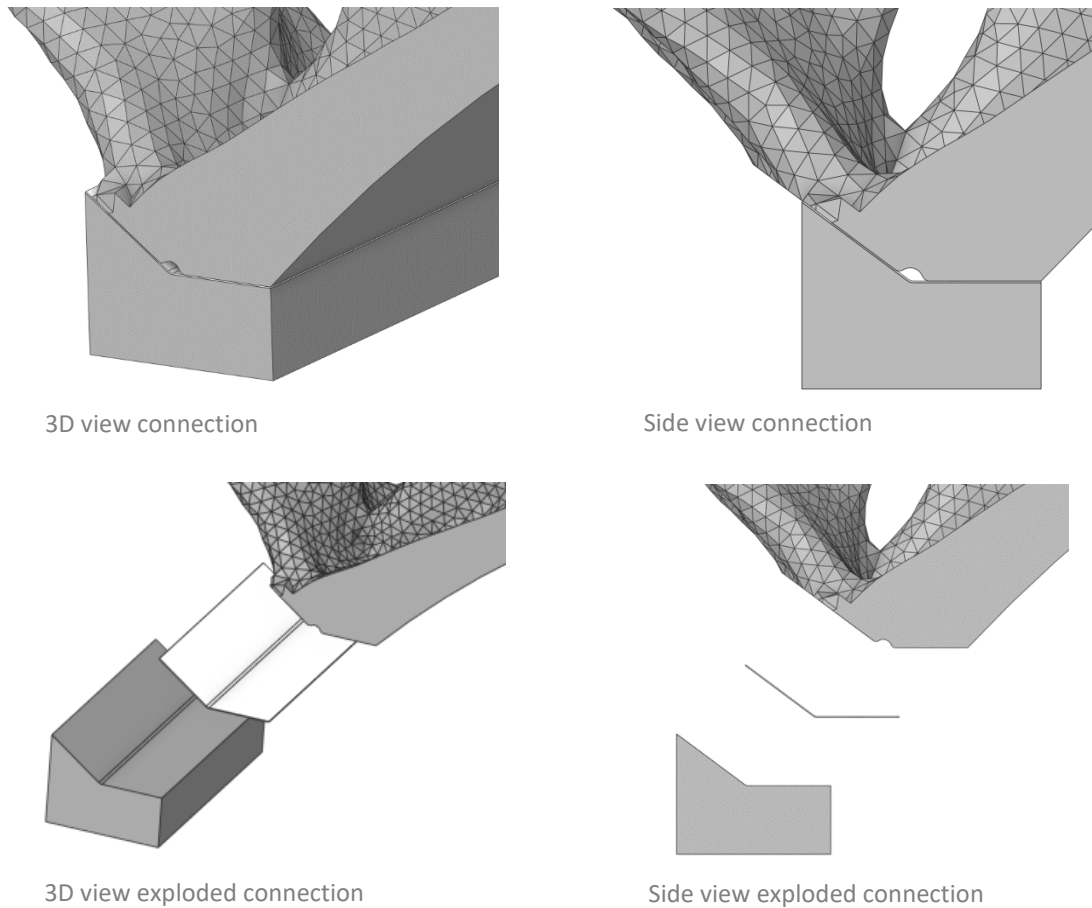
Figure 8.22 Connection between the outer element and foundation.

8.5 Conclusion overall shape

The final design given in Figure 8.23 is most suited to produce in cast glass. Using the right connections and dividing the bridge into manageable pieces ensures that the bridge can abide uneven settlement and asymmetric loads. With this design, enough tolerance and robustness can be built into the design. The fabrication and construction process is also more straightforward than with the other design options, and it is simpler to replace the float glass top layer and cast glass elements in case of a damaged element.
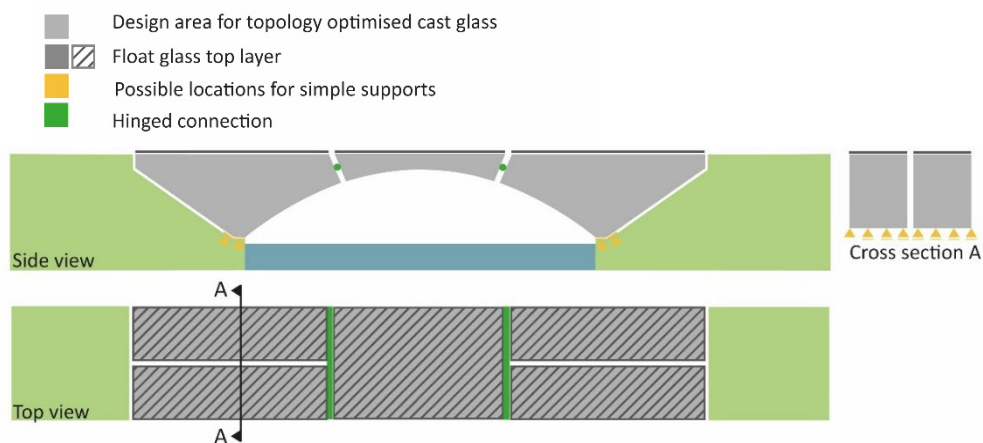
Figure 8.23 Structural scheme of final bridge design.

9. Case study

An HP Zbook with an Intel(R) Core (TM) i7-4700MQ CPU @2.40GHz and an 8.00 GB installed RAM was used for the optimisation. When making structural calculations with a finite element program or performing a topology optimisation, the capacity of the computer was a limiting factor.

9.1 Input materials

In Table 9.1, the material properties can be found that are used in the finite element analysis. The float glass top layer is made from heat strengthened soda lime float glass; the cast glass support structure is made from borosilicate glass; the transition between the cast glass; and the foundation is simplified as stiff material.

Table 9.1 Material properties for soda-lime glass, borosilicate glass, and stiff material.

	Unit	Soda-lime glass	Borosilicate glass	Stiff material
Young's modulus	MPa	69000	63000	1000000
Poisson's ratio	-	0.23	0.2	0.2
Thermal expansion coefficient	10^{-6} K^{-1}	8.5	3.4	0
Mass density	kg/m^3	2460	2230	0.01
Tensile Ultimate Strength	MPa	63.5	4.5	-

For the non-linear analysis, polyurethane is used as an intermediary layer between the cast components and between the cast components and the stiff material. The Mooney-Rivlin 2 Parameter is used to model the hyperplastic properties of polyurethane. The material properties and used constants are given in Table 9.2.

Table 9.2 Material properties for polyurethane, From (Granta Design TEAM, 2019).

	Unit	polyurethane
Mass density	kg/m^3	1200
Material constant C10	MPa	0.67
Material constant C01	MPa	0.168
Incompressibility parameter D1	1/MPa	0.0012
Tensile Ultimate Strength	MPa	45.17

The final bridge consists out of three primary materials, borosilicate glass, soda-lime glass and polyurethane.

9.2 Structural analysis before topology optimisation

A balance must be found during topology optimisation between the mesh size and the time an optimisation takes. There are various restrictions on meshing, connections, joints, support types, and loads when using Ansys.

9.2.1 Input geometry

In Figure 9.1, the input geometry is given. The green elements are made from borosilicate glass, and the grey element is made from a stiff material. Only one-fourth of the bridge is optimised to reduce the total size of the model. The total volume of the element is equal to 3.6 m³, which is equivalent to approximately 8000 kg.

The Level Set optimisation is used. This method needs a tetrahedral mesh with a mesh size at least 4.4 times finer than the maximum member size. The maximum member size is set at 180 mm, which means the mesh size should be 40 mm. Multiple branches can merge during topology optimisation resulting in larger member sizes. With a maximum member size of 180 mm implemented in the topology optimisation process, elements are obtained with maximum member sizes of 210 mm.

Figure 9.1 Input geometry with in green the cast glass elements and in grey the elements made from stiff material.

9.2.2 Supports

A fixed support is used to model the interaction between the foundation and soil, and frictionless support is used to mimic symmetry. The blue areas in Figure 9.2 are the frictionless supports, and the yellow area is the fixed support.

Figure 9.2 Support of the bridge with in blue the frictionless support and in yellow the fixed support.

9.2.3 Interfaces

The connection 'no separation' is used to mimic the behaviour of the intermediary layer in between the cast glass elements. This contact type is free to slide but unable to separate. The weight of the bridge is relatively high and ensures the contact areas to be under compression. Because of the lack of friction between the elements, only normal force can be transferred. This is beneficial in the final model since it results in a topology that is optimised on transferring normal forces between the cast glass components and between the cast glass and the supports.

9.2.4 Loads

A distinction is made between four loads. These are loads due to dead weight, a vertical load, a horizontal load perpendicular to the structure, and a horizontal load parallel to the structure. The vertical load is built up out of the dead weight of the float glass top layer, the vertical wind load, and the traffic load. It is assumed that the 10 kN point load can only occur once every square meter. This means the point load is the most determining vertical load for traffic. In the simplified model, the point load is schematized as 10 kN/m². It is decided only to consider the vertical loads since they are significantly higher than the horizontal loads. The loads used in the model are given in Table 9.3. For every load case, the highest load is put into the topology optimisation process.

The maximum length of a single borosilicate cast element is approximately 4 meters. With an expansion coefficient of $3.4 \cdot 10^{-6}$ the maximum expansion for a temperature difference of 60 ℃ is equal to $0.81\ mm$. During the design of the supports and connections, this value is considered. But during topology optimisation and structural analysis, the temperature is not considered.
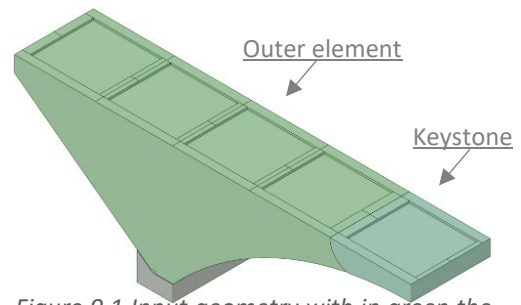
82
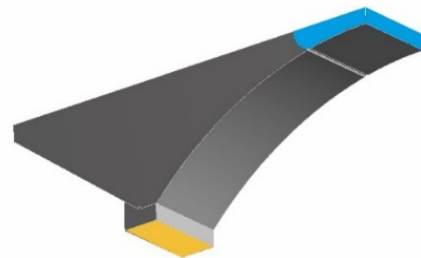
Table 9.3 Loads used for topology optimisation.

	Worst case scenario
$g_{d,soda\ lime}$	$1.24\ kN/m^2$
$g_{d,borosilicate}$	$3122\ kg/m^3$
$q_{fd,vertical}$	$15\ kN/m^2$
$q_{d,wind,vertical}$	$0.86\ kN/m^2$

The load is inserted onto the model on the grid structure (surfaces with a colour gradient in Figure 9.3). It is decided not to model the float glass top layer because this increases the size and complexity of the model. The load is applied linear with at midspan of every gridline the highest load. In Figure 9.3, the highest loads are given in red and the lowest loads in blue. This way, the load transfer from the float glass layer to the cast glass grid structure is mimicked. The loads from Table 9.3 are multiplied by 5 to obtain the load at the midspan of each section. An example for the deadweight of the float glass layer + wind load applied along with line A as shown in Figure 9.3, is given in Figure 9.4. The difference

Figure 9.3 Schematisation of the vertical load on a grid structure.

between the model's results with float glass and the model with the simplified grid load is around 5%, where the simplified grid model gives higher deformations and higher stresses.
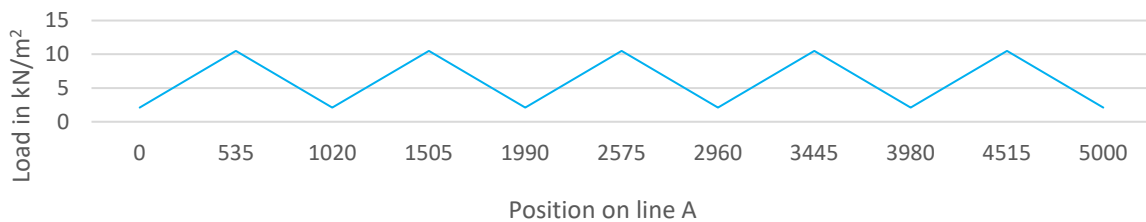
Figure 9.4 Load pattern along with line A in Figure 9.3 for deadweight float glass top layer + wind load.

Topology optimisation is sensitive to the load that is applied before optimisation. It is crucial to make a distinction between the different loads, load cases and load combinations. Since only one-fourth of the bridge is optimised, the load combinations that can be considered are limited. In Figure 9.5, seven load combinations are given. All these load cases are implemented in the topology optimisation model.

After implementing the different load cases, the topology optimisation was carried out. This was followed by a structural analysis with a maximum point load of 15 kN. It was found that the structure could not carry this point load. Which meant a different approach had to be found for this load. This point load could be anywhere on the top surface of the bridge. For the top float glass layer, the most determining location is in the centre of the pane. Since this pane is edge supported, the most determining location for the cast glass is on the grid. The highest peak stress with this load occurs at the midspan of the bridge. Since it is impossible to use a stress constraint in the model, a new strategy must be found. A simple calculation was done to ensure the cast structure can withstand a point load of 15 kN in all places. In this calculation, a two-sided clamped beam of 1 meter was taken with a point load of 15 kN acting at the midspan of the beam. With the maximum allowable stress of 4.5 N/mm² and a width of 100 mm, the minimum height of the beam should be 160 mm. This height is added to the topology optimisation process by setting a minimum thickness for the exclusion region.
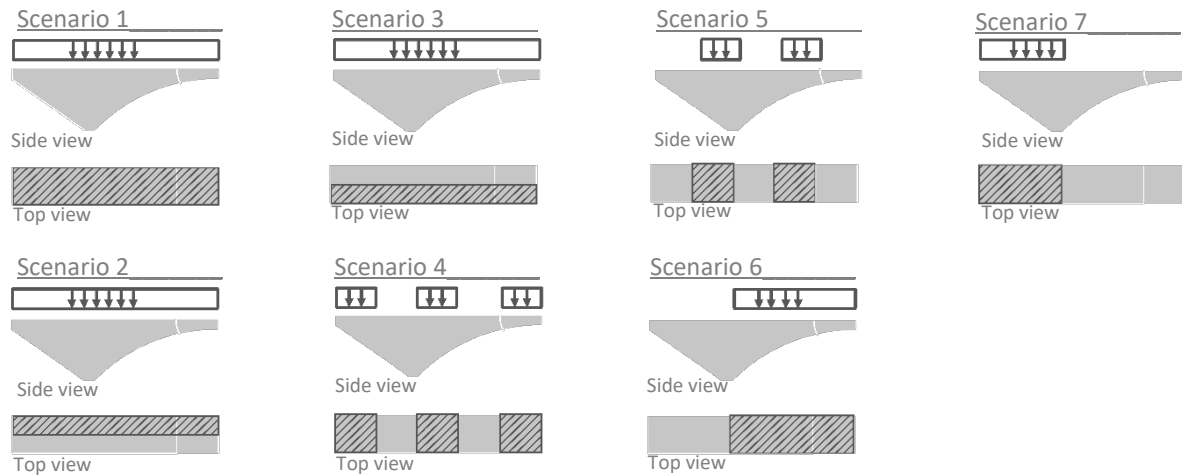
Figure 9.5 Possible load combinations: the dead weight and wind load are applied on the entire surface. Traffic load given in dark grey is applied to the areas as indicated in the figure.

9.2.5   Structural analysis

The structural analysis, which is done before topology optimisation, should be linear. Since glass behaves linearly during loading and large deflections are not expected, no significant problems are expected from this limitation. A non-linear analysis is essential to model the intermediary layers' approximate behaviour at the different connections.

9.3 Topology analysis

There are different ways to optimise in Ansys. Optimisation can be done with a density-based solver (SIMP), a Level Set solver, and a lattice optimisation solver. Most solvers are density-based or Level Set. With density-based optimisation, optimisation is linked to the density of an element and with Level Set optimisation, the optimisation is done with shape functions. A weakness of the density-based method is the absence of clearly defined boundaries. Because of this, the designer should almost always interpret the poorly defined geometry. The Level Set method changes the boundaries of the design during the optimisation process, which results in an optimised design with clear boundaries and smooth contours. Therefore, it is decided to use the Level Set method during the optimisation. An additional advantage of the Level Set method is that an exclusion thickness can be set, which is not possible with the density-based function.

The objective function chosen for this optimisation is to minimize compliance with a mass response constraint. After multiple optimisations, a mass constraint in the 30-35% range was found to give acceptable results when testing the model on stress limits.

The most crucial aspect when designing a cast glass bridge is the maximum dimensions of the cross-sections. The bigger the cross-section, the longer the annealing time. The maximum thickness was set at 210 mm. The maximum member size in the model is set to 180 mm. Connecting members merge and can form cross-sections larger than 180 mm. To ensure the 210 mm thickness is not exceeded, the maximum member size is set to 180 mm. The minimum member size cannot be set for the Level Set method. During multiple optimisations rounds, the results did not contain members with a non-acceptable small cross-section.

The design region consists out of two bodies the outer element and keystone. Excluded from this region is the grid structure that supports the float glass top layer and the contact surface between the two bodies. The grid structure is excluded to ensure that the material is in the right spot to support the float-glass top layer. The contact surface is excluded to ensure that enough material is left at the connections. The exclusion is set at 160 mm, as explained in section 9.2.4.

After 36 iterations in 12 hours and 3 minutes, an optimised design was obtained. Only 2800 kg of the initial 8000 kg of material was left, equal to 35% of the original mass. The outcome of the optimisation can be found in Figure 9.6.

Optimisation type: Level Set
Excluded: Top surface & contact surface (160 mm)
Mesh type: Tetrahedral
Element order: Quadratic
Maximum mesh element size: 40 mm
Mesh elements: 481484
Mesh nodes: 672642
Maximum thickness member: 180 mm
Percent to retain: 30-35%
Optimisation time: 12 hours and 3 minutes
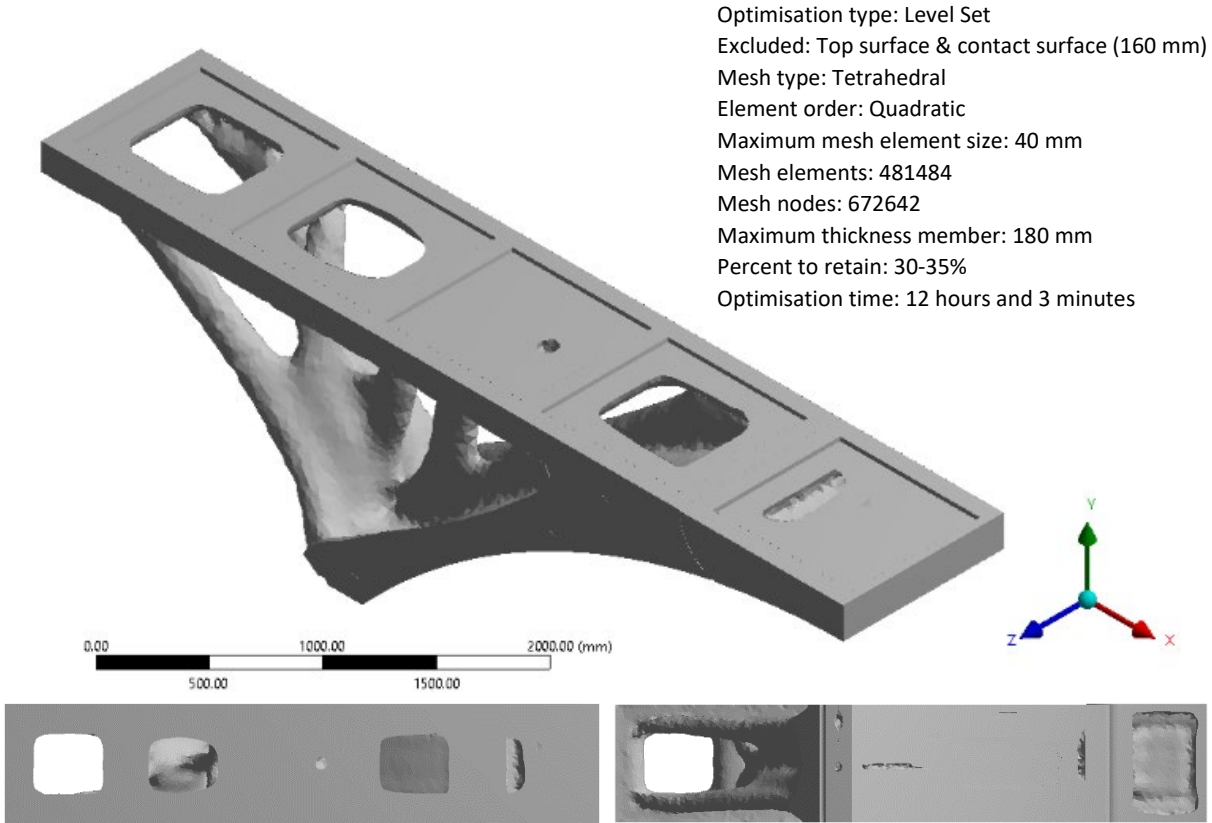
Figure 9.6 Outcome of the topology optimisation process.

9.4 Post-processing

Post-processing is done in Ansys Spaceclaim. Post-processing is needed to reduce the complexity of the design. With the less complex design, structural calculations can be done. During the post-processing, various tools are used to produce a smooth structure. It is noteworthy that some of the surfaces are very straight compared to the more fluent surfaces. This can be partly ascribed to the topology optimisation, which leaves the material at the spots where it is most needed and partly on choices made during post-processing. More information about post-processing is given in appendix D.

After the initial structural analysis, it was found that the stresses were too high when a point load was exerted on the keystone. Because of this, it was necessary to increase the cross-section of the keystone at some points. The model can be found in Figure 9.7.

Figure 9.7 Post-processed optimised model.

9.5 Structural analysis after topology optimisation of one-fourth of the bridge

Multiple linear analyses are done to model the overall structural behaviour. Since glass behaves linearly and large deformations are not expected. During the first structural verification, linear analysis is used.

9.5.1 Input geometry

In Figure 9.8, the input geometry is given. The green elements are made from borosilicate glass, and the grey element is made from a stiff material. The reduced weight of the structure is equal to 2800 kg. During the structural calculations of one-fourth of the bridge, the float glass top layer is also modelled.

A tetrahedral mesh is used with a maximum size of 50 mm and a quadratic element order.
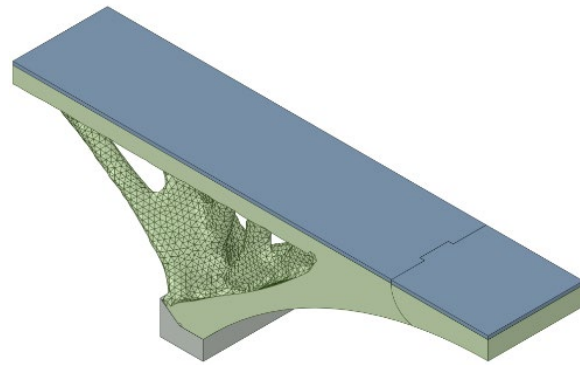
Figure 9.8 Input geometry with in green the topology optimised cast glass elements, in grey the elements made from a stiff material and in blue the float glass top layer.

9.5.2 Supports

In Figure 9.9 (a), the structural model is given for an equally distributed load. In Figure 9.9 (b), the structural model is given with a point load on the most critical location. The labels A and B in this figure indicate frictionless supports, and they are used to mimic symmetry. The labels C and D show an additional constraint of movement in the z-direction, and label G indicates the fixed support.
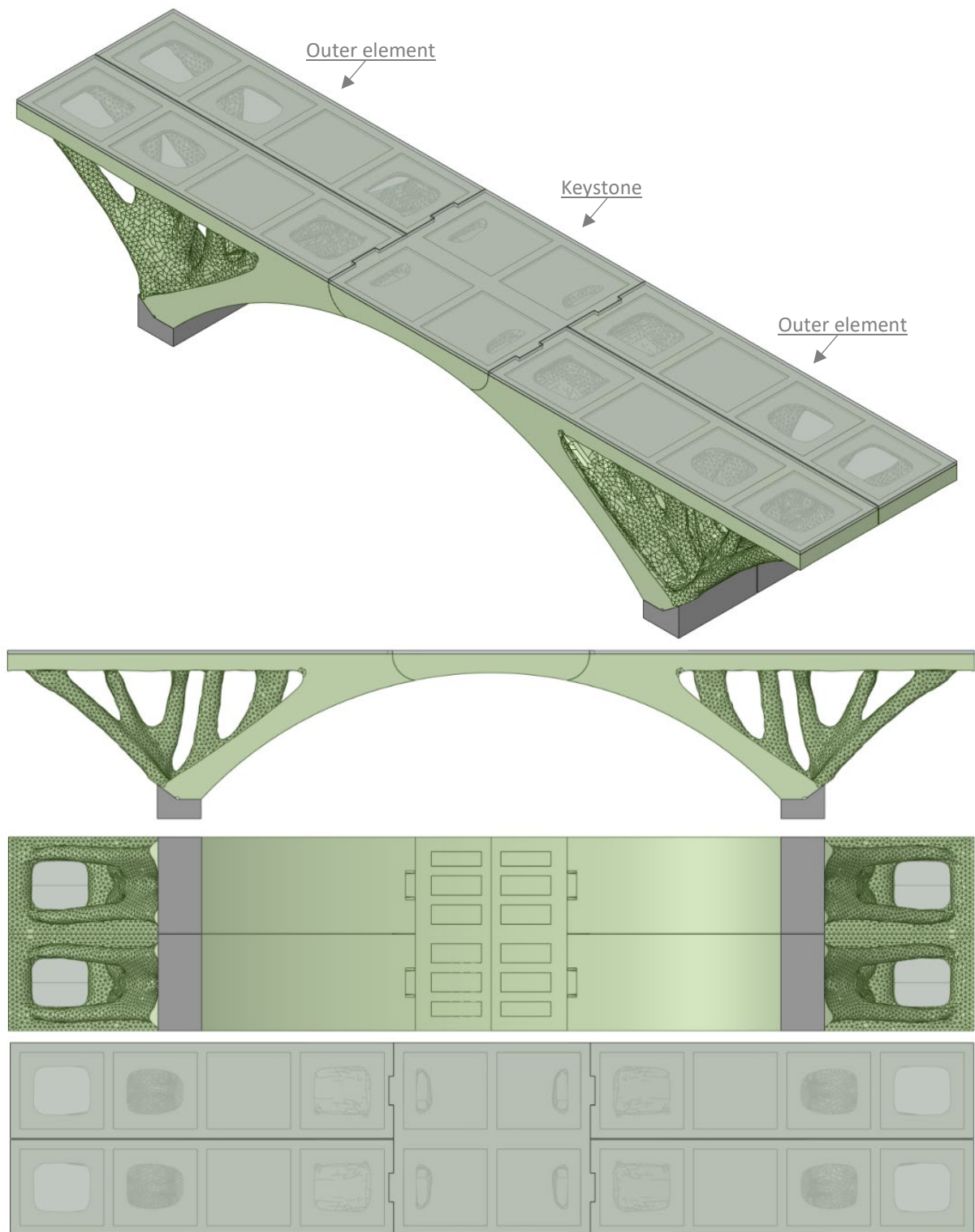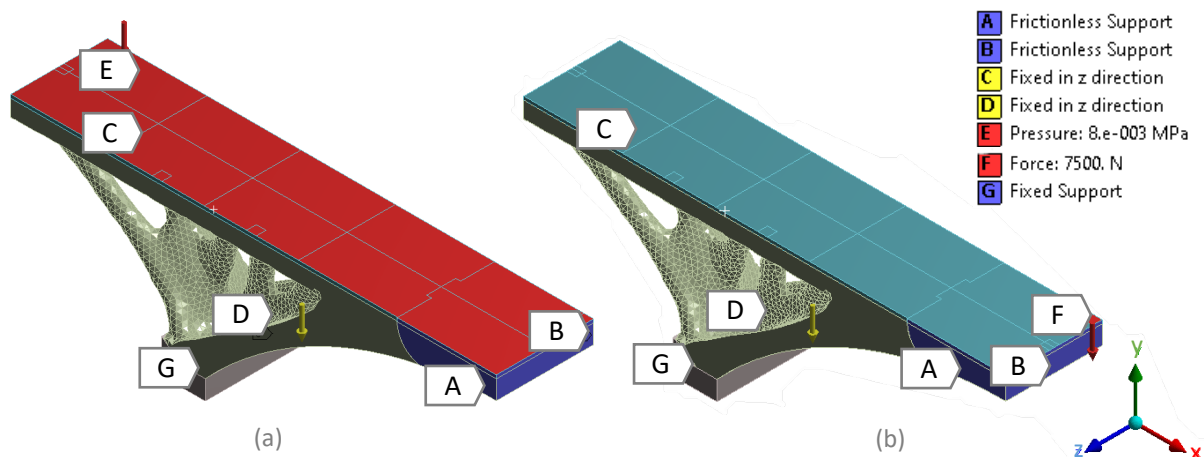

Figure 9.9 Structural model of one-fourth of the bridge. (a) structural model for an equally distributed load. (b) structural model for the point load on the most critical location.

9.5.3 Interfaces

For this structural analysis, the connection 'no separation' is used to mimic the behaviour of the interlayer in between the cast glass elements and between the cast glass outer element and foundation.

9.5.4 Loads

During the initial check on the structural behaviour of one-fourth of the model, it was found that the horizontal loads $q_{fk,parallel}$, $q_{wind,perpendicular}$, and $q_{wind,parallel}$ result in a tensile stress increase of around 0.05 MPa. Compared to the maximum principal stress from the vertical load that is exerted on the surface by traffic, this value is negligible. The temperature load will also not form a problem during the lifetime of the bridge. Because the bridge can rotate, the expansion and shrinkage due to temperature differences can be taken up by the supports and connections without increasing the

stresses significantly. Only the dead weight, vertical traffic load and vertical wind load are considered during the structural verification of the entire bridge. The highest load is found when using load combination 2 from Table 6.1. The loads with included factors are given in Table 9.4.

Table 9.4 loads from load combination 2 from Table 6.1 exerted on the topology optimised bridge.

	L.C.2
$g_{,soda\ lime}$	$3075\ kg/m^3$
$g_{,borosilicate}$	$2788\ kg/m^3$
$q_{f,vertical}$	$7.5\ kN/m^2$
$Q_{fv;vertical}$	$15\ kN$
$q_{wind,vertical}$	$\pm0.26\ kN/m^2$

Since the bridge is topology optimised, it is essential to test it on multiple load scenarios. The different load scenarios are given in Figure 9.10. Scenario 1 until 7 consider equally distributed loads, and scenario 8 considers a point load. For scenario 8, it was decided to only perform the structural analysis for the point load on the most disadvantageous location. However, the point load could be exerted everywhere on the surface, resulting in high stresses near those locations.
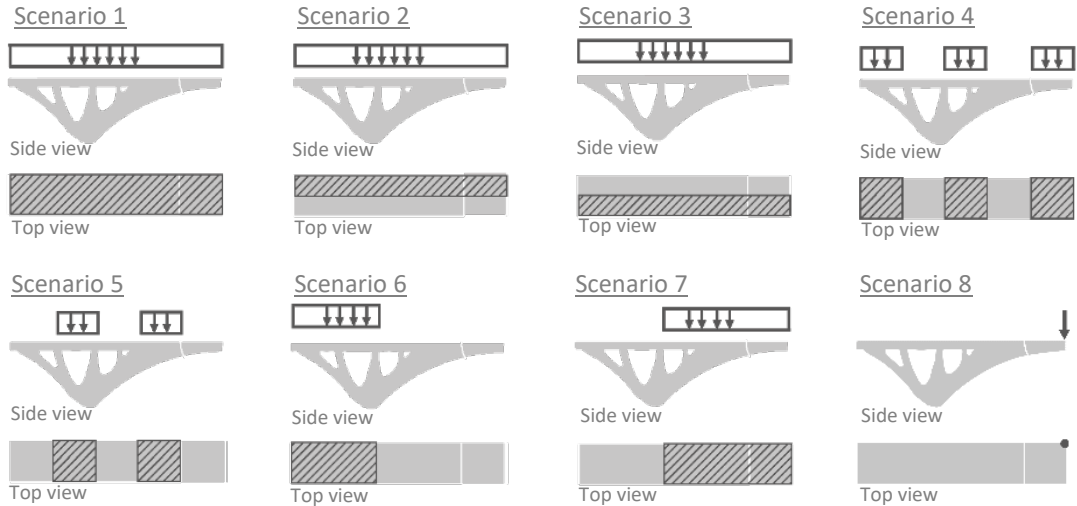
Figure 9.10 Load scenarios used for the structural analysis of one-fourth of the bridge.

9.5.5 Structural analysis

The maximum deformation and maximum tensile stress for the eight load scenarios are given in Table 9.5. From the structural analysis, it can be concluded that scenarios 1 and 8 are most determining for the keystone and scenario 7 is most determining for the outer element. The results from scenario 1 are given in Figure 9.11, the results from scenario 7 are given in Figure 9.12, and the results from scenario 8 are given in Figure 9.13.

Table 9.5 Outcome of linear structural analysis of one-fourth of the bridge.

	Loads (side and top view)	Max deformation	Max principal stress
Unit		mm	MPa
S.1		0.13	1.67
S.2		0.10	1.19
S.3		0.10	1.30
S.4		0.12	1.54
S.5		0.08	0.99
S.6		0.05	0.66
S.7		0.015	2.47
S.8		0.19	3.08

Type: Total Deformation
Unit: mm
Time: 1

0.13217 Max
0.1175
0.10282
0.088145
0.07347
0.058795
0.04412
0.029445
0.01477
9.4584e-5 Min

Top view   Bottom view

Type: Maximum Principal Stress
Unit: MPa
Time: 1

1.6732 Max
1.4348
1.1963
0.95787
0.71942
0.48098
0.24254
0.0040939
-0.23435
-0.47279 Min

Top view   Bottom view
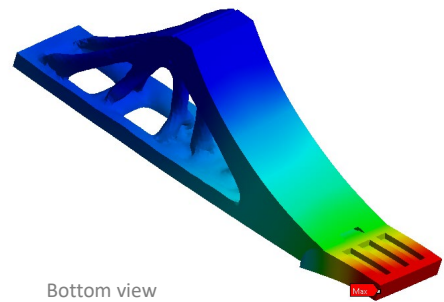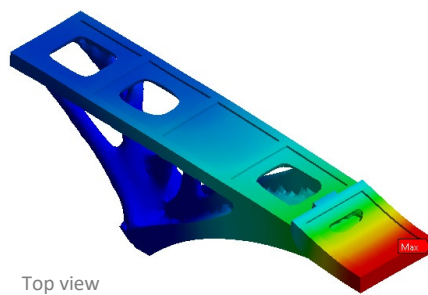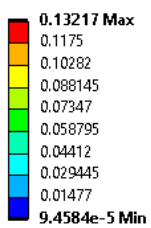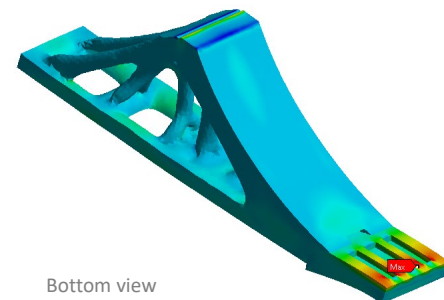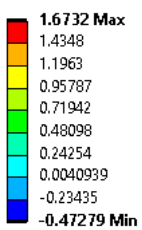
Figure 9.11 Plots from maximum deformation and principal stress of load scenario 1.
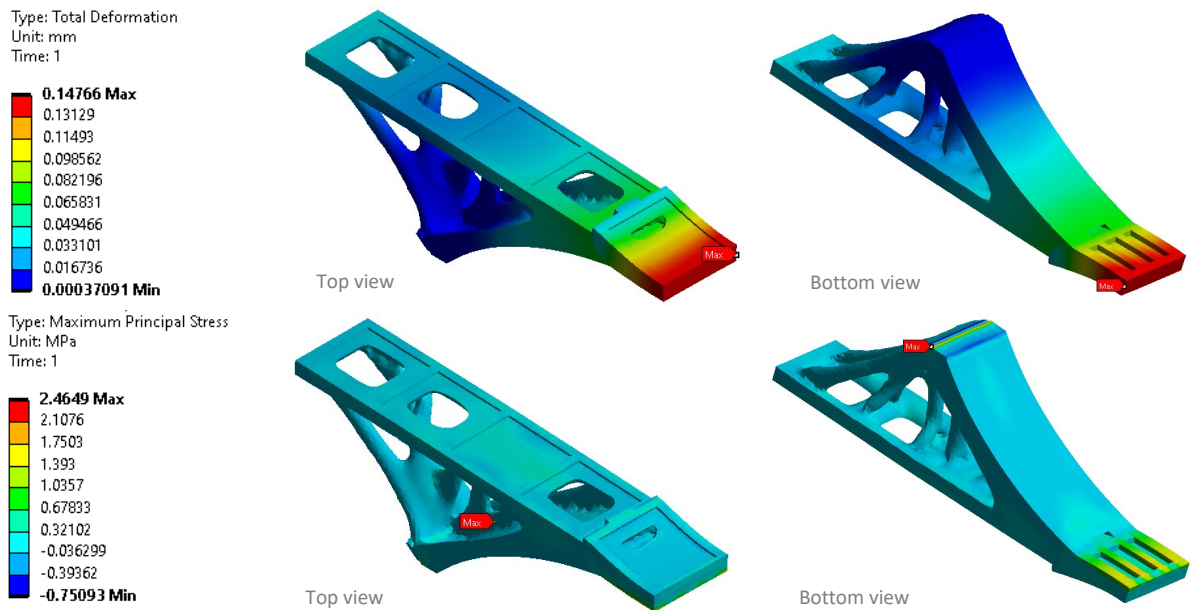
Figure 9.12 Plots from maximum deformation and principal stress of load scenario 7.
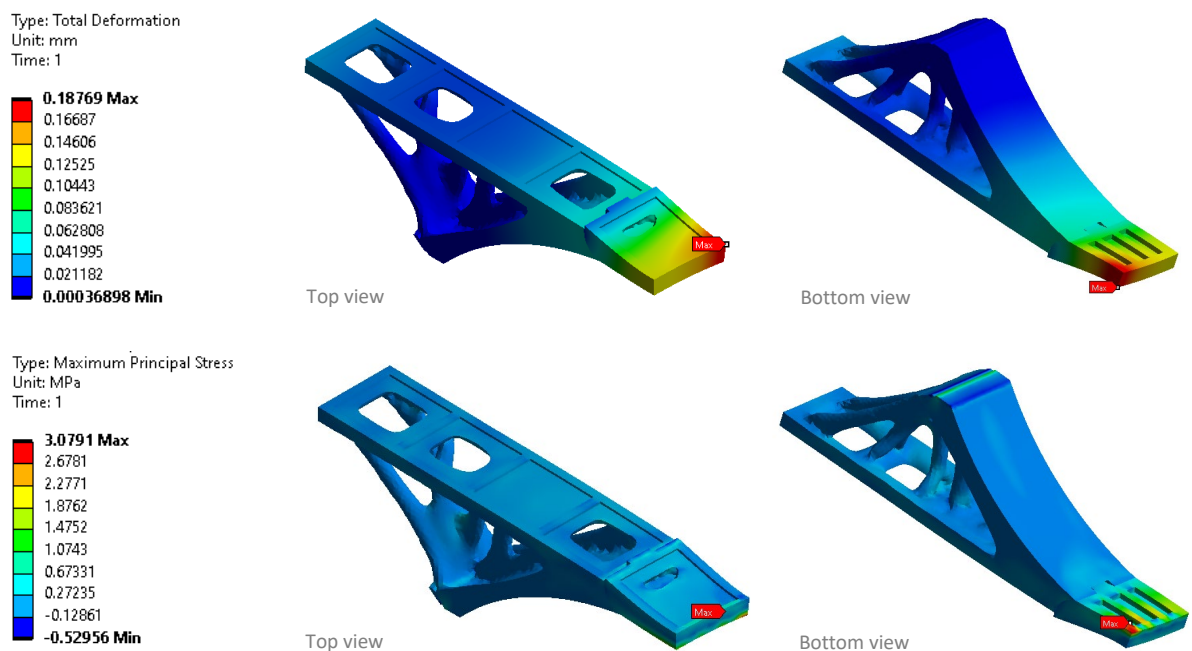
Figure 9.13 Plots from maximum deformation and principal stress of load scenario 8.

9.5.6   Interpretation of the result

The maximum tensile stress is found when a point load is applied at midspan. This stress is equal to 3.1 MPa, which is lower than the maximum allowable flexural stress for borosilicate glass. At the connection between the cast glass and foundation, a stress gradient is observed. This gradient occurs due to the simplification of the contact faces. In reality, the polyurethane interlayer distributes the stresses over the support surface. The maximum deformation is equal to 0.19 mm. The maximum allowable deformation is equal to 24 mm. The results of the structural analysis do not give the correct approximate behaviour for the deformation.

9.6 Structural analysis after topology optimisation of the entire bridge

The analysis for the entire bridge is done in four cycles, in every cycle, a step is made towards a bridge that is analysed closer to reality. The first cycle is a linear analysis, the second cycle is a non-linear analysis with a polyurethane interlayer and fixed supports, the third cycle is a non-linear analysis with a polyurethane interlayer and horizontal elastic supports, and the fourth cycle is a non-linear analysis with a polyurethane interlayer, elastic supports and a settlement of 10 mm of one of the supports.

9.6.1   Input geometry

Two different models are used. Model one consists out of borosilicate glass and stiff material and is used for the linear analysis. In the second model, a polyurethane interlayer with a thickness of 3 mm is added. Because of the non-linear behaviour of this material, a non-linear analysis must be done. Figure 9.14 (a) shows the exploded version of the first model, this model is used during analysis cycle 1. Figure 9.14 (b) shows the exploded version of the second model, this model is used during analysis cycle 2, 3, and 4.

(a)   (b)
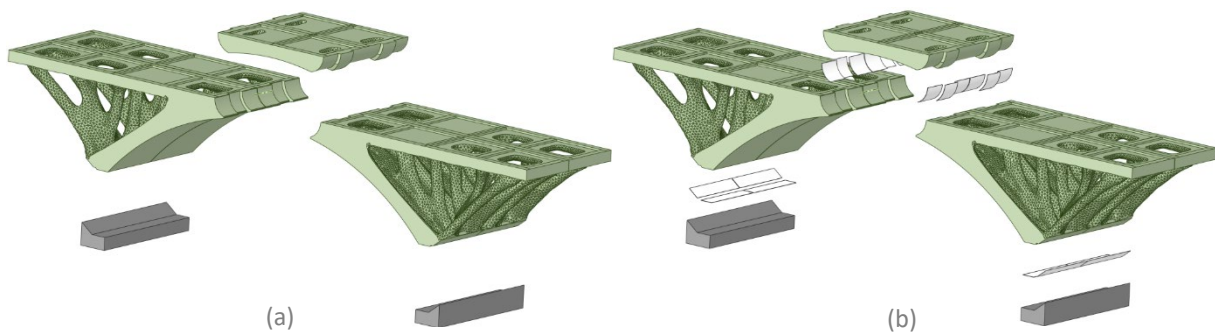
Figure 9.14 Input geometry for (a) linear and (b) non-linear analysis. The elements in green are the topology optimised cast glass elements, in grey the elements made from a stiff material, and in white the elements made from polyurethane.

9.6.2   Meshing

A tetrahedral mesh is used with a maximum size of 60 mm and a quadratic element order.

9.6.3   Supports

The support conditions for the first analysis cycle are given in Figure 9.15. During this analysis, the foundation is fixed, and the outer elements have an extra restraint in the z-direction.

(a)   (b)
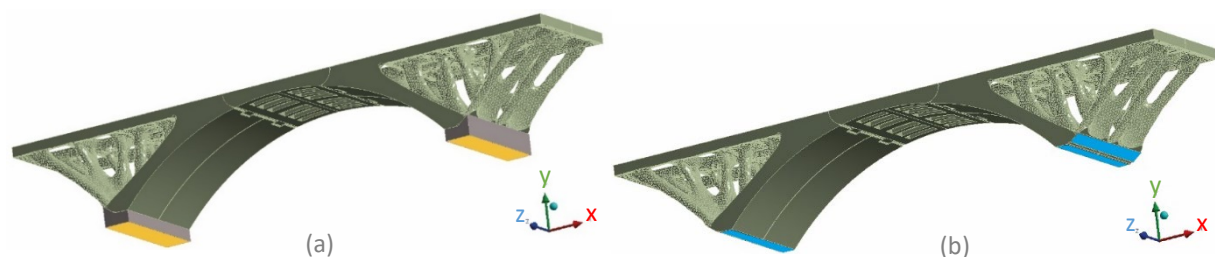
Figure 9.15 Support conditions for linear analysis cycle. (a) Yellow indicates the fixed connection, (b) blue indicates an additional constraint to restrain movement in the z-direction.

During the second analysis, the foundation is still fixed. However, the additional constraint in the z-direction is removed, this constraint is not needed because the interlayer restricts movement. For the third analysis, the fixed support is replaced by elastic horizontal supports and displacement supports

for the y- and z-direction. Since the bridge is optimised with fixed supports, low elastic horizontal supports result in high stresses and more significant bending moments. With a low elastic horizontal support, the horizontal support reactions are also lower. After a few iterations, the horizontal elastic support is chosen to be 0.08 N/mm^3 on both sides. With this horizontal elastic support, the structure deforms 1 mm when a load of 100 kN is applied. The support conditions for cycle three are given in Figure 9.16.

Figure 9.16 Support conditions for non-linear analysis cycle with an elastic supported foundation in the x-direction. Red indicates the restrained surface in the x- and z-direction, and in green, the horizontal elastic support.

For load cycle four, one of the restrained horizontal surfaces is replaced by elastic supports in the vertical direction. For the other restrained surface, a displacement is added of 10 mm in the y-direction. For the elastic vertical support, 0.2 N/mm^3 is assumed. This results in a deformation of 0.5 mm when a load of 165 kN is applied.

9.6.4 Interfaces

In analysis cycle 1, the connection 'no separation' is used to mimic the behaviour of the intermediary layer in between the cast glass elements and between the cast glass outer element and foundation. For analysis cycle 2, 3, and 4, a polyurethane interlayer is used. These layers are schematised as bonded to the cast elements and foundation.

9.6.5 Loads

Only the dead weight, vertical traffic load and vertical wind load are considered during the structural verification of the entire bridge. The loads used are given in Table 9.6.

Table 9.6 Loads on topology optimised bridge.

	L.C.2
$g_{,soda\ lime}$	$3075\ kg/m^3$
$g_{,borosilicate}$	$2788\ kg/m^3$
$q_{f,vertical}$	$7.5\ kN/m^2$
$Q_{fv;vertical}$	$15\ kN$
$q_{wind,vertical}$	$\pm0.26\ kN/m^2$

In the model for the entire bridge, it was decided not to model the float glass top layer. Instead, the same approach was applied, as mentioned in section 9.2.4. In Figure 9.17 (a), the highest loads are given in red and the lowest loads in blue. The maximum point load should also be considered to check for local effects. The most disadvantageous location of the point load is indicated with the red arrow in Figure 9.17 (b).

(a)

(b)
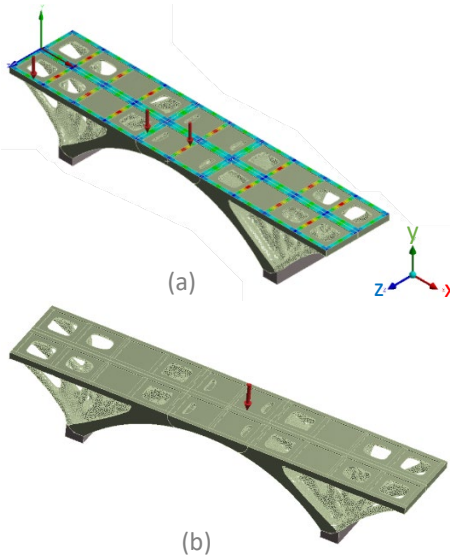
Figure 9.17 Load configuration for the entire bridge. (a) load configuration for an equally distributed load. (b) load configuration for the point load on the most critical location.

The bridge is tested on multiple load scenarios. Scenario 1 until 15 show equally distributed loads and scenario 16 shows a point loaded bridge. It is decided to only do the structural analysis for the point load on the most disadvantageous location. However, the point load could be exerted everywhere on the surface, resulting in high stresses near those locations. The different load scenarios are given in Figure 9.18. A selection is made on which scenarios are most important to do structural analysis on. Scenario 1 provides the highest vertical support force, and scenario 11 gives the highest horizontal support force. Scenario 2 provides the highest support moment around the x- and y-axis and scenario 11 or 12 around the z-axis. The most significant displacement and stress are expected to occur for load scenario 16. Scenario 14 and 15 are most important for the bridge's stability and the pressing out of the keystone.
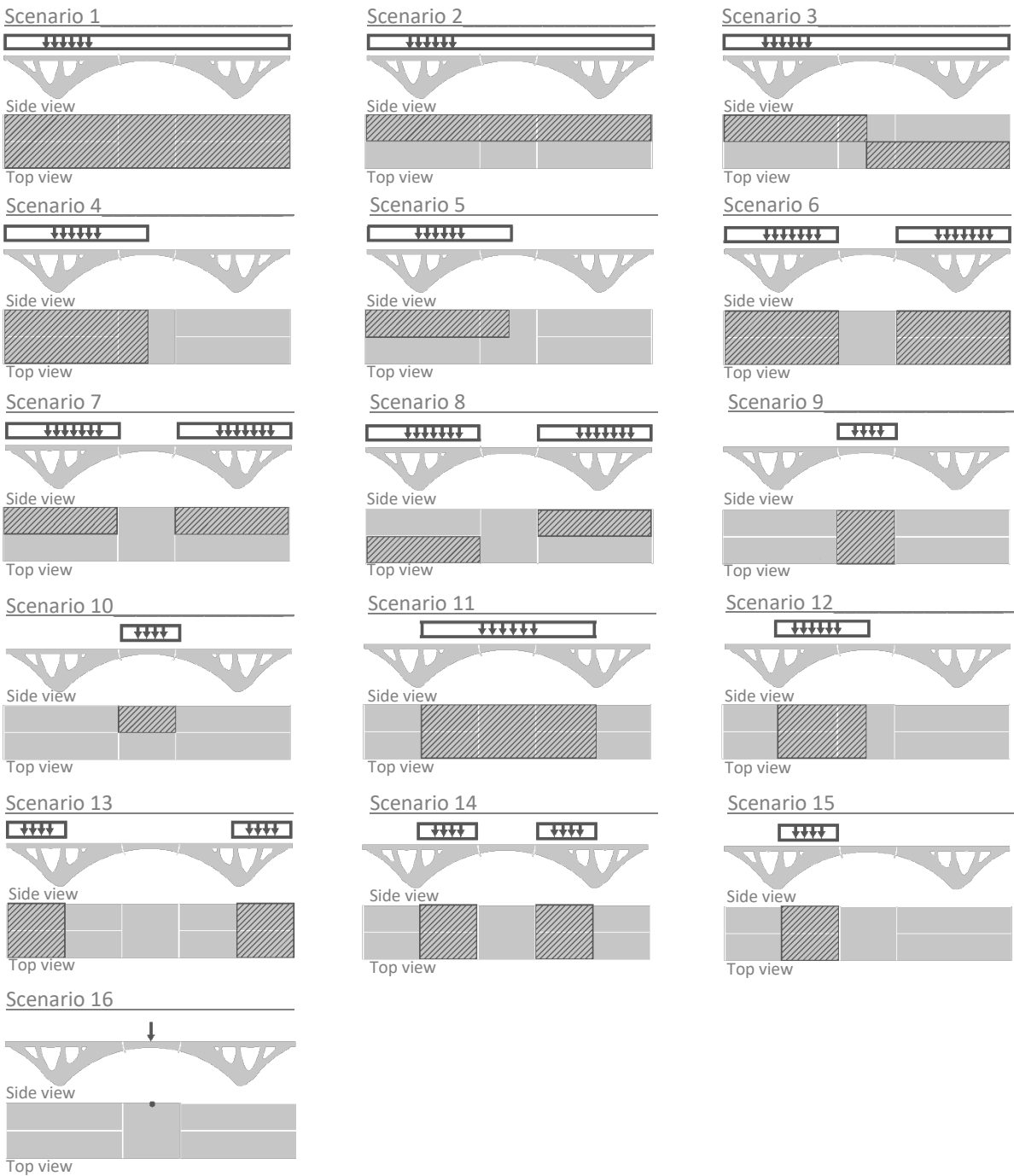
Figure 9.18 Possible load scenarios for the entire bridge.

9.6.6   Structural analysis

The maximum deformation, maximum tensile stress, maximum support forces, maximum support moments, and maximum contact pressure for the eight most essential load scenarios are given in Table 9.7. The contour plots for the maximum deformation, principal stress, and pressure for boundary condition cycle 4, load scenario 1, are shown in Figure 9.19, and for boundary condition cycle 4, load scenario 16 in Figure 9.20.
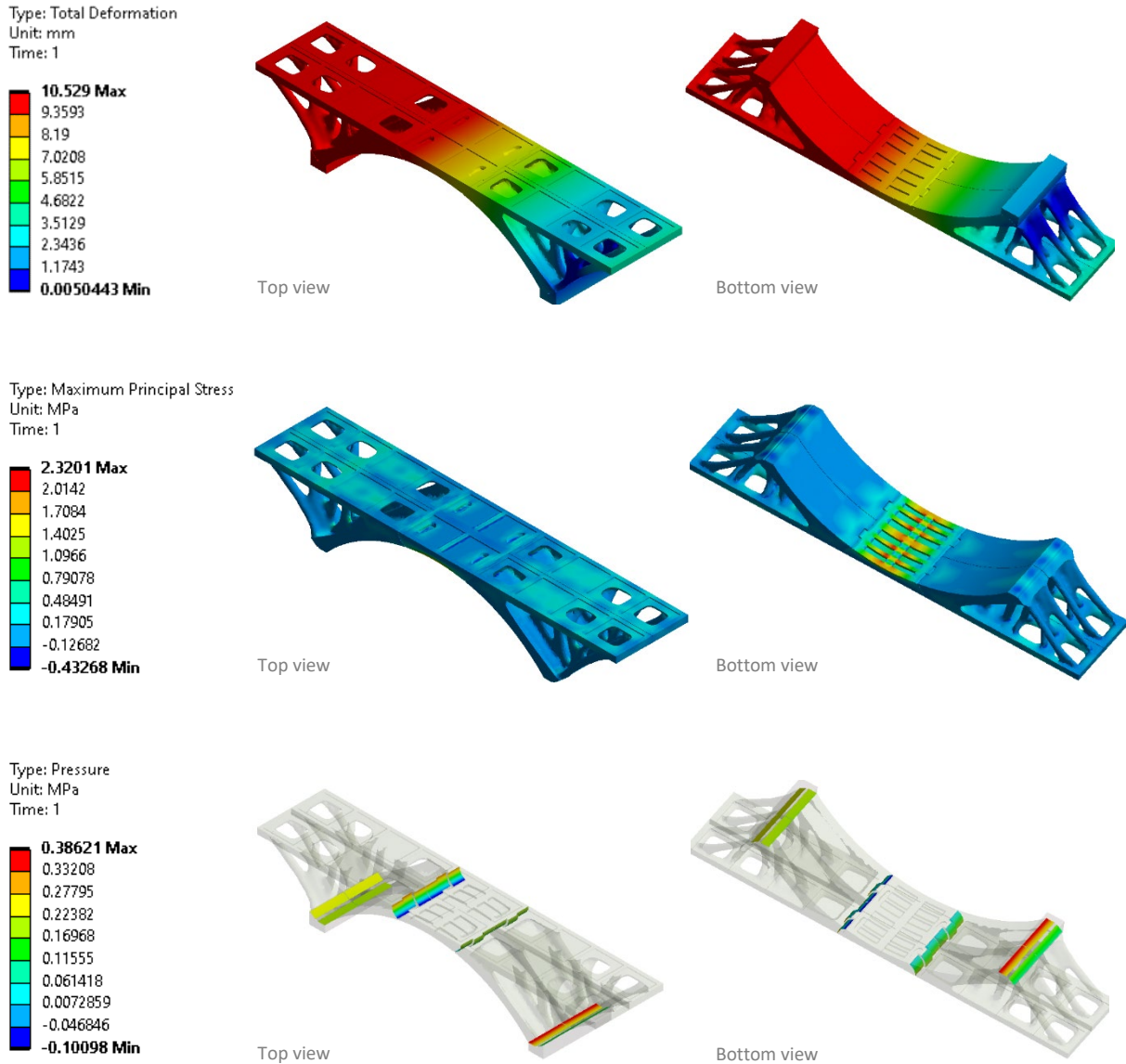
Figure 9.19 Contour plots for boundary conditions cycle 4, load scenario 1.

Table 9.7 Maximum output values from structural analysis of cycle one till four of the eight most crucial load scenarios.

Unit	Loads (side and top view)	Max deformation mm				Max tensile stress MPa				Max force at support kN					Max moment at support kNm					Max contact pressure MPa			
		1	2	3	4	1	2	3	4		1	2	3	4		1	2	3	4	1	2	3	4
S. 1		0.2	0.9	2.8	10.5	2.1	1.6	2.4	2.3	x	73	80	64	77	x	0	0	0	0	+3.6	+0.3	+0.55	+0.38
										y	165	165	166	167	y	0	0	0	0	-2.9	0	-0.05	-0.10
										z	0	0	0	0	z	5	14	19	30				
S. 2		0.1	0.9	2.3	11.0	1.7	0.8	1.3	1.6	x	55	59	49	57	x	21	20	20	22	+2.6	+0.27	+0.44	+0.36
										y	123	123	122	125	y	6	4	4	2	-2.3	0	-0.06	-0.18
										z	0	0	0	0	z	3	12	10	17				
S. 11		0.2	1.0	3.4	10.9	3.1	1.4	2.4	2.4	x	89	98	79	93	x	0	0	0	0	+6.2	+0.28	+0.64	+0.39
										y	132	132	132	133	y	0	0	0	0	-5.7	0	-0.14	-0.12
										z	0	0	0	0	z	5	17	23	27				
S. 12		0.3	1.9	3.5	11.1	4.4	1.2	1.9	2.2	x	62	71	58	66	x	0	0	0	0	+6.0	+0.35	+0.59	+0.69
										y	119	121	122	118	y	0	0	0	0	-5.4	-0.13	-0.22	-0.34
										z	0	0	0	0	z	37	22	24	24				
S. 14		0.1	0.8	2.5	10.6	2.0	0.9	1.1	1.7	x	57	69	57	67	x	0	0	0	0	+4.0	+0.21	+0.42	+0.31
										y	114	114	114	116	y	0	0	0	0	-3.7	0	-0.07	-0.14
										z	0	0	0	0	z	2	13	14	17				
S. 15		0.2	1.4	2.7	10.4	2.3	1.1	1.2	2.0	x	47	56	47	54	x	0	0	0	0	+4.0	+0.25	+0.42	+0.44
										y	110	109	110	107	y	0	0	0	0	-3.3	-0.10	-0.16	-0.27
										z	0	0	0	0	z	19	17	16	18				
S. 16		0.2	1.0	2.3	11.2	3.8	3.2	3.7	3.8	x	48	56	46	54	x	7	7	7	8	+2.94	+0.20	+0.37	+0.33
										y	89	89	89	87	y	8	7	7	4	-2.39	-0.03	-0.08	-0.17
										z	0	0	0	0	z	2	12	8	9				

Type: Total Deformation
Unit: mm
Time: 1
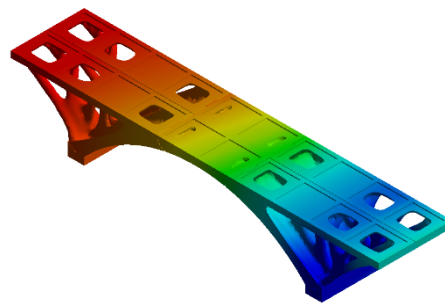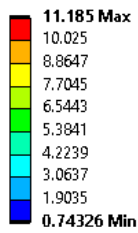
11.185 Max
10.025
8.8647
7.7045
6.5443
5.3841
4.2239
3.0637
1.9035
0.74326 Min

Top view   Bottom view

Type: Maximum Principal Stress
Unit: MPa
Time: 1

3.7835 Max
3.3268
2.8702
2.4136
1.9569
1.5003
1.0437
0.58707
0.13044
-0.32619 Min
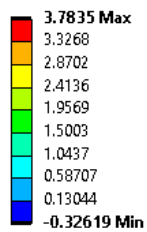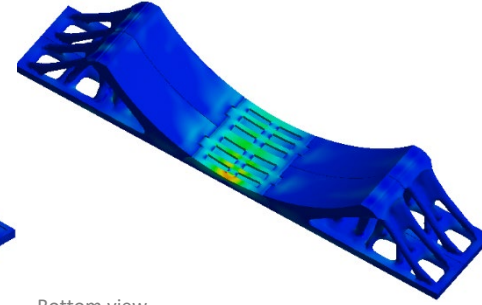
Top view   Bottom view

Type: Pressure
Unit: MPa
Time: 1

0.33346 Max
0.27762
0.22178
0.16594
0.1101
0.054264
-0.0015756
-0.057415
-0.11325
-0.16909 Min
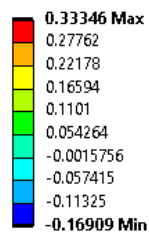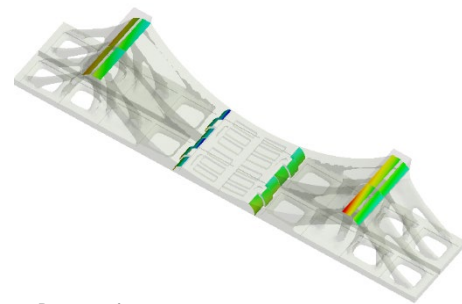
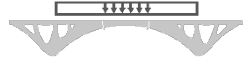Top view   Bottom view

Figure 9.20 Contour plots for boundary conditions cycle 4, load scenario 16.

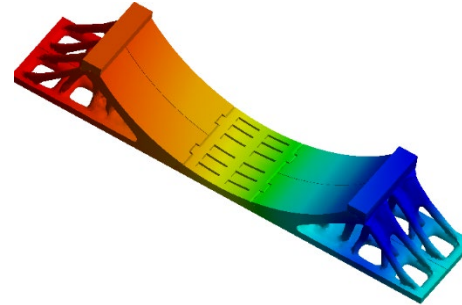### 9.6.7   Manual verification

Simplified manual calculations are used to check the outcome of the FEM model. First, the reaction forces are compared to the forces that are applied on the bridge. Second, the stability is verified with the use of thrust lines. Third, the stresses inside the connections are compared with the manually calculated stresses. Fourth, the buckling load is calculated. The manual verifications can be found in Appendix E.

9.6.8   Interpretation of the result

The contour plots show that the structure is not fully stressed until its ultimate capacity. The bridge should be able to withstand a point load of 15 kN everywhere on the surface. This results in higher stresses near the point of application. When comparing the structural analysis for the different boundary conditions, several conclusions can be drawn:

- The highest observed tensile stress and deformation are lower than the maximum allowable flexural stress (4.5 MPa) and deformation (24 mm).
- The point load, scenario 16, gives the highest tensile stresses, followed by the equally distributed load of scenario 11.
- When comparing the non-linear analysis with the linear analysis, significant differences are found between the solutions. Mainly on the deformation and contact pressure. The linear analysis gives a good approximation of the tensile stresses when compared to the non-linear analysis.

96

- The maximum tensile stress found in cycle 1 scenario 11, 12, 14 and 15 is higher than the results from cycle 2 until 4. These are singularities in the model. Because of the complexity of the model, a singularity is not easy to remove. Non-linear analysis with a soft intermediary material was done to check the actual maximum tensile stress in the model.
- The maximum deformation, maximum tensile stress, maximum support moment, and maximum contact pressure increase significantly by adding elastic horizontal supports. At the same time, the horizontal support force decreases. The horizontal elastic support must be stiff to ensure sufficient stability. To make the bridge better resistant to horizontal and vertical deformation. The optimisation process should be on half of the entire bridge (in the longitudinal direction) and should include unequal settlement.
- The results for contact pressure in cycle 1 are high compared to the contact pressures in cycle 2 till 4. This is due to the type of contact face that was used during this cycle.
- Since the interlayer is bonded to the elements, a negative contact pressure (tensile stress) is observed. This is not possible in reality. However, since the stresses are low, it is assumed that these stresses do not cause a problem.
- It might be possible to optimise the structure further since not every section is fully stressed. This is not done due to time limitations.

9.7 Safety

A scenario is tested were one of the outer element breaks. During this scenario, only the dead weight of the structure is taken into account. The same boundary conditions are taken as in cycle 3 (elastic foundation, with no settlement). In Figure 9.21, the results from the structural analysis are given. The analysis shows that when one of the outer elements breaks, the structure does not collapse. This is not the case when the keystone breaks since this makes the structure unstable. However, since the keystone is a massive element and mainly in compression, structural failure is not expected. A float glass top layer is added with a sacrificial layer to prevent damage to the cast structure. On the sacrificial layer, a ceramic fritted pattern is added to increase the slip resistance.
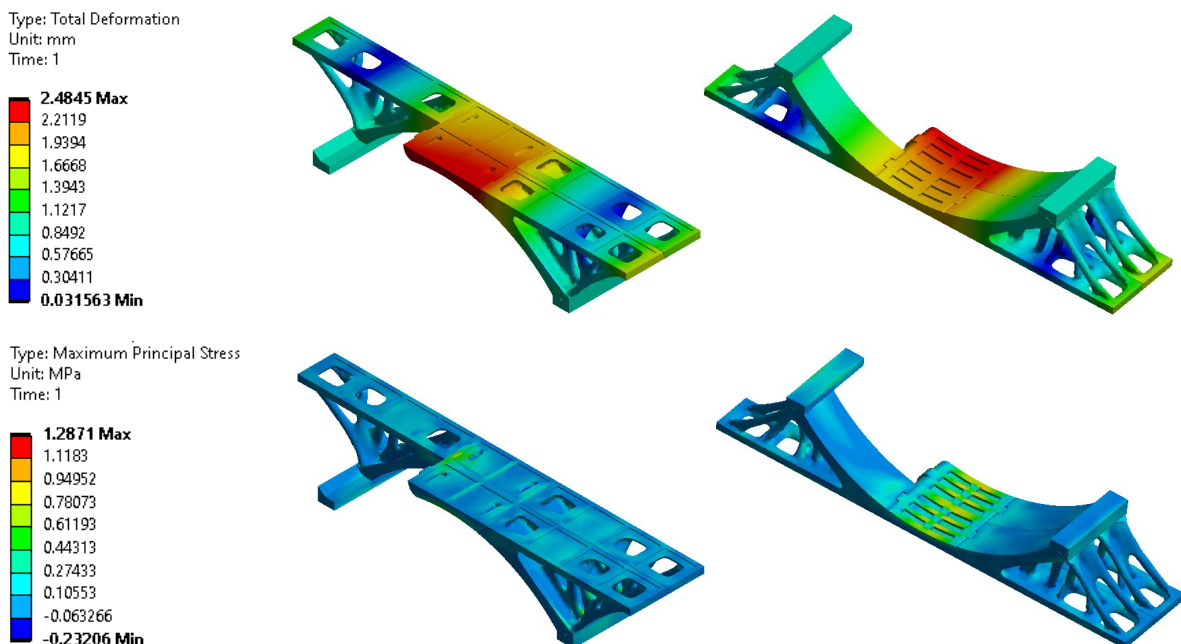
Figure 9.21 Structural verification of post breakage behaviour.

9.8 Post-processing

During post-processing, the model is shrink-wrapped with a gap size of 5 mm. It is advised to use a value lower than this to obtain an even more smoothened structure. Due to hardware limitations, it is decided to use 5 mm. This results in a faceted body that is suitable for post-processing. By going over each part of the structure with the smoothing tool, all sharp edges, corners and geometric features smaller than 20 mm were removed. The final post-processed bridge design is shown in Figure 9.22.
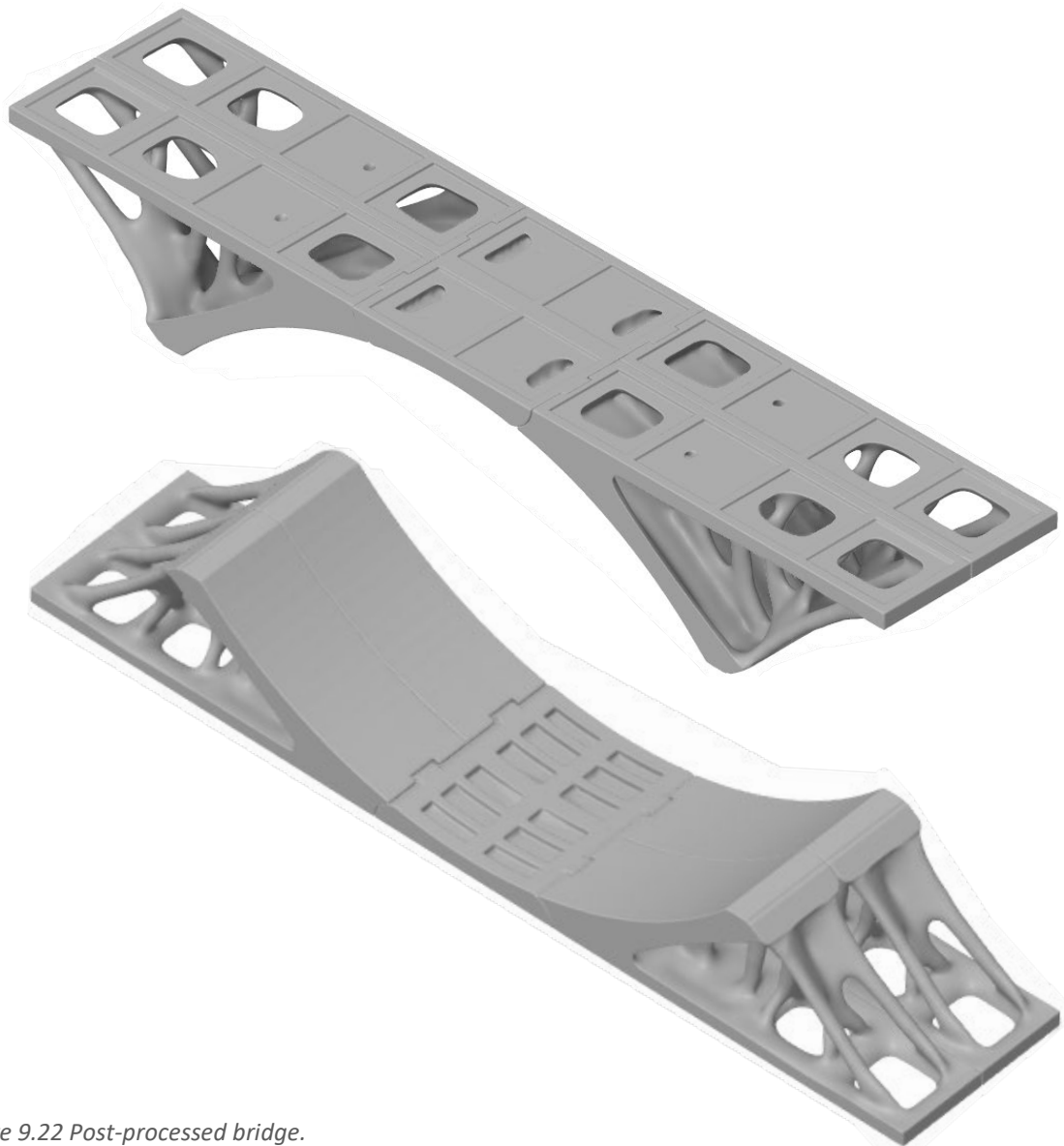
Figure 9.22 Post-processed bridge.

9.9 Manufacturing and Construction

This section explains what to do after the bridge design is finished and how to manufacture and construct the bridge. Due to time limitations, it was not possible to test the production method. In previous years experiments were done to test the use of 3D printed sand moulds for casting glass. Future researchers should investigate the production process further.

9.9.1 Producing the bridge

The bridge design is finalized in the post-processing step. After this step, the mould can be designed, the elements can be cast and post-processed, and the bridge can be assembled. The process is illustrated in Figure 9.23. The entire process consists out of 6 steps. In Table 9.8, the constraints from the literature research are recapped. Additionally, the step is given for when each constraint is applied.
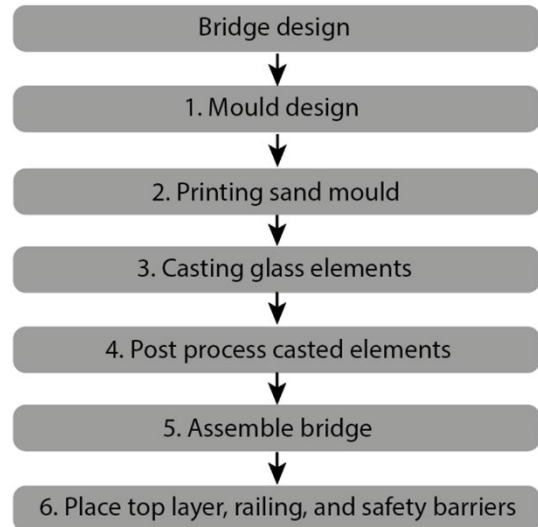
Figure 9.23 Production and construction process for the topology optimised cast glass bridge.

Table 9.8 Overview of constraints followed from literature research and in which step of the production process they are applied.

	Input values / Constraints	Step
Manufacturing		
Minimum wall thickness mould	4 mm	1
Maximum dimension of a mould element	$4\ by\ 2\ by\ 1\ meter$	1
Other constraints	Minimum mould divisions, interlocking nodes, screw holes, a pouring cup, vent pipes, and risers should be added	1

9.9.2 3D printed sand mould

Additive manufactured sand moulds combine sand with binder jetting/extrusion. The largest sand printer on the market can create elements with an accuracy in the range of 0.2 mm with a maximum dimension of 4 meters by 2 meters by 1 meter.
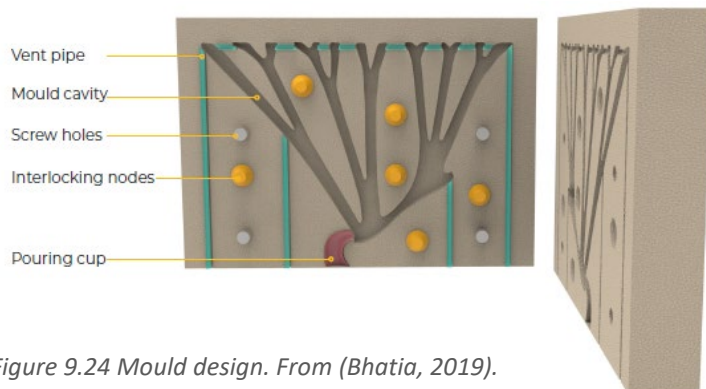
Figure 9.24 Mould design. From (Bhatia, 2019).

From experiments done by Bhatia (2019) followed that the inorganic and cold hardening phenolic binder remained intact during the casting of glass. Crystal cast was found to be a suitable coating to increase the surface quality. In Figure 9.24, an example of a mould design is given.

For the mould design, it is essential to ensure that the unused sand can be removed after the printing and that the coating can be applied to every surface within the mould. The division of the mould should be done such that every part is accessible. Interlocking nodes and/or screw holes are needed to connect the different parts (Bhatia, 2019). For the casting process, a pouring cup is needed that has a

larger diameter than the nozzle. Additionally, vent pipes are necessary to avoid the possible development of air entrapments inside the element. Risers might be helpful to cope with the excess material when the mould is filled up. The minimum thickness of the walls was calculated to be 4 mm (Bhatia, 2019). In Figure 9.25, an example of a 3D printed mould is given.

Figure 9.25 Removal of residual sand after printing. From (Jipa et al., 2016).

Multiple mould elements should be connected since the casted element has a larger dimension than the maximum dimension of a single mould element. In Figure 9.26, an example is given of how the mould could be split. To finalise the mould, a pouring cup, vent pipes, and risers should be added to the mould design.

The mould is split into 10 separate pieces that are connected with interlocking nodes. Splitting the mould into multiple segments results in an easier process to treat the surface of the mould before casting. The elements can be stacked like Lego blocks and stay in place via the interlocking nodes and gravity.

Interlocking nodes

3D printed sand moulds

Glass wool blanket

Concrete container
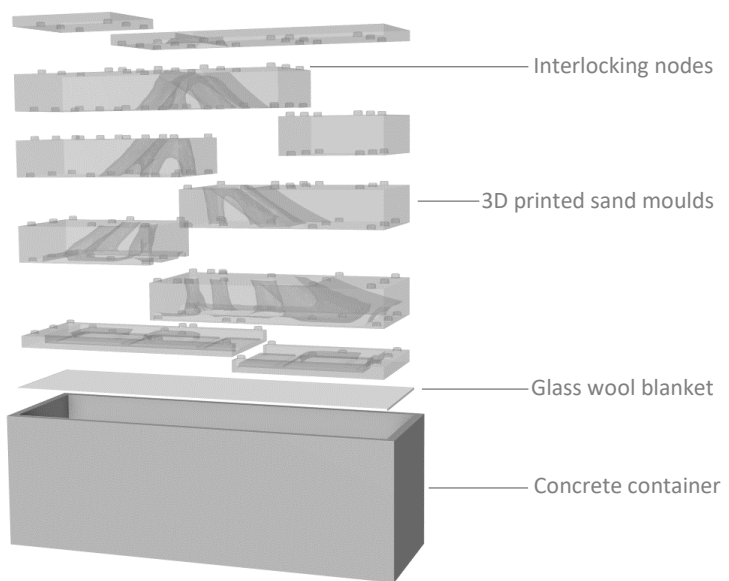
Figure 9.26 Assembly of the casting setup

The concrete container functions as a base for the casting process. A glass wool blanket is added to accommodate for the difference in expansion between the concrete and glass. Besides kiln casting via the pouring cup, big pieces of glass are spread inside the mould before casting to reduce the time needed for casting.

9.9.3 Casting

The bridge is made from borosilicate glass and is kiln cast. During kiln casting, the glass is remolten, poured and annealed in the same oven. Annealing is the primary treatment of glass. During this process, the glass transforms from liquid to solid. The thickness of each cross-section is smaller than 210 mm, which results in an approximate annealing time of one month.

9.9.4 Post-processing cast elements

After casting, the bridge has to be post-processed to remove deficiencies caused by the seepage of glass through the seams of the mould. The interlayer used between elements is 3 mm. Because of this, the surface of the cast glass elements at the connections needs to have high accuracy.

9.9.5   Detailling

In this section, the details are given for the bridge. In Figure 9.27, a cross-section is given of the bridge with the locations of the details. Detail A, given in Figure 9.28, shows the connection between the keystone and outer element. Detail B, given in Figure 9.29, shows the connection between the outer element and foundation. Detail C, given in Figure 9.30, shows the connection between the outer element and the footpath
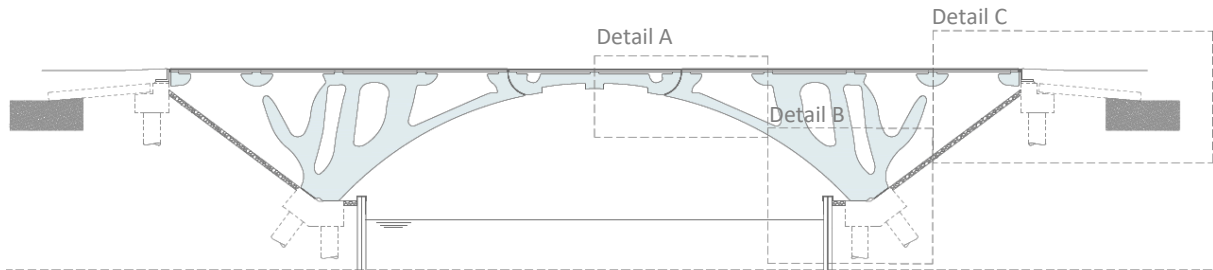
Figure 9.27 Cross-section of the bridge.
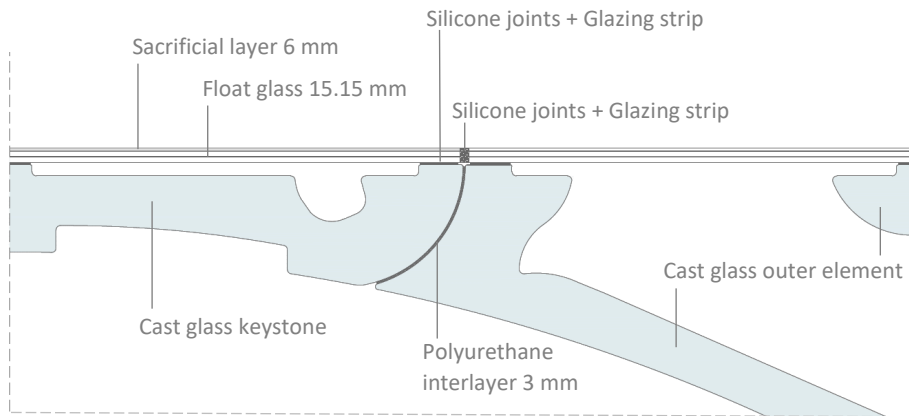
Figure 9.28 Detail A, the connection between the keystone and outer element.
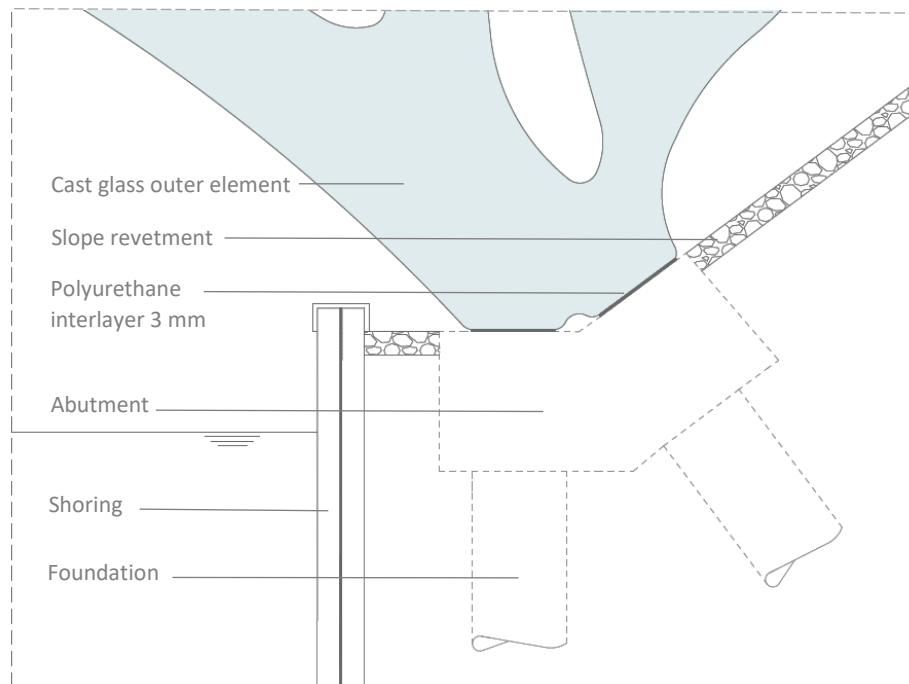
Figure 9.29 Detail B, the connection between the outer element and foundation.
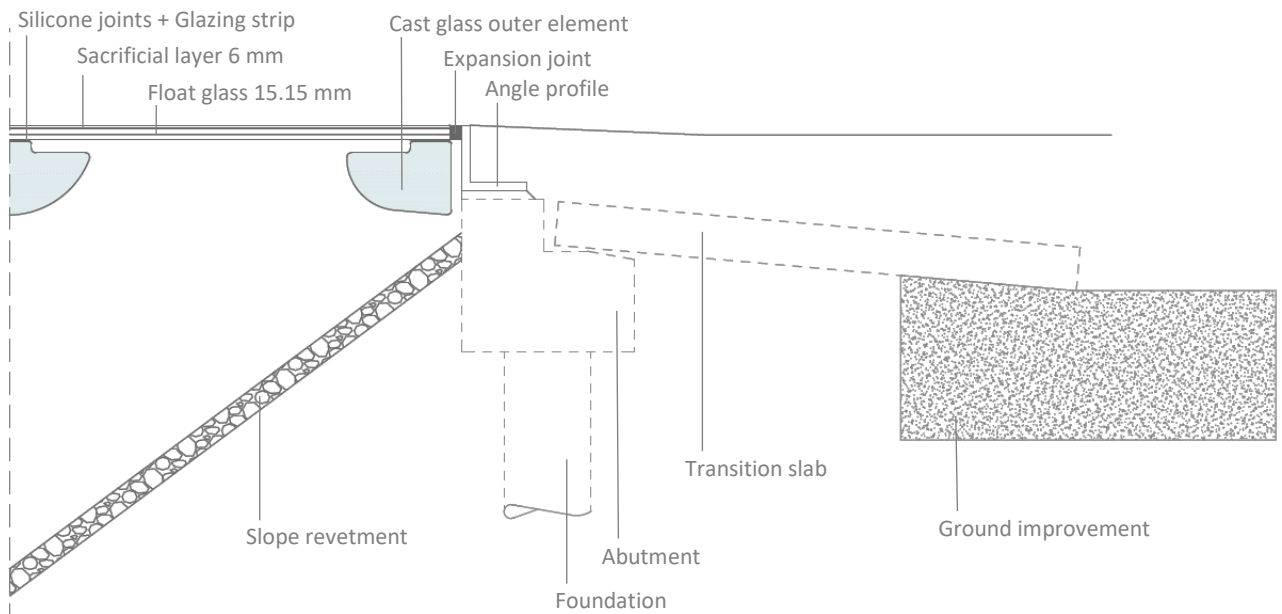
Figure 9.30 Detail C, the connection between the outer element and the footpath.

9.10 Conclusion case study

During topology optimisation, the bridge's mass was restrained, and it was optimised to minimize compliance. The topology optimisation resulted in a bridge that is feasible to produce. The cross-sections of all members are less than 210 mm, which results in an annealing time that is approximately one month. The weight of the outer element is 2400 kg, and the weight of the keystone is 1700 kg. This is below the maximum weight set for a cast element. An impression of the design is given in Figure 9.31.
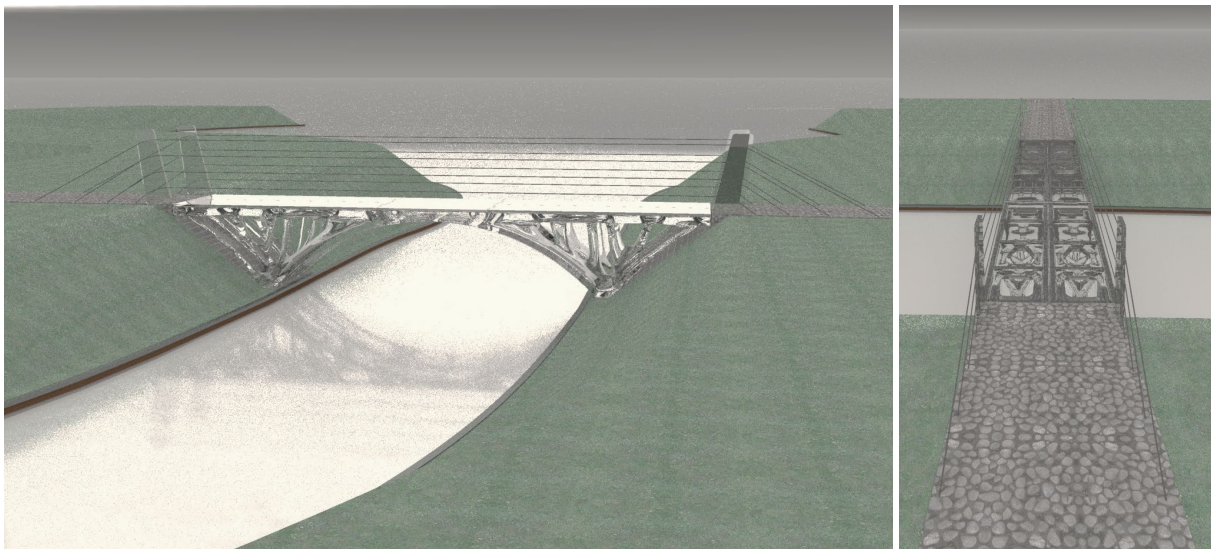
Figure 9.31 3D impression of the bridge

The bridge's design is strong, stiff, and stable according to the finite element analysis and manual verifications. The different load scenarios added to the model before optimisation results in a safe design. The point load has the most impact on the topology of the structure. This load results in a less optimised structure with a thicker grid structure. A smaller maximum point load would result in a leaner structure.

During the verification of the bridge, multiple analysis cycles were done, linear and non-linear. The non-linear analysis gives better results for the deformation, stresses, and contact pressure. The results for the horizontal loads, vertical loads and support moments are comparable between the different cycles. The horizontal elastic stiffness was found essential to obtain similar results. When the stiffness is lower, the horizontal loads become smaller, and the deformation and maximum stress become bigger. When looking at the contact pressure, it can be observed that tensile stresses occur at the support and the interface between the cast elements. The contact face between the interlayers and elements is bonded. In reality, this contact depends on friction and normal forces only. Since the contact pressures are small, it is assumed that the contact pressures will not significantly influence the model. If it does become a problem, a solution could be to use glue at the interface between the elements and interlayers.

To produce a stable bridge, the horizontal stiffness of the bridge must be 10^8 N/mm. This value can be reduced by adding a horizontal deformation as a load scenario before topology optimisation. Due to computer limitations, only one-fourth of the bridge was optimised. Half of the entire bridge should be modelled (in the longitudinal direction) before optimisation to implement the unequal settlement and horizontal deformation into the optimisation process. The line of thrust of the bridge, as shown in Appendix E.3, indicates that the bridge is stable.

Before topology optimisation, the connections were tested with linear analysis. The contact faces 'no separation' were used (no separation and no friction). In reality, there is friction due to the interlayer used. The results from the non-linear analysis show that the deformation of the elements due to asymmetric settlement is different from the deformation from the linear analysis. A smaller height difference between the elements is observed than expected.

In an additional test, the robustness of the bridge is checked. During this analysis, one of the outer elements was left from the model. During this test, the deformation and stresses were still in an acceptable range. This is not the case when the keystone breaks since this makes the structure unstable. However, since the keystone is a massive element and mainly in compression, structural failure is not expected.

Part 4

Conclusion, Discussion and Recommendations

The goal of this research is to show how a cast glass pedestrian bridge can be designed. The main research question is as follows:

How can a virtually monolithic glass pedestrian bridge be designed and constructed feasibly by using topology optimisation while considering external influences?

Six sub-questions are answered to obtain the answer for the main research question.

SQ1: What are the characteristic properties of glass, and how can it be used as a structural material in a cast glass structure?

Glass is a brittle material with a low capacity for tensile stresses and a high capacity for compressive stresses. When glass is used in large quantities with large cross-sections, the annealing process can take a long time and require a significant amount of energy.

In this thesis, a design is made for a bridge with a cast glass support structure and a float glass bridge deck. Borosilicate glass is used for the cast support structure since it has an excellent thermal shock performance and a shorter annealing time than soda-lime glass. Soda-lime is used for the float glass bridge deck because of its higher strength.

The maximum cross-section for the cast support structure is set at 210 mm, resulting in an approximate annealing time of one month. Sharp edges and corners are avoided to reduce unequal cooling and reduce the risk of too high internal stresses. Additionally, elements with small cross-sections are removed during the design phase, and the material gradually changes to reduce internal stresses. A polyurethane layer is used as an interlayer between cast elements.

SQ2: What are the fundamental principles of additive manufacturing, and how can it be used for glass structures?

Additive manufacturing, also known as 3D printing, produces shapes by depositing material layer by layer. 3D printing glass is still in its infancy, causing limitations on an element's maximum size and transparency. Therefore, the choice is made to use kiln casting in combination with 3D printed sand moulds with an inorganic binder. This type of mould performs best for a topology optimised design. The 3D printed sand mould needed during casting is divided into multiple pieces. The largest sand printer on the market can create elements with an accuracy in the range of 0.2 mm with a maximum dimension of 4 meters by 2 meters by 1 meter.

The final mould is divided at strategic places into 10 pieces. Interlocking nodes are added to connect the different parts of the mould. Additionally, a pouring cup, vent pipes, and risers should be added to the mould design. Fragile elements are removed from the structure during the design phase: geometric features are minimal 20 mm, and the minimum wall thickness of the mould is 4 mm.

SQ3: What are the fundamental principles of topology optimisation, and how can it be used for glass structures?

When using topology optimisation, the material is automatically added and removed based on an objective function. The objective function used for most topology optimisation problems is to minimise the weight or compliance of an element with stress or volume restrictions. An approach that considers the difference between tensile and compressive strength is not yet successfully implemented. Only the maximum tensile stress could be used during a stress-based optimisation with glass as the material, resulting in a structure that does not fully utilise its compressive strength. Compliance-based optimisation is better for glass since it results in a design that uses the compressive capacity of the glass more beneficially. For this method the stresses must be checked at the end of each optimisation and more post-processing is needed.

The most implemented optimisation methodologies are Solid Isotropic Material with Penalization, Level Set, and Bidirectional Evolutionary Structural Optimisation. The Level Set method is found to be most suitable and is used during the design phase of the bridge.

SQ4: What are the structural design principles of the new pedestrian bridge made from cast glass?

Glass is a brittle material with a low tensile strength compared to its compressive strength. An arch bridge is the only bridge type that can be executed entirely in compression, without pre-tensioning. The requirements on the bridge design are based on the dimensions of the current bridge. Additionally, the maximum dimension of a truckload (13.6 m x 2.48 m x 2.5 m) and the maximum hoist capacity of a crane (3t) are considered. Furthermore, the design is made so that maintenance to the waterway is possible. For the maintenance, a clear width is needed of 3.1 m and a clear height of 1 m. The design life of the bridge is 50 years with consequence class 3. The loads considered during structural analysis are the deadweight, vertical traffic load (distributed and point), and vertical wind load.

SQ5: How does the weather affect the bridge, and how should this be incorporated in the bridge's design?

The bridge is made from borosilicate glass. This type of glass is used to reduce the effect of temperature on the cast structure of the bridge. Supports and connections are designed in such a way that they do not restrain the deformation from temperature. The parallel and perpendicular loads from the wind are not considered during the design phase of the bridge because they are negligible compared to the structure's weight.

Due to the rain or snow, the bridge might become slippery. Therefore, on the sacrificial layer, a ceramic fritted pattern is added to increase the slip resistance. In addition, a sealant is used that is suitable for outdoor use to prevent the ingress of moisture between the elements. The sealant and the interlayer used are: UV-light resistant, water-resistant, slow-burning, and have an operating temperature between -20°C and 50°C.

SQ6: Which type of topology optimisation and which software is most suitable for designing a glass bridge, and how are this type and software used for the final design?

Plug-ins for McNeel Rhinoceros/Grasshopper and the software package Ansys are compared. This comparison shows that Ameba, one of the plug-ins, is the best available plugin for topology optimisation but is unsuitable to use for glass structures. The main reason for this is because it is not possible to add a cross-sectional constraint to the optimisation process. The Trade-off matrix that followed from comparing the different tools resulted in Ansys being the most suitable software for designing the cast glass bridge.

Ansys Workbench 2019 R3 mechanical is used during finite element analysis and topology optimisation. The implemented application Ansys Spaceclaim is used as pre- and post-processor. During the design phase of the glass bridge, the compliance-based objective function and Level Set method was used. This method results in an optimised design with clear edges and smooth contours. When using the Level Set method in Ansys, all mesh elements should have a tetrahedral shape. Implementing a maximum member size requires a mesh density that is 4.4 times finer than its maximum member. Before the optimisation process, only linear contacts can be used, such as 'bonded' or 'no separation' contacts, and only fixed joints can be used during structural analysis. Thermal loads cannot be used as input for topology optimisation in Ansys.

In the first variant study, multiple 2D shapes are optimised to determine which shape is most suited for the bridge's final design. The second variant study focuses on the 3D shape of the bridge and how the bridge is split into multiple segments. The weight of the final optimised bridge is reduced by 65%. Due to symmetry in the design, it was possible to limit hardware requirement. During the optimisation, seven different load scenarios are implemented, and for the point load, a region is excluded from optimisation. It is not possible to implement unequal settlement to the bridge before optimisation since only one-fourth of the bridge is optimised. After optimisation, linear and non-linear finite element analysis showed that the structure is safe. The model used for non-linear analysis is presented in Figure 10.1.
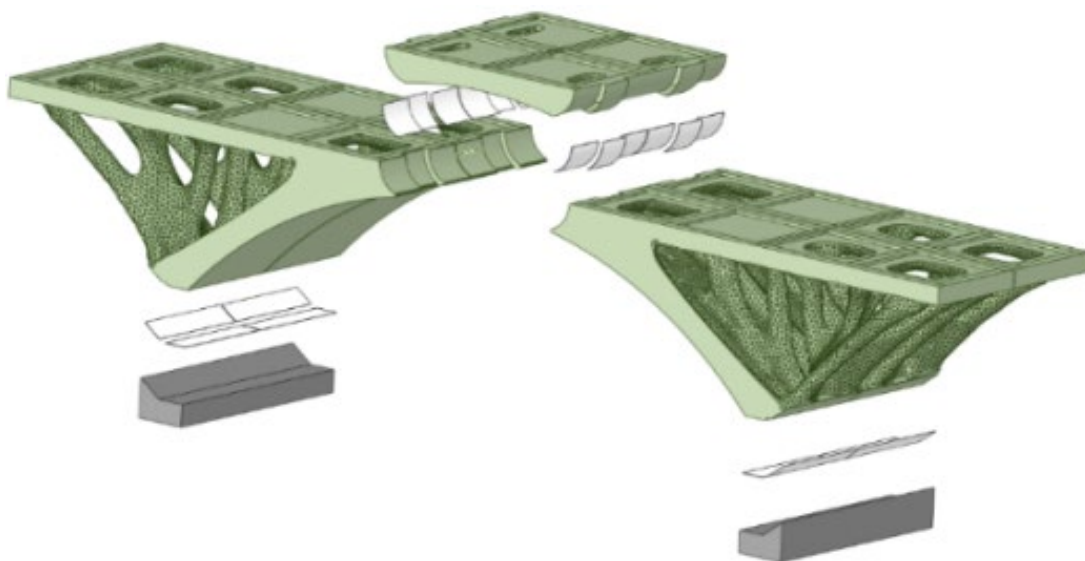

Figure 10.1 Exploded view of the model used during non-linear structural analysis.

In the sections below, the topics: material, topology optimisation, bridge design, and experimental validation are discussed.

11.1 Material

In the past decades, an increasing number of structures have been designed and built using glass as a structural component. Glass is a suitable material for the building industry due to its translucent property and refraction of light. The focus of this thesis is on solid cast glass elements. The main reason to focus on this production method is the possibility to use glass in different shapes and sizes.

Borosilicate glass is used for the cast support structure. This type of glass has the advantage of having a shorter annealing time than soda-lime glass, and the expansion and shrinkage are lower than soda-lime glass. Predicting the annealing time is not a straightforward process and depends on different conditions, which might result in a longer annealing time as expected. The thermal expansion and shrinkage of the bridge could be significant, even more, when using soda-lime glass during casting. When these aspects can be better predicted, it might be interesting to explore the use of soda-lime glass.

Creating a topology optimised bridge via a different production process or with another material, results in a different final design. An advantage of these alternative methods is the lack of limitations caused by the annealing time and the reduced cost due to the more straightforward production process.

11.2 Topology optimisation

During the design phase of the bridge, topology optimisation was used to obtain a more optimal structure by reducing its weight and changing the material distribution. It was found that when optimisation is done on multiple load cases instead of a single load case, the optimisation process is more challenging. The process with multiple load cases requires a more creative approach for implementing the different load cases and requires a higher computational capacity. The optimal solution is not found during this process. However, the new design is more feasible to produce and uses the material more efficiently than before optimisation.

For topology optimisation with a stress constraint, it is not yet possible to distinguish between the tensile and compressive strength of a material. Stress based optimisation might not be beneficial for structures that can be loaded in many different ways. Many different load scenarios would result in an unmanageable large model, especially when point loads are considered. With compliance-based optimisation, this is a less significant problem. However, more time is required for checking the stresses and post-processing at the end of each optimisation process.

11.3   Bridge design

Arch shaped bridges are better in transferring loads to the supports via compression compared to other bridge topologies. In this thesis, a circular shaped arch is used in the design. During structural validation, it is found that the horizontal elastic supports of the bridge needs to be high to ensure the stability of the bridge. This stability could be increased by changing the shape of the arch, the location of the supports, the shape of the connections, the material used in the connections, and by adding material to move the centre of gravity of the outer elements towards the supports.

A sacrificial layer is added to the bridge deck. This measure ensures the bridge's safety in case of too high impact loads on the top surface. The bridge is located in a park above a waterway that is not accessible for boats (only for maintenance boats). Therefore, a collision of a boat with the bridge is not expected. Additionally, a barrier prevents vehicles from passing the bridge. In the unlikely event of a collision where one of the outer elements entirely breaks, the remaining structure does not collapse. This is not the case when the keystone breaks since this makes the structure unstable. However, since such an event is improbable and the keystone is a massive element mainly in compression, structural failure is not expected.

11.4   Experimental validation

Due to time limitations and restrictions on lab work, it was not possible to do experiments to validate the structural behaviour and production method. However, from previous research, it can be concluded that additive manufactured sand moulds is a promising type of mould for cast glass. Nevertheless, it is doubtful whether elements with the dimensions required for the designed pedestrian bridge (4 m x 1 m x 1.5 m) will ever be cast in glass. However, the process followed in this thesis shows that a topology optimised cast bridge can be designed that fulfils all constraints.

Several gaps are found in the knowledge surrounding topology optimised cast glass structures that require further research. These are:

- A topology optimisation method should be developed that takes into account the difference between tensile and compressive strength. When using compliance-based optimisation, the optimised element does not fully utilize the compressive strength of the glass. By implementing the different strengths, glass could be used in a more advantageous manner.

- Combining glass with additional materials such as steel is an interesting topic to research. For instance, the steel could be implemented as a second load path or used to prestress the glass. A safer element could be obtained this way that uses more of the compressive strength of glass.

- 3D printed sand moulds should be further researched. This should include flow analysis of glass inside the mould and how the glass shrinks when cooled. By knowing the behaviour of glass inside the mould, the design of the element and the mould could be modified to make the casting process better. Additionally, research should be performed to determine the surface finish resulting from different coatings. A bad surface finish after casting requires significant post-processing to obtain a smooth and transparent element.

- For large cast elements, a good way to estimate annealing time is missing and requires further research. The annealing time of an element is difficult to predict. Since the material is not entirely equally distributed, the annealing process could take more time than expected.

- More research should be done on the thermal expansion and shrinkage of optimised cast components. A thermal load is more crucial for elements made from soda-lime glass than from borosilicate glass. Since the cross-sections are not equal, the expansion and shrinkage could be a problem.

- A strategy should be found to implement an unequal settlement and horizontal support stiffness before topology optimisation. Doing this results in a bridge that needs a lower elastic horizontal support and can better withstand unequal settlement.

- Creating a topology optimised bridge via a different production process or with another material should be researched. Changing the production process or material will result in a different final design. An advantage of these alternative methods can be that there are no limitations caused by the annealing time. When using float glass for the main structural components the most important limitation is the maximum number of layers that can be laminated. When using concrete as loadbearing material, adding reinforcement is simpler, resulting in a more slender structure with a larger flexural strength and higher redundancy.

- Experiments should structurally validate the optimised design of the bridge. This includes validation of the stresses inside the bridge, on the connections, and on the structure's dynamics.

Abbey, T. (2017). Topology Optimization Methods. Retrieved from https://www.digitalengineering247.com/article/topology-optimization-methods/

abc.net.au. (2021). Glass bridge in China shatters, leaving tourist trapped partway across. Retrieved from https://www.abc.net.au/news/2021-05-10/tourist-in-china-left-trapped-after-glass-bridge-shatters/100128310

Albeck-Ripka, L. (2021). A Glass Bridge. Gale-Force Winds. A Moment of Terror High in the Air. *The New York Times*. Retrieved from https://www.nytimes.com/2021/05/11/world/asia/china-glass-bridge-stranded.html

Aurik, M. (2017). *Arched Glass Masonry Bridge.* (Master of Science). Delft University of Technology Delft.

Aurik, M., Snijder, A., Noteboom, C., Nijsse, R., & Louter, C. (2018). Experimental analysis on the glass-interlayer system in glass masonry arches. *Glass Structures & Engineering, 3*(2), 335-353. doi:10.1007/s40940-018-0068-7

Baumgartner, A., Harzheim, L., & Mattheck, C. (1992). SKO (soft kill option): the biological way to find an optimum structure topology. *International Journal of Fatigue, 14*(6), 387-393. doi:https://doi.org/10.1016/0142-1123(92)90226-3

Belblidia, F., & Bulman, S. (2002). A hybrid topology optimization algorithm for static and vibrating shell structures. *International Journal for Numerical Methods in Engineering, 54*, 835-852. doi:10.1002/nme.450

Bendsøe, M. P., & Kikuchi, N. (1988). Generating optimal topologies in structural design using a homogenization method. *Computer Methods in Applied Mechanics and Engineering, 71*(2), 197-224. doi:https://doi.org/10.1016/0045-7825(88)90086-2

Bendsoe, M. P., & Sigmund, O. (2003). *Topology Optimization; Theory, Methods and Applications*. Berlin/Heidelberg Germany: Springer-Verlag.

Berg, C. (2015). *Brief Dutch Design Manual for Bicycle and Pedestrian Bridges*. Delft: IPV Delft.

Bhatia, I. (2019). *Shaping transparent sand in sand.* (MSc). Delft University of Tehnology Delft.

Bialkowski, S. (2017). *tOpos GPGPU Accelerated Structural Optimisation Utility for Architects.* Paper presented at the eCAADe.

Bristogianni, T., Oikonomopoulou, F., Yu, R., Veer, F. A., & Nijsse, R. (2020). Investigating the flexural strength of recycled cast glass. *Glass Structures & Engineering, 5*(3), 445-487. doi:10.1007/s40940-020-00138-2

Buchanan, C., & Gardner, L. (2019). Metal 3D printing in construction: A review of methods, research, applications, opportunities and challenges. *Engineering Structures, 180*, 332-348. doi:https://doi.org/10.1016/j.engstruct.2018.11.045

Bullseyeglass. (2009). *Monitoring Kiln Temperatures for Successfull Annealing* Retrieved from https://www.bullseyeglass.com/images/stories/bullseye/PDF/TechNotes/technotes_07.pdf

Chicago. (n.d.). Millennium Park — Crown Fountain Facts & Figures. Retrieved from https://www.chicago.gov/city/en/depts/dca/supp_info/millennium_park_-crownfountainfactsfigures.html

Clayton, R. (n.d.). Slip Resistant Options for Walk on Glass. Retrieved from https://technical.iqglassuk.com/technical-advice/slip-resistant-options-walk-on-glass/

Collins, C. (2018). Autodesk Teams Up with NASA's Jet Propulsion Laboratory to Explore New Approaches to Designing an Interplanetary Lander. Retrieved from https://adsknews.autodesk.com/news/nasas-jet-propulsion-lab-teams-autodesk-explore-new-approaches-designing-interplanetary-lander

Cummings, K. (2001). *Techniques of kiln-formed glass*. London/Philadelphia, UK/USA: A&C Black Publishers Limited/University of Pennsylvania Press.

Curbell Plastics. (2021). SentryGlas® XTRA™ Data Sheet (at Curbell Plastics). In C. Plastics (Ed.).

Damen, W. (2019). *Topologically Optimised Cast Glass Grid Shell Nodes: Exploring Topology Optimisation as a design tool for Structural Cast Glass elements with reduced annealing time.* (MSc Master thesis). Delft University of Technology, Delft. Retrieved from http://resolver.tudelft.nl/uuid:2afbfe96-c9bf-44d7-bfaa-d8a710fa1ce2

Dillenburger, B., & Hansmeyer, M. (2013). *The Resolution of Architecture in the Digital Age.* Paper presented at the International Conference on Computer Aided Architectural Design Futures Shanghai, China.

DSV Global Transport and Logistics. (n.d.). What are the flatbed trailer dimensions? Retrieved from https://www.dsv.com/en/our-solutions/modes-of-transport/road-transport/trailer-sizes/open-trailer

Engelsmann Peters. (2008). Seele all-glass bridge. Retrieved from https://www.engelsmannpeters.de/en/portfolio_page/seele-ganzglasbruecke/

esmadrid. (2004). Monument to the Victims of 11-M. In. Madrid: esmadrid.

Freiman, S. (2007). *Global roadmap for ceramics and glass technology*. Hoboken, New Jersey: John Wiley & Sons, Inc. .

Fuji, K. (2013). Optical Glass House / Hiroshi Nakamura & NAP. In: Nacasa & Partners Inc. .

Galjaard, S., Hofman, S., Perry, N., & Ren, S. (2015). *Optimizing Structural Building Elements in Metal by using Additive Manufacturing*.

Gemeente Delft. (2019). *Ontwerpspecificatie standaard bruggen delftse stijl* Delft: Gemeente Delft

GMTO. (2020). Giant Magellan Telescope, primary mirror. Retrieved from https://www.gmto.org/resources/

Hackney, P., & Wooldridge, R. (2017). Optimisation of Additive Manufactured Sand Printed Mould Material for Aluminium Castings. *Procedia Manufacturing, 11*, 457-465. doi:10.1016/j.promfg.2017.07.136

Hailu Shimels, G., Dereje Engida, W., & Fakhruldin Mohd, H. (2017). A comparative study on stress and compliance based structural topology optimization. *IOP Conference Series: Materials Science and Engineering, 241*, 012003. doi:10.1088/1757-899x/241/1/012003

Haldimann, M., Luible, A., & Overend, M. (2008). *Structural Use of Glass*. Zurich, Switzerland: IABSE-AIPC-IVBH.

Hartsuijker, C., & Welleman, H. (2009). *Introduction to continuum mechanics* [7](pp. 79). Retrieved from http://icozct.tudelft.nl/TUD_CT/CT4145/collegestof/files/CT4145Lecture_Notes-version7.pdf

Heugten, R. (2013). *Load-bearing glass columns: the stacked column.* (Master). TU Eindhoven, Eindhoven.

Hoogenboom, P. C. J. (2014). *Shell analysis course handout*

Hummel, K. (2018). Leidse Catharinabrug aan de Aalmarkt door DP6 wint internationale betonprijs. In Aalmarkt-Leiden-25-08-2017_0035-HR-bewerkt-1024x367.jpg (Ed.): de Architect

IAAC. (2017). 3D printed bridge. In.

Inamura, C. (2020). *Glass Additive Manufacturing.* Paper presented at the Challenging Glass Ghent University.

Institution of Structural Engineers. (2014). Structural Use of Glass in Buildings (2nd Edition). In: Institution of Structural Engineers.

Jiang, L., & Chen, S. (2017). Parametric structural shape & topology optimization with a variational distance-regularized level set method. *Computer Methods in Applied Mechanics and Engineering, 321*, 316-336. doi:https://doi.org/10.1016/j.cma.2017.03.044

Jipa, A., Bernhard, M., Meibodi, M., & Dillenburger, B. (2016). *3D-Printed Stay-in-Place Formwork for Topologically Optimized Concrete Slabs*. Paper presented at the TxA Emerging Design + Technology, San Antonio, Texas, USA.

Klein, J., Stern, M., Franchin, G., Kayser, M., Inamura, C., Dave, S., . . . Oxman, N. (2015). Additive Manufacturing of Optically Transparent Glass. *Mary Ann Liebert, Inc., 2*. doi: 10.1089/3dp.2015.0021

Leary, M., Merli, L., Torti, F., Mazur, M., & Brandt, M. (2014). Optimal topology for additive manufacture: A method for enabling additive manufacture of support-free optimal structures. *Materials & Design, 63*, 678-690. doi:https://doi.org/10.1016/j.matdes.2014.06.015

Lehman, R. (n.d.). The mechanical properties of glass In.

Li, Z. (2020). Jue Chair. Retrieved from https://www.bilibili.com/s/video/BV1ZK4y1a7ER

Matthews, D. (2017). Crown Fountain Through The Years In: DNAinfo.

McLellan, G. W., & Shand, E. B. (1984). *Glass Engineering Handbook*. United States of America: McGrawHill.

Meibodi, Giesecke, R., & Dillenburger, B. (2019). *3D printing sand molds for casting bespoke metal connections.* Paper presented at the Intelligent and Informed - Proceedings of the 24th International Conference on Computer-Aided Architectural Design Research in Asia, CAADRIA 2019.

Meibodi, Jipa, A., Giesecke, R., Shammas, D., Bernhard, M., Leschok, M., . . . Dillenburger, B. (2018). *Smart slab: Computational design and digital fabrication of a lightweight concrete slab.* Paper presented at the Recalibration on Imprecision and Infidelity - Proceedings of the 38th Annual Conference of the Association for Computer Aided Design in Architecture, ACADIA 2018.

Mirzendehdel, A., Rankouhi, B., & Suresh, K. (2017). Strength-Based Topology Optimization for Anisotropic Parts. *Additive Manufacturing, 19*. doi:10.1016/j.addma.2017.11.007

MIT Media Lab. (n.d.). GLASS II Architectural-Scale Glass 3D Printing. Retrieved from https://mediatedmattergroup.com/glass-ii

MX3D. (n.d.). MX3D Bridge. Retrieved from https://mx3d.com/projects/mx3d-bridge/

Naous, D. (2020). *Topologically Optimised Cast Glass Shell.* (MSc.). Delft University of Technology, Delft.

Oikonomopoulou, F. (2019). *Unveiling the third dimension of glass: Solid cast glass components and assemblies for structural applications.* (Doctor). Delft University of Technology, Delft. Retrieved from http://resolver.tudelft.nl/uuid:16f1560f-1739-492c-bd95-3f47bf096182

Oikonomopoulou, F. (2020). *Guidelines for the structural calculation of glass structures*

Oikonomopoulou, F., Bristogianni, T., Barou, L., Veer, F. A., & Nijsse, R. (2018). The potential of cast glass in structural applications. Lessons learned from large-scale castings and state-of-the art load-bearing cast glass in architecture. *Journal of Building Engineering, 20*, 213-234. doi:https://doi.org/10.1016/j.jobe.2018.07.014

Pereira, T., Kennedy, J. V., & Potgieter, J. (2019). A comparison of traditional manufacturing vs additive manufacturing, the best method for the job. *Procedia Manufacturing, 30*, 11-18. doi:https://doi.org/10.1016/j.promfg.2019.02.003

Querin, O. M., Victoria, M., Alonso, C., Ansola, R., & Martí, P. (2017). *Topology design methods for structural optimization*. Oxford: Academic Press.

Rael, R., & Fratello, V. S. (2014). Quake Column & Involute Wall.

Richards, B., & Gilbert, D. (2006). *New Glass Architecture*: Laurence King.

Rippmann, M., Liew, A., Van Mele, T., & Block, P. (2018). Design, fabrication and testing of discrete 3D sand-printed floor prototypes. *Materials Today Communications, 15*, 254-259. doi:10.1016/j.mtcomm.2018.03.005

Rubem, O., Montedo, O., Hotza, D., Oliveira, A., Meszaros, R., Travitzky, N., & Greil, P. (2012). Crystallisation Kinetics of a -Spodumene-Based Glass Ceramic. *Advances in Materials Science and Engineering 4.*

(2009). *STRESS, OUT! Avoiding painful breaks and strains* [

Scagliola, D., & Brakkee, S. (2019). MVRDV's transparent brick store in amsterdam re-opens for Hermès. In: desinboom.
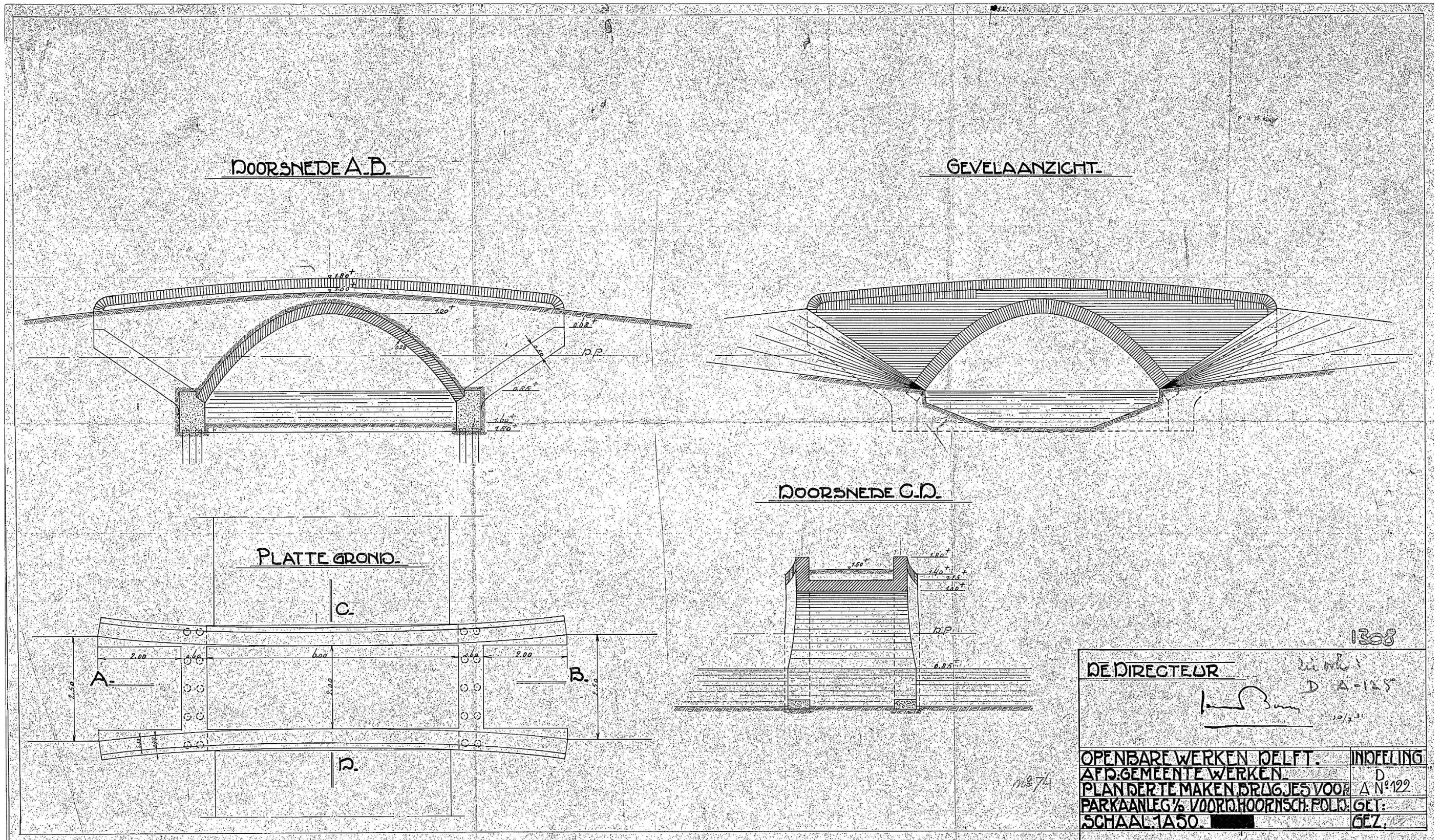
Sedak. (2018). Glass laminate of superlatives. Retrieved from https://www.sedak.com/fileadmin/user_upload/news/Pressemitteilungen/Englisch/2018061 9_PM_Glasstec_2018_EN.pdf

Smit, R. (Producer). (2020). Delftse mysteries: Hoeveel bruggen zijn er precies in Delft? Retrieved from https://indebuurt.nl/delft/genieten-van/mysteries/delftse-mysteries-hoeveel-bruggen-zijn-er-precies-in-delft~101512/

Snijder, A. H., Nijsse, R., & Louter, C. (2018). The glass truss bridge. *Heron, 63*(1/2), 139-157. Retrieved from http://heronjournal.nl/63-12/7.pdf

Snijder, A. H., van der Linden, L. P. L., Goulas, C., Louter, C., & Nijsse, R. (2020). The glass swing: a vector active structure made of glass struts and 3D-printed steel nodes. *Glass Structures & Engineering, 5*(1), 99-116. doi:10.1007/s40940-019-00110-9

Spoorzone, D. (n.d.). Projectgeschiedenis Spoorzone Retrieved from https://www.spoorzonedelft.nl/

Starink, P. (2016). Rode stalen draagconstructie Symbiobrug. *Architectuur NL*. Retrieved from https://www.architectuur.nl/nieuws/rode-stalen-draagconstructie-symbiobrug/

Stefanaki, M. (2020). *Glass Giants: Mass-optimized massive cast glass slab.* (MSc). Delft University of Technology, Delft.

Suzuki, K., & Kikuchi, N. (1991). A homogenization method for shape and topology optimization. *Computer Methods in Applied Mechanics and Engineering, 93*(3), 291-318. doi:https://doi.org/10.1016/0045-7825(91)90245-2

Tektoniek. (2016). Catharinabrug leiden. Retrieved from https://www.tektoniek.nl/evenementen/catharinabrug-leiden

Toetenel, C. (2020). Stop de verloedering van het Wilhelminapark! . *Delft op Zondag*. Retrieved from https://www.delftopzondag.nl/nieuws/algemeen/92091/-stop-de-verloedering-van-het-wilhelminapark-

Vantyghem, G., De Corte, W., Shakour, E., & Amir, O. (2020). 3D printing of a post-tensioned concrete girder designed by topology optimization. *Automation in Construction, 112*, 103084. doi:https://doi.org/10.1016/j.autcon.2020.103084

Veer, F., & Rodichev, Y. (2011). The structural strength of glass: Hidden damage. *Strength of Materials, 43*, 302-315. doi:10.1007/s11223-011-9298-5

Vogel, W. (1994). *Glass Chemistry*. Berlin and Heidelberg GmbH & Co. .

Voxeljet, A. G. (n.d.). Additive manufacturing of sand casting molds Retrieved from https://www.voxeljet.com/anwendungen/sandguss/

Wang, M., Wang, X., & Guo, D. (2003). A level set method for structural topology optimization. *Computer Methods in Applied Mechanics and Engineering, 192*, 227-246. doi:10.1016/S0045-7825(02)00559-5

Watson, D. M. (1999). Practical Annealing by Dan Watson. Retrieved from http://www.gafferglass.com/technical/practical-annealing-by-dan-watson/

Wilde, A. (2018). Catharinabrug Leiden door DP6 wint internationale betonprijs. *de Architect* Retrieved from https://www.dearchitect.nl/techniek/nieuws/2018/11/catharinabrug-leiden-door-dp6-wint-internationale-betonprijs-101202326?_ga=2.39923429.632055215.1598860660-1925493722.1596628720

Wurm, J., & Peat, R. (2007). *Glass Structures: Design and Construction of Self-supporting Skins*: Boston.

Xia, L., Xia, Q., Huang, X., & Xie, Y. M. (2018). Bi-directional evolutionary structural optimization on advanced structures and materials: a comprehensive review. *Archives of Computational Methods in Engineering, 25*(2), 437-478.

Xie, Y. M., & Steven, G. P. (1997). *Evolutionary Structural Optimization*. London: Springer.

Appendix

(Gemeente Delft, 2020)

DOORSNEDE A.B.

GEVELAANZICHT.

DOORSNEDE C.D.

PLATTE GROND.

DE DIRECTEUR

OPENBARE WERKEN DELFT. | INDEELING
AFD: GEMEENTE WERKEN. | D
PLAN DER TE MAKEN BRUGJES VOOR | A N° 122
PARKAANLEG % VOORD. HOORNSCH. POLD. | GET:
SCHAAL 1A50. | GEZ.

B. Strength, deflection, loads

B.1 Calculation maximum strength and deflection

A distinction is made between the float glass top layer made from heat strengthened soda lime float glass and the cast glass supporting structure made from borosilicate glass.

B.1.1 Float glass top layer

The float glass top layer is heat strengthened with rounded corners. The flexural strength for this type of glass can be calculated with equation B.1 from NEN 2608:2014.

$$f_{mt;u;d} = \frac{k_a \cdot k_e \cdot k_{mod} \cdot k_{sp} \cdot f_{g;k}}{\gamma_{m;A}} + \frac{k_e \cdot k_z \cdot (f_{b;k} - k_{sp} \cdot f_{g;k})}{\gamma_{m;V}} \tag{B.1}$$

where:

$k_a = 1.0$ Factor for surface effect, which for concentrated loads and all other situations is taken to be equal to 1.

$k_e = 1.0$ Edge quality factor for fully tempered glass loaded in plane

$k_{mod} = 0.29$ Factor for load time which is 0.29 for floors and balconies that have corrosion constant C = 16

$k_{sp} = 1.0$ Factor for surface structure which is 1.0 for float glass

$k_z = 0.9$ Factor dependant on the zone of the pane. For fully tempered glass, this factor is equal to 0.9

$f_{g;k} = 45 \ N/mm^2$ Characteristic value for flexural strength of float glass

$f_{b;k} = 120 \ N/mm^2$ Characteristic value for flexural strength of fully tempered float glass.

$\gamma_{m;A} = 1.8$ Material factor for glass

$\gamma_{m;V} = 1.2$ Material factor for pre-tensioned glass

When filling in these values into (B.1) the following flexural strength is obtained.
$$f_{mt;u;d} = 63.5 \ N/mm^2$$

B.1.2 Cast glass

The flexural strength for cast glass is obtained similarly as described in section B.1.1. Since borosilicate glass is used during casting and the equations given in NEN2608:2014 for calculating bending-tensile strength are based on float glass, this strength gives a rough estimation only.

$$f_{mt;u;d} = \frac{k_a \cdot k_e \cdot k_{mod} \cdot k_{sp} \cdot f_{g;k}}{\gamma_{m;A}} \tag{B.2}$$

where:

$k_a = 1.0$ Factor for surface effect, since the connecting area between the cast glass with the top layer is relatively small, it is assumed that this factor is equal to 1.0.

$k_e = 1.0$ Factor for edge quality, since the edge quality does not apply to cast glass, it is assumed that this factor equals 1.0.

$k_{mod} = 0.29$	Factor for load time which is 0.29 for floors and balconies that have corrosion constant C = 16
$k_{sp} = 0.8$	Factor for surface structure. This factor is lower for cast glass than float glass and is assumed to be comparable to figure glass.
$f_{g;k} = 35\ N/mm^2$	Value for flexural strength for borosilicate glass is assumed to be 10 N/mm^2 lower for borosilicate glass. This assumption is based on the values given in (Bristogianni, Oikonomopoulou, Yu, Veer, & Nijsse, 2020)
$\gamma_{m;A} = 1.8$	Material factor for glass.

When filling in these values into (B.2), the following flexural strength is obtained.

$f_{mt;u;d} = 4.5\ N/mm^2$

B.1.3 Maximum deflection

The maximum allowable deflection according to NEN 2608:2014 for laminated glass for an unsupported edge must satisfy the following inequality:

$$u_{max} \leq L_z/100 \qquad \text{(B.3)}$$

where:

$$L_z = length\ of\ the\ unsupported\ edge$$

For the middle of the glass, the following condition should be fulfilled:

$$u_{dia,max} \leq \frac{L_{dia}}{65} \leq 50 \qquad \text{(B.4)}$$

where:

$$L_{dia} = length\ of\ the\ largest\ diagonal$$

The overall deflection should not succeed the following inequality:

$$u_{max} \leq L/250 \qquad \text{(B.5)}$$

where:

$$L = length\ of\ the\ unsupported\ part\ or\ length\ of\ the\ bridge$$

With a four-sided line supported float glass top pane, the maximum deflection can be calculated with (B.4) and results in a maximum deflection of:

$$u_{dia,max} \leq \frac{L_{dia}}{65} \leq 50 \quad \text{with:} \quad L_{dia} = \sqrt{1000^2 + 1000^2} = 1414.2\ mm$$

$$u_{dia,max} = \frac{1414.2}{65} = 21.8\ mm$$

The maximum deflection of the entire bridge can be calculated with (B.4). With a span of 6 meters, the maximum deflection is equal to:

$$u_{max} = \frac{6000}{250} = 24\ mm$$

B.2 Actions on a pedestrian bridge

For the design of the bridge, the Eurocodes and the Dutch National Annex is used. The permanent load, traffic load, wind load, and temperature load is considered. The design life of the bridge is 50 years, and a consequence class of 3 is assumed.

B.2.1 Loads on a bridge

It is assumed that the bridge, in this case, is not accessible for maintenance vehicles and emergency services. A barrier should be added to prevent vehicles from passing the bridge. The horizontal force caused by people walking over the bridge should be considered and is 10% of the total distributed load. There is also a dynamic load that is caused by people or by the wind. The dynamic load caused by people and by wind is negligible due to the small size of the bridge and its high dead weight compared to its slenderness. Because of this, the dynamic loads are not considered.

B.2.1.1 Permanent load

The only permanent load on the bridge is the self-weight. For the top layer, this can be calculated with $g_{k;toplayer}$ and for the cast glass structure, this can be calculated with $g_{k;cast}$.

$$g_{k;toplayer} = 24.6 \cdot 0.036 = 0.89 \ kN/m^2 \qquad \text{(for 2 panes with t = 15 mm and 1 pane}$$
$$\text{with t = 6 mm)}$$

$$Q_{k;cast} = 22.3 \cdot Volume \qquad kN$$

B.2.1.2 Traffic load

Two load cases must be considered. The third load case, which is caused by service vehicles, is not considered. The traffic load is determined according to NEN-EN 1991-2+C1:2015:

The first load case is a horizontal distributed load with a horizontal load corresponding to 10% of the vertical load.

$$q_{fk;vertical} = 5 \ kN/m^2$$
$$q_{fk;horizontal} = 0.5 \ kN/m^2$$

The second load case is a concentrated load applied on an area of 100 mm x 100 mm and must be considered when regarding local effects.

$$Q_{fvd;vertical} = 10 \ kN$$

B.2.1.3 Wind load

The wind load is determined according to NEN-EN 1991-1-4+A1+C2:2011/NB:2019+C1:2020. The wind loads for the different directions are given in Table B.1.

$$F_{wind} = \frac{1}{2} \cdot \rho \cdot v_b^2 \cdot C \cdot A_{ref,x} \qquad \text{(B.6)}$$

where

$\rho = air \ density \ (1.25 \ kg/m^3)$
$v_b = basic \ wind \ speed$
$C = wind \ load \ factor$
$A_{ref,x} = reference \ area$

This can be rewritten as:

$$F_{wind} = q_{wind} \cdot A_{ref,x}$$

where

$$q_{wind} = \frac{1}{2} \cdot \rho \cdot v_b^2 \cdot C \tag{B.7}$$

To calculate the basic wind speed v_b, the following equation can be used:

$$v_b = c_{dir} \cdot c_{season} \cdot v_{b,0} \tag{B.8}$$

where

$c_{dir} = 1.0$ (wind direction factor)
$c_{season} = 1.0$ (season factor)
$v_{b,0} = 27 \, m/s$ (windspeed for region 2)

To calculate the wind load factor C, the following equation can be used:

$$C = c_e \cdot c_{f,x} \tag{B.9}$$

where

$c_e = exposure\ factor$

$$c_{f,x} = \begin{cases} 2.2 \ (for\ a\ horizontal\ wind\ load\ perpendicular\ to\ the\ bridge) \\ 0.4 \cdot 2.2 = 0.88 \ (for\ a\ horizontal\ wind\ load\ parrallel\ to\ the\ bridge) \\ \pm 0.9 \ (for\ vertical\ wind\ loads) \end{cases}$$

To calculate the exposure factor c_e, the following equation can be used:

$$c_e = \frac{q_p(z)}{q_b}$$

where

$q_p(z) = 0.58 \, kN/m^2$ (for a bridge located in area 2 that is cultivated, with a height z, lower than 7 m.)

$$q_b = \frac{1}{2} \cdot \rho \cdot v_b^2$$

By using equation (B.6) and (B.7), equation (B.9) can be rewritten as:

$$q_{wind} = q_p(z) \cdot c_{f,x}$$

Table B.1 Distributed wind loads

Direction	$q_{wind} \, [kN/m^2]$
Horizontal, Perpendicular	1.28
Horizontal, Parallel	0.51
Vertical	± 0.52

B.2.1.4 Temperature load

The temperature load is calculated according to NEN-EN 1991-1-5+C1:2011. The temperature load is not specified for glass. However, since the thermal conductivity for glass ($\lambda = 1.14 \, W/mK$ for borosilicate glass and $\lambda = 1.06 \, W/mK$ for soda-lime glass) is comparable with the thermal coefficient of concrete ($\lambda = 1.16 - 1.71 \, W/mK$) it is assumed that the glass bridge behaves similarly as a concrete bridge with deck type three.

The temperature values that should be used in the Netherlands are:

$T_{max} = 30 \, °C$
$T_{min} = -25 \, °C$

For a concrete bridge with deck type three, the following equations apply:
$$T_{e,min} = T_{min} + 8$$
$$T_{e,max} = T_{max} + 2$$

The following equations can be used to calculate the temperature increase or decrease:
$$\Delta T_{N,con} = T_0 - T_{e,min}$$
$$\Delta T_{N,exp} = T_{e,max} - T_0$$
where
$$T_0 = 10\ °C$$

By combining the equations, the following results are obtained:
$$\Delta T_{N,con} = 27\ °C$$
$$\Delta T_{N,exp} = 22\ °C$$

It will most likely happen that temperature differences occur in the vertical direction between the top and bottom of the bridge due to sunlight exposure. For a concrete plate without a wear layer, the following results are obtained:
$$\Delta T_{M,heat} = 15 \cdot 0.8 = 12\ °C$$
$$\Delta T_{M,cool} = 8 \cdot 1.1 = 8.8\ °C$$

The following equations can be used to combine the temperature increase or decrease with the temperature differences between the top and bottom of the bridge. The most adverse effect should be chosen:
$$\Delta T_m + \omega_N \cdot \Delta T_n \qquad or \qquad \omega_M \cdot \Delta T_m + \Delta T_n$$
where
$$\omega_N = 0.35$$
$$\omega_M = 0.75$$
Which gives a maximum temperature increase or decrease that is equal to $\Delta T_{max} = 36\ °C$.
$\Delta T_n = 27\ °C$ in contraction and $\Delta T_m = 0.75 \cdot 12 = 9\ °C$ degrees difference between top and bottom of the deck.

Figure B.1 Loads and zones for horizontal barrier (NEN-EN 1991-1-1)

B.2.1.5 Loads on a railing
The railing consists out of two zones. The height of zone A is defined as 0.1 meters from the top. The point load should be applied on 200 mm x 200 mm at the most unfavourable location

Equally distributed load:	$q_{rep} = 3\ kN/m$	Zone A 5 min
Concentrated load:	$F_{rep} = 1\ kN$	Zone A 5 min
	$F_{rep} = 0.7\ kN$	Zone B 5 min
	$F_{rep} = 0.5\ kN$	Zone A+B for 7*24h

B.2.2 Load combinations
The load combinations are set up according to NEN-EN 1990+A1+A1/C2:2019. A distinction is made between serviceability state and ultimate limit state. With the ultimate limit state partial and combination factors are included. The load combinations can be calculated according to Table B.2

Table B.2 Calculation of load combinations

Permanent load		Dominant variable load	Accompanying loads
Unfavourable	Favourable		
$\gamma_{G,j,sup} G_{k,j,sup}$	$\gamma_{G,j,inf} G_{k,j,inf}$	$\gamma_{Q,1} Q_{k,1}$	$\gamma_{Q,i} \psi_{0,i} Q_{k,i}$

B.2.2.1 Partial factors

The partial factors for a structure with Consequence Class III are given in Table B.3. This consequence class is chosen because a cast glass bridge is a new type of structure, and the collapse of such a bridge would not be beneficial for the development of cast glass structures in the future. The consequence of loss of human life is normal.

Table B.3 Partial factors γ for CC3

Load type	Symbol	Partial factor
Permanent	$\gamma_{G,j,sup}$	1.40
	$\gamma_{G,j,sup}$	1.25
	$\gamma_{G,j,inf}$	0.9
Traffic	$\gamma_{Q,Traffic}$	1.5
Wind	$\gamma_{Q,Wind}$	1.65
Temperature	$\gamma_{Q,Temp}$	1.65

B.2.2.2 Combination factors

Because there are three variable loads and it is unlikely these loads coincide, partial factors should be used. The factors are given in Table B.4.

Table B.4 Combination factors ψ_0

Load type	Symbol	Partial factor
Traffic	$\psi_{0,Traffic}$	0.4
Wind	$\psi_{0,Wind}$	0.3
Temperature	$\psi_{0,Temp}$	0.3

B.2.2.3 Load combinations

The load combinations used during the validation of the topology optimised structure are given in Table B.5.

Table B.5 Load combinations

	Permanent	Traffic	Wind	Temperature
L.C. 1	**1.40**	$1.5 \cdot 0.4$	$1.65 \cdot 0.3$	$1.65 \cdot 0.3$
L.C. 2	1.25	$\mathbf{1.5 \cdot 1.0}$	$1.65 \cdot 0.3$	$1.65 \cdot 0.3$
L.C. 3	1.25	$1.5 \cdot 0.4$	$\mathbf{1.65 \cdot 1.0}$	$1.65 \cdot 0.3$
L.C. 4	1.25	$1.5 \cdot 0.4$	$1.65 \cdot 0.3$	$\mathbf{1.65 \cdot 1.0}$

C. Software research

C.1 Ameba

Ameba is a relatively new topology optimisation tool developed by Xie Technologies. The plugin is based on the Bi-directional Evolutionary Structural Optimisation (BESO) algorithm. There is a discounted student version with the same capabilities as the professional version.

Setting up the design is done in Grasshopper in combination with Rhino (see Figure C.1). Before the optimisation is started, the design space is meshed. This function is embedded in Ameba. When using the mesh function, it is essential to set your computers decimal sign to a point instead of a comma. There are various meshing algorithms implemented in the program. The maximum number of elements for a meshed 2D structure is equal to 500.000, and for a 3D structure, it is equal to
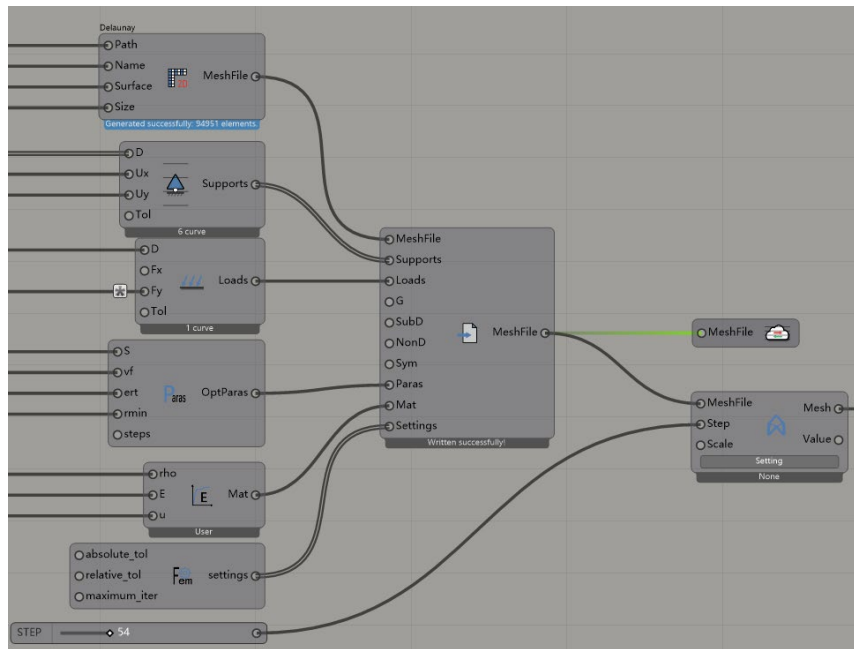

Figure C.1 Setting up design space in Grasshopper

200.000. A point support or plane support can support the structure. No rotational restrictions can be added. A point load, line load, surface load, and domain load can be added to the model. It is not possible to add moments. The plug-in can handle multiple load cases. Additionally, a sub-design domain, non-design domain, and symmetry axis can be added. The optimisation can be done based on Von Mises, Strain Energy Density (compliance), and Frequency.

An advantage of Ameba is the cloud computing function, which gives fast results if the geometry is not too complex. However, still, some deficiencies were found during computation at the time of testing. For example, implementing a railing into the 3D design was found quite tricky, and many times no results were obtained.

After 2D optimisation, the design can be rebuilt to a NURBS surface, and after 3D optimisation, the model can be re-meshed within the plugin. Other functions include simplification of the mesh and smoothing of the mesh.
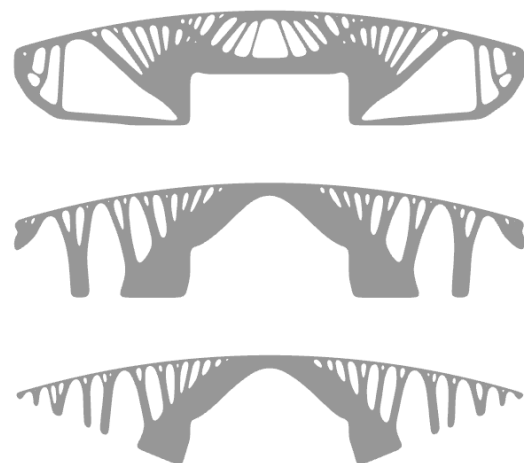

Figure C.2 2D variant study

In Figure C.2, a 2D variant study is given. By changing the boundary conditions, three shapes are obtained. At the opening for boats, the cross-section of the arch is too large. At other points, the cross-section is too small. A disadvantage of Ameba is the lack of cross-sectional constraints. Because of this, it is necessary to do much post-processing after optimisation to obtain a feasible design. After optimisation, it is necessary to export the model to a different program to check the structural capacity. With these 2D designs, it is possible to design a bridge by extruding the 2D design with a glass pane on top of it. Figure C.3 gives an example of such a structure.
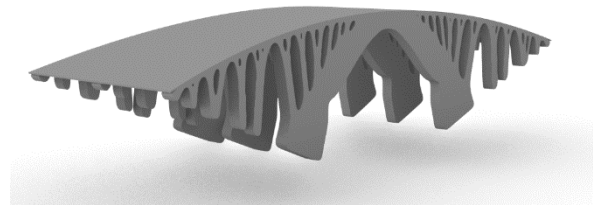

Figure C.3 3D bridge constructed from a 2D topology optimised design.

Various designs were made to test the 3D design function of Ameba. Complicated designs took much time, and some optimisations did not give any result at all. Figure C.4 gives an example of a small topology optimised glass railing design.

Figure C.4 topology optimised railing

Ameba has some great potential to become a good topology optimisation plugin for Grasshopper. At the moment of testing, it has still some problems. Ameba is less suitable for the optimisation of cast glass structures. This is mainly because it is impossible to add rotational constraints to the supports, add bending moments, and add a minimum or maximum cross-sectional constraint.

C.2 Karamba 3D

Karamba3D is developed as a parametric structural engineering tool. With this plugin, it is possible to analyse shells, frames, and trusses. Implemented in this tool are algorithms to optimise cross-sections, beams, and shells. The tool uses BESO during optimisation. Setting up the design is done in Grasshopper in combination with Rhino. With a 2D design, it is possible to optimise on compliance. Different load cases can be added, their influence on an element is added up before optimisation. Since Karamba3D does not have an option to optimise in 3D, it is unsuitable for designing the glass bridge.

C.3 Peregrine

Peregrine has a free non-commercial option of their software for students and lecturers. At the moment of exploring this plug-in, this software is still in development, and lots of features such as multiple domains and buckling are not implemented yet.

Peregrine is an easy to use and fast plug-in for Grasshopper. Setting up the design is done in Grasshopper in combination with Rhino. Before the optimisation is started, the design space is meshed into triangles. This process is not included in the plugin and should be done with other components in Grasshopper. A point load, line load, and surface load can be added to the model. However, it is not possible to add moments. A point support or plane support can support the structure, but no rotational restrictions can be added. The plug-in can handle multiple load cases. However, when using multiple load cases, the behaviour is assumed to be plastic, which means only ductile material can be optimised with multiple load cases. In addition, only CHS sections can be set as section types. The material

properties of this section can be changed. Additionally, predefined user nodes can be added and a joint/cost ratio.

After the optimisation, you can get the nodes, lines, and section sizes. Additionally, the forces are given for each element. Post-processing components are included in the program, including simplification tools, setting a limit for the maximum number of nodes, and the minimum member size. Furthermore, there is a component with which crossover nodes can be modelled and a component with which nodes can be merged.

It is pretty easy to do a parameter study with the number of nodes, different load cases and different supports. In

Gallery information:
Reference vol: 7.3824E-001
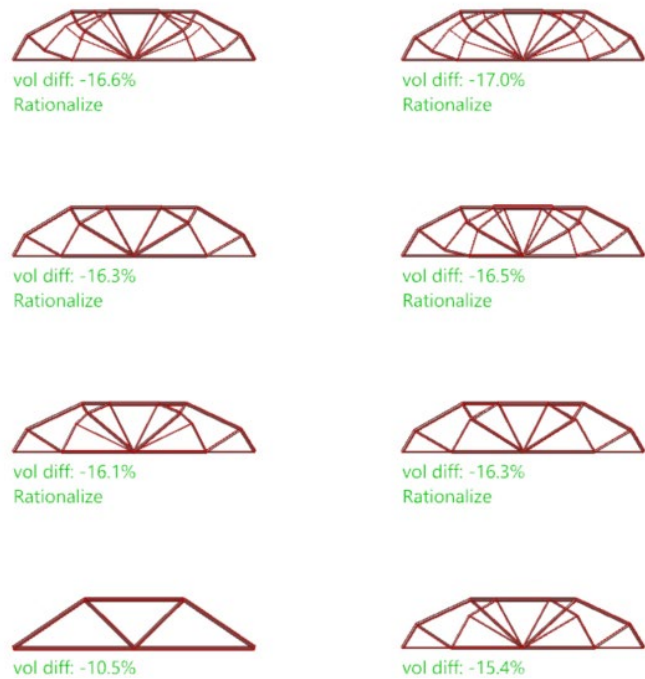Sorting weight: Volume(3), Complexity,(0)

vol diff: -16.6%
Rationalize

vol diff: -17.0%
Rationalize

vol diff: -16.3%
Rationalize

vol diff: -16.5%
Rationalize

vol diff: -16.1%
Rationalize

vol diff: -16.3%
Rationalize

vol diff: -10.5%

vol diff: -15.4%

Figure C.5 Parameter study for a simple supported beam with a point load.

Figure C.5 and Figure C.6, a parameter study and the associated Grasshopper script is given. After optimisation, it is possible to post-process the design and to see the forces in each bar. Manual post-processing needs to be done to make the structure producible (for example designing the nodes).
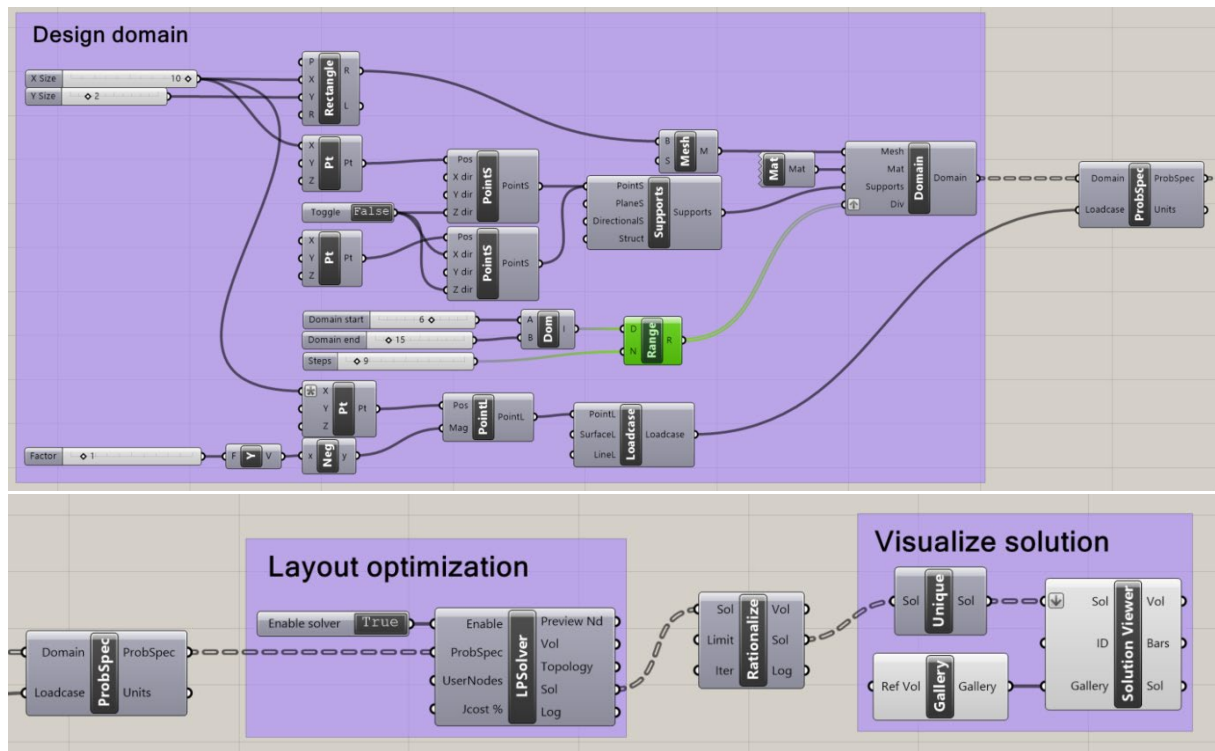

Figure C.6 Setting up design space in Grasshopper

Peregrine is not suitable for optimising cast glass structures with the functionalities it has at the moment of testing the program. It isn't easy to join all bars into a single element from the optimised design without adding spheres at each node. This process can be done in Rhino itself, but due to the complexity of the model and the number of different elements, the program crashed every time this was tried. It was not researched if another program could do this. However, it is still a promising plug-in. The optimised design consists of beams and nodes. This type of design is more suitable to produce with glass rods and steel nodes. Additionally, a drawback of this program is its assumption of plastic behaviour when using multiple load cases. For brittle materials, another solution should be found when optimising on multiple load cases.

C.4 Millipede

Millipede is a free structural analysis plug-in for Grasshopper. The developers discontinued developing and updating the software. It is not possible to go to their website, and it is impossible to download the plug-in via the conventional way. When opening the plug-in, it warns you that this version of millipede has expired and that a newer version should be downloaded from their website. However, the plug-in still works when this message is disregarded. Since there is no manual, it is difficult to find out how the plug-in works.

Setting up the design is done in Grasshopper in combination with Rhino. Before the optimisation is started, the design space is transformed into a FE model meshed into triangles. A point load, line load or surface load or load region can be added to the model. It is not possible to add a moment. Multiple load cases can be added to the optimised object. The structure can be supported by a plane or by a domain, and rotational restrictions can be added.

After optimisation, the object can be re-meshed within this plug-in. Further, post-processing is needed, which should be done with another Grasshopper plug-in. After optimisation, the stress lines can be given, but no further structural analysis of the optimised object can be done within the plugin.

The lack of support types and the discontinuation of the software make millipede unsuitable for optimising cast glass structures. Additionally, an important aspect is cross-sectional constraints which are not possible to implement with this plug-in.

C.5 tOpos

tOpos is a relatively new free topology optimisation plugin for Grasshopper. This plugin gives faster results in comparison to other topology optimisation plugins. This is because the plugin is designed to use GPU for the acceleration of the computation. This means that this plugin is only fast when used on computers with an NVIDIA graphics card that has Cuda Computation Capability that is higher or equal to 3.0. There is an option to use this plugin in CPU mode, which still gives the same result but takes longer to run (Bialkowski, 2017). Because of the lack of documentation and manual, it is unclear what hidden feature the program has. Underneath are the findings of various test scenarios.

The topology optimisation in tOpos is compliance-based and is done according to the SIMP methodology. Setting up the design is done in Grasshopper in combination with rhino. Before the optimisation is started, the design space is meshed into triangles. This can be done within the plugin. A point load, line load, surface load and volume load can be added to the model, and it is not possible to add a moment. The structure can be supported by defining a volume. It is impossible to say how this volume supports the structure (fixed, simply supported, hinged).

12

After optimisation, an iso mesh or voxel mesh can be plotted. Additionally, the principal stresses can be plotted from the initial results. It is not possible to re-mesh or smoothen the mesh within the plugin. However, this can be done with 'Smooth Mesh' included in Grasshopper or 'Weaverbird's Catmull-Clark Subdivision', which is included in the free plug-in weaverbird.
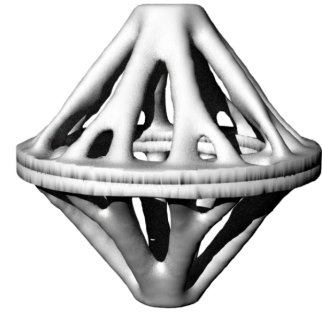

Figure C.7 Topology optimised Christmas ornament

With this plugin, multiple designs were made. For example, a topology optimised Christmas ornament. In Figure C.7 and Figure C.8, this ornament is given with the associated Grasshopper script. After the smooth-mesh component, some manual alterations were done to prepare the file for 3D printing.

tOpos is less suitable for the optimisation of cast glass structures. This program is not ideal because it is impossible to add moments and because it is not possible to define specific support conditions and min/max cross-sectional constraints. The missing of a manual is also not ideal when figuring out the capabilities of a software program.
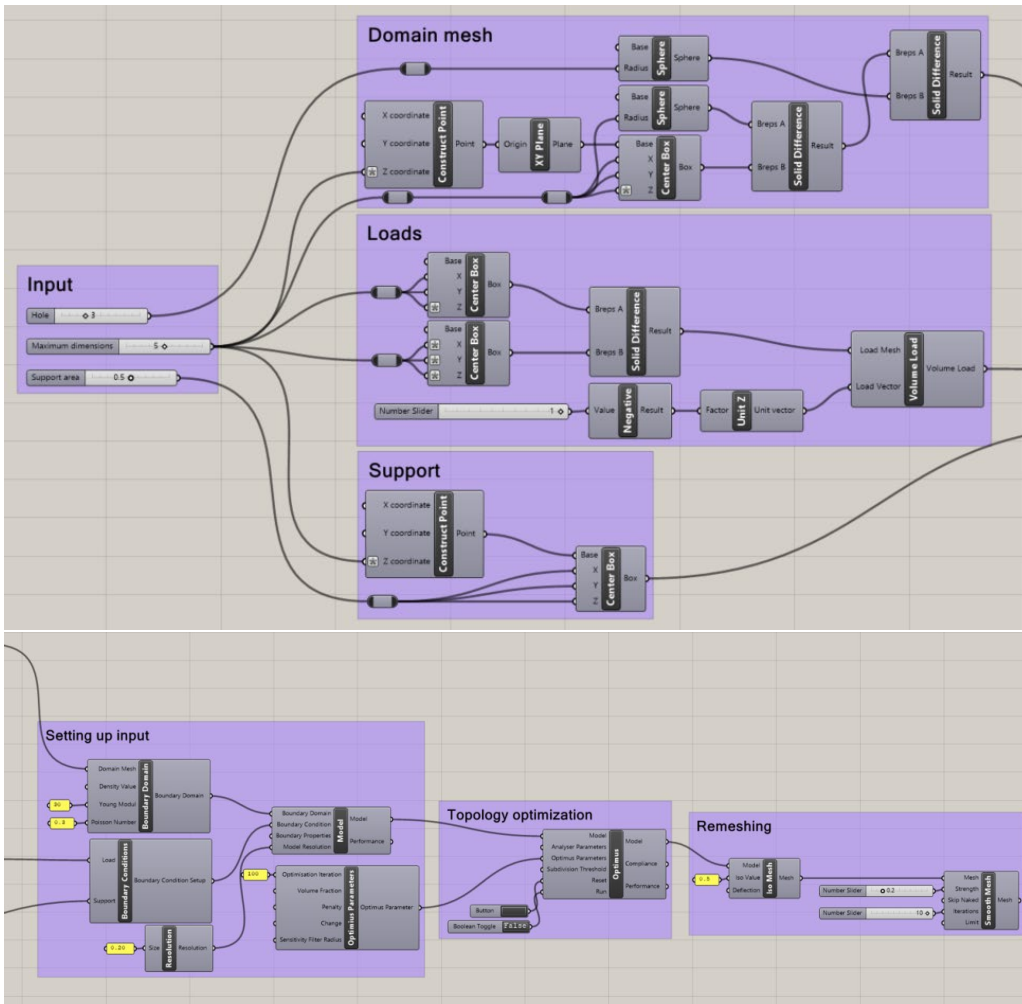

Figure C.8 Setting up design space in Grasshopper

1. As input for Spaceclaim, the original un-optimised model is needed and the result from the optimisation process. Both models are given in Figure D.1.
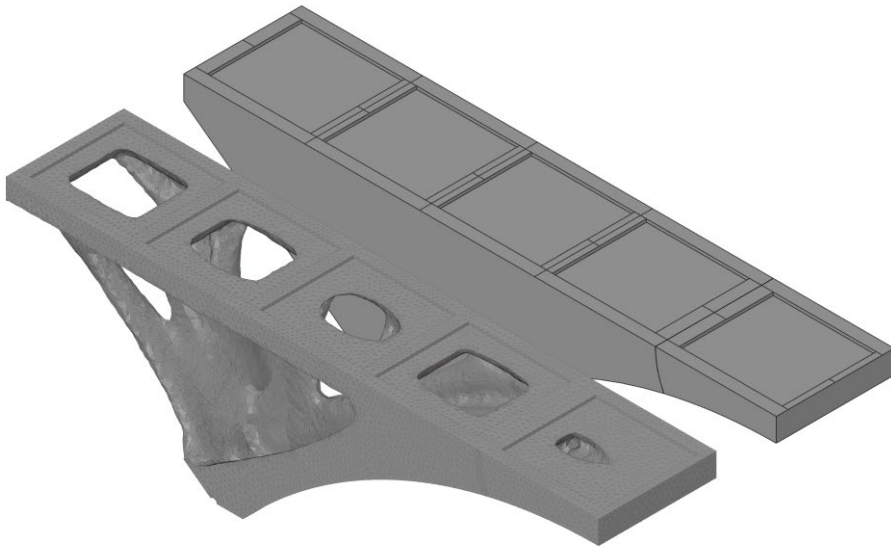

Figure D.1 Optimised faceted body and un-optimised model.

2. Since the optimised model is not exact anymore, the original model is needed to get some exact shapes. These faces and the solid model are given in Figure D.2
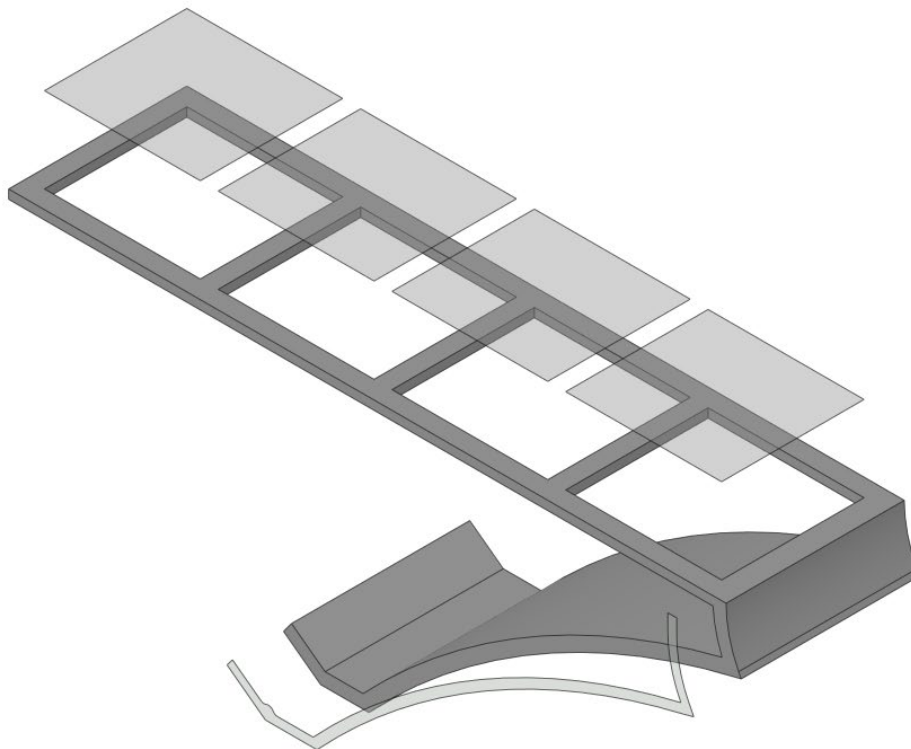

Figure D.2 Body and surfaces extracted from the un-optimised model

3. In this case, the solid model made in step 2 needs to be a little bit bigger near the connections and near the arch, as indicated in red in Figure D.3. This is needed to make sure that in a later step, these surfaces are not faceted.
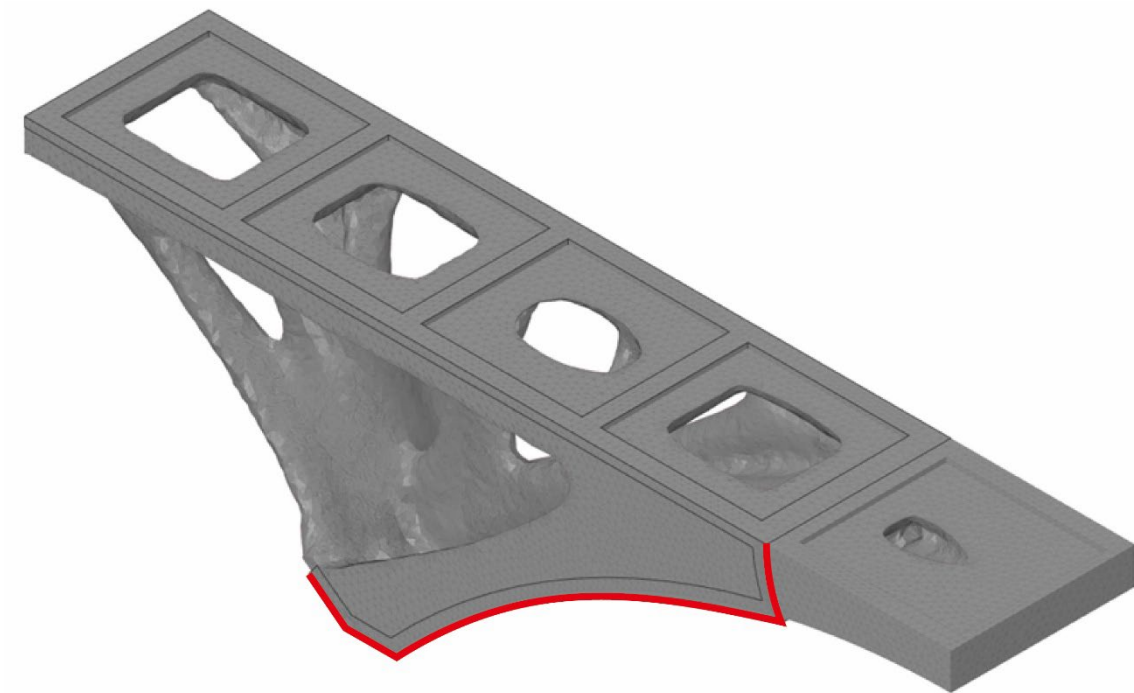

Figure D.3 Area in red needs to be extruded extra to ensure these surfaces are not faceted.

4. The faceted body is shrink-wrapped with the shrinkwrap tool on the facets tab. A maximum Gap size of 50 mm is implemented, and the box preserve features is checked with an angle threshold of 40°. The result of this step is given in Figure D.4.
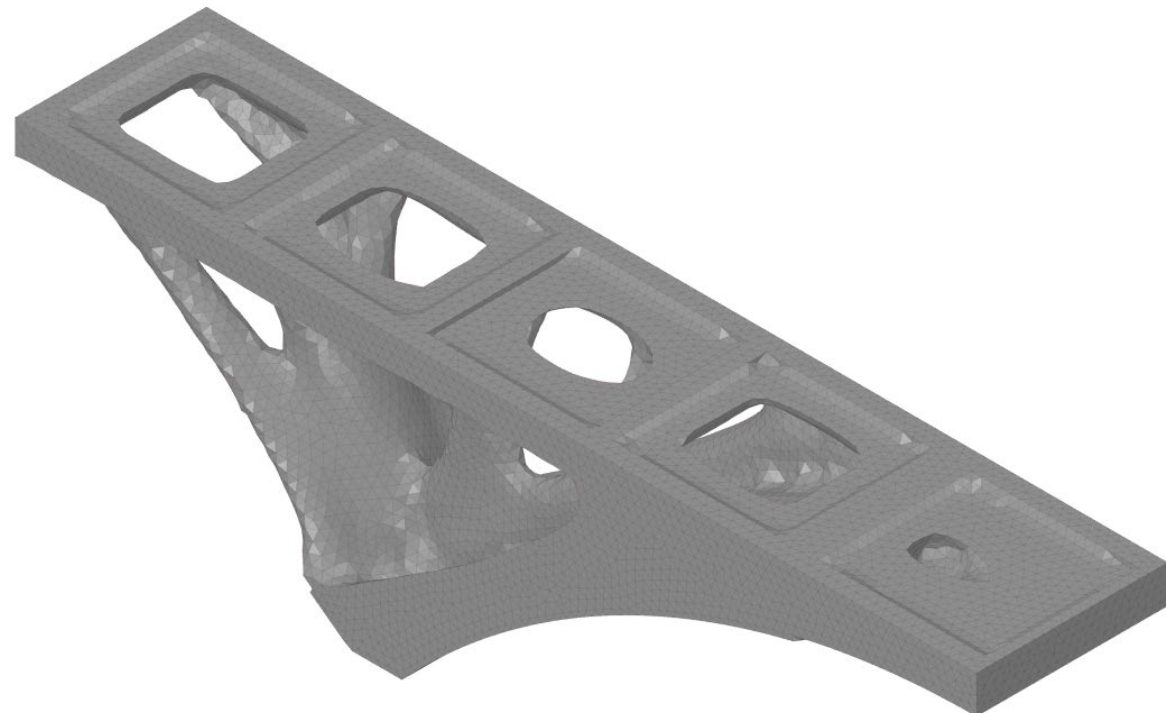

Figure D.4 Result of the shrink-wrapping process.

5. This faceted body is converted to a solid with merge faces on. The result of this step is given in Figure D.5
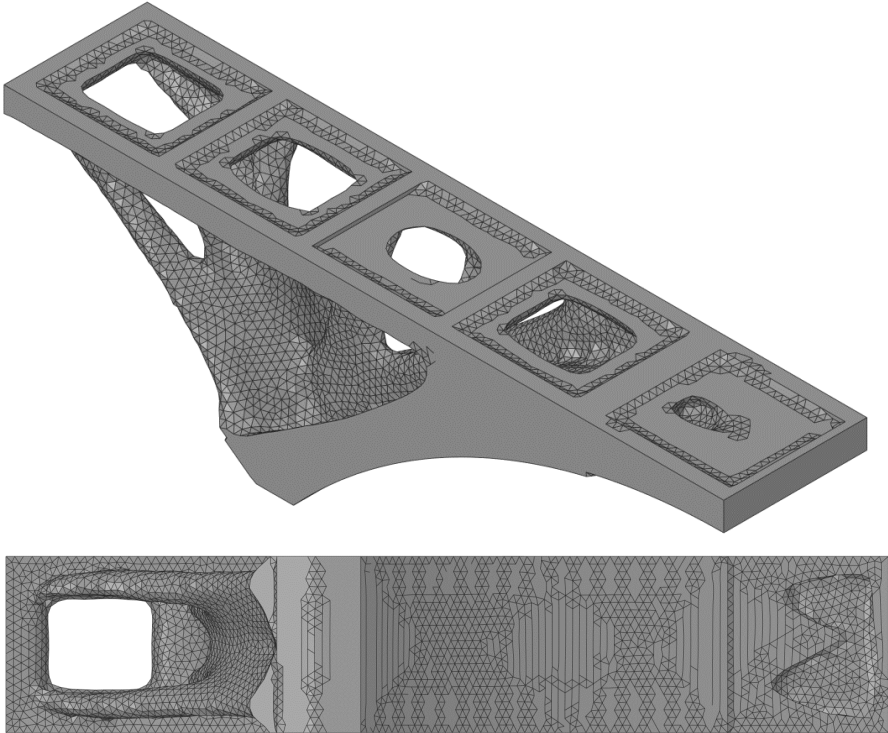

Figure D.5 Result of the conversion of a faceted body into a solid body.

6. Then the parts that should be smooth or need to have a straight angle are cut out with the pull tool. The surfaces made in step 2 are needed during this step. The result is given in Figure D.6.
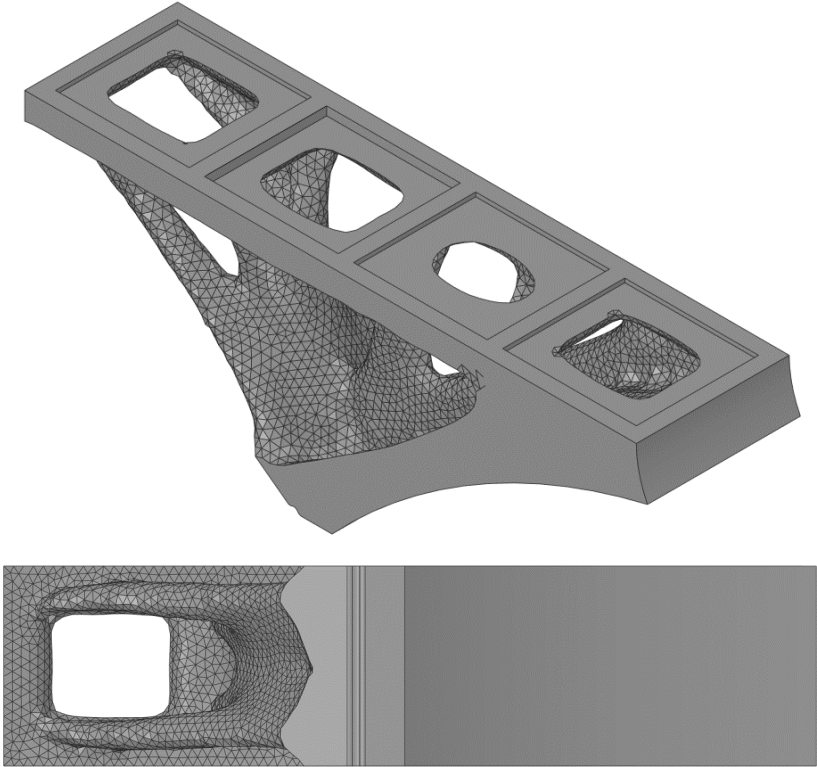

Figure D.6 Results from pull/push action done with surfaces from step 2.

7. Step 2 till 6 are repeated for the middle section. The result of this part is given in Figure D.7.
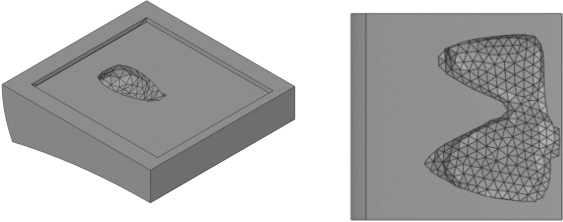

Figure D.7 Result of the post-processing of the middle section.

8. The result is mirrored 4 times to obtain the final model. In the final step, the top surface and support elements are also modelled. The final model is given in Figure D.8.
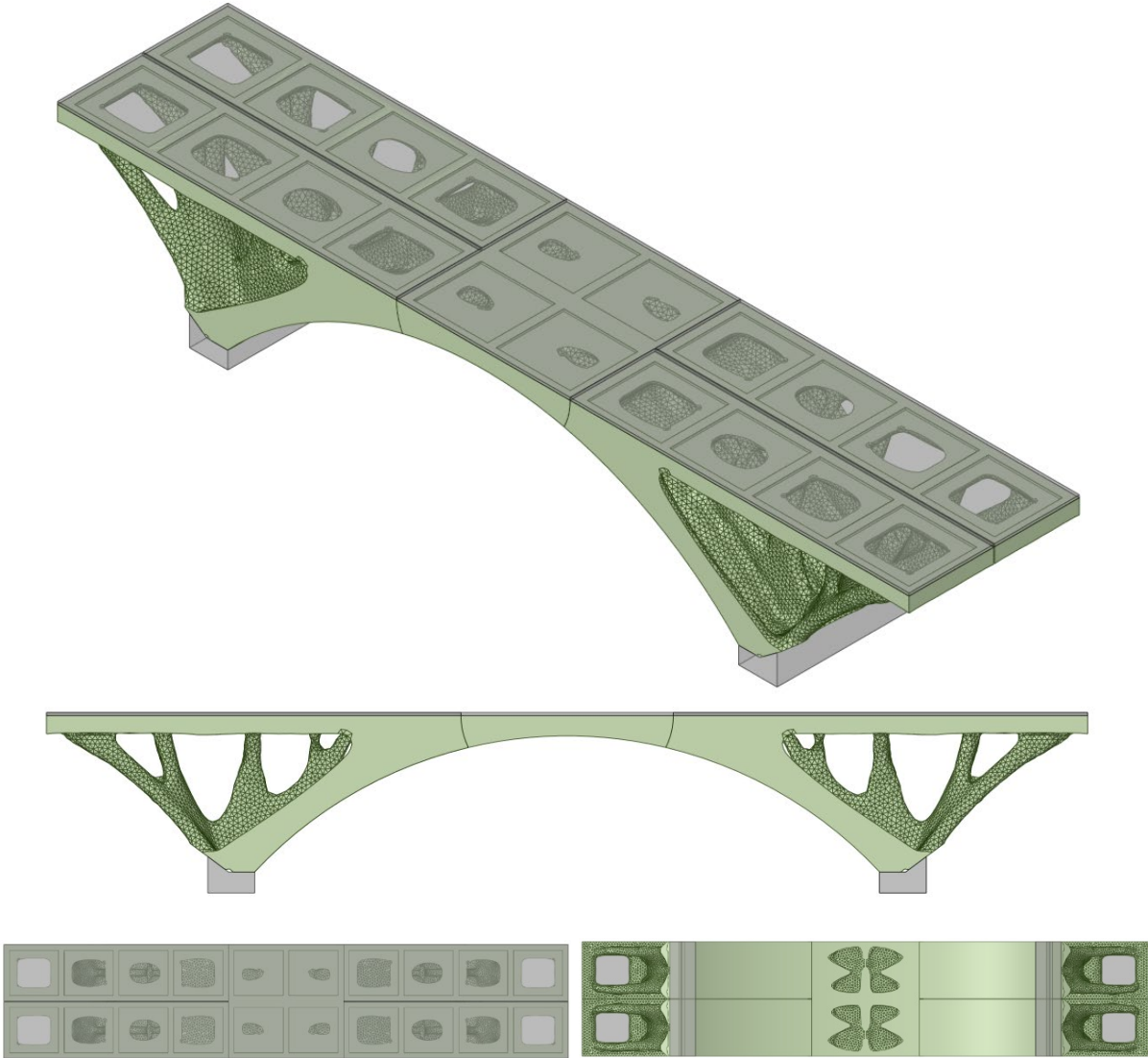

Figure D.8 Final FEM model

E. Manual verification

Simplified manual calculations are used to check the outcome of the FEM model. First, the reaction forces are compared to the forces that are applied on the bridge. Second, the stability is verified with the use of thrust lines. Third, the stresses inside the connections are compared with the manually calculated stresses. Fourth, the buckling load is calculated. The manual verifications can be found in Appendix E.

E.1 Reaction forces verification

The verification of reaction forces is done for boundary condition cycle 3 scenario 1. The total pressure that should be applied on the top surface for load case 2 is equal to 7.8 kN/m^2, which is equal to a total load of 156 kN. The weight of the soda-lime glass top layer for load case 2 is equal to 3075 kg/m^3 with a total thickness of 36 mm the total weight of the float glass 1.1 kN/m^2, which is equal to a total load of 22 kN. The weight of the borosilicate cast glass for load case 2 is equal to 2788 kg/m^3. The outer elements have a volume of 1.07 m^3 which is equal to a total dead load of 30 kN for each outer element (120 kN total). The keystone has a volume of 0.75, which is equal to a total dead load of 21 kN. The total load that is exerted on the supports is around 320 kN. The total vertical support forces from the FEM model are equal to 330 kN. The deviation between the results is most likely from the simplification of the forces on the top surface.

E.2 Stability analysis with the line of thrust

When looking at the stability of the bridge, it is essential that the line of thrust can go through the supports and connections. The most governing scenarios for the bridge are scenario 14 and scenario 15. The verification for the stability is done for boundary condition cycle 3. The loads from deadweight and the variable loads with corresponding points of application are given in Table E.1. The thrust line and force polygon for scenario 14 is given in Figure E.1, and for scenario 15 is given in Figure E.2. As can be seen, the thrust line goes through the supports and the connections.

Table E.1 Loads and application points used for drawing thrust line.

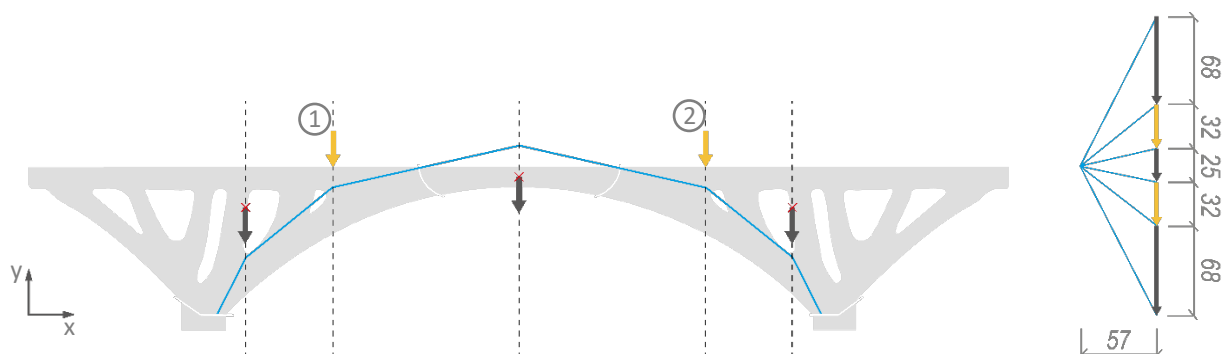|	Loads [kN]	Point of application	
		x [mm]	y [mm]
outer element 1+2 & floatglas layer 1+2	68	2210	1066
keystone + floatglas layer	25	5000	1408
outer element 3+4 & floatglas layer 3+4	68	7790	1066
Resultant force 1	32	3000	1500
Resultant force 2	32	7000	1500

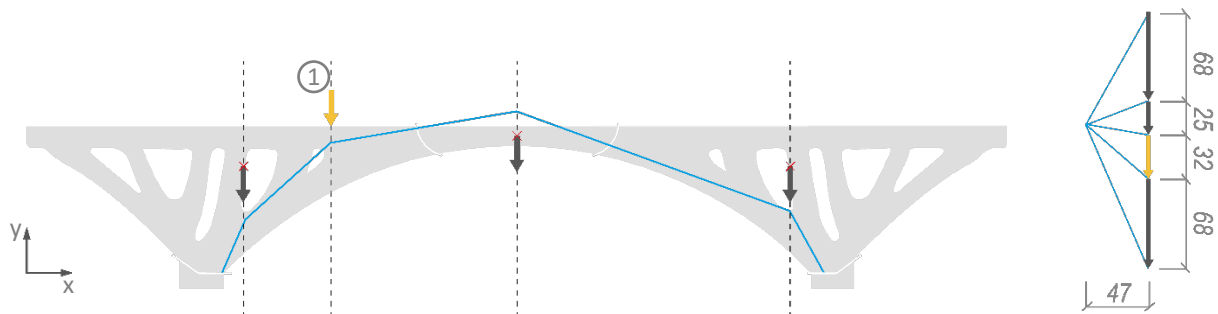*Figure E.1 Thrust line and force polygon for scenario 14 cycle 3.*

Figure E.2 Thrust line and force polygon for scenario 15 cycle 3.

E.3 Stress verification inside connections

The reaction forces at the supports for load scenario 14 cycle 3 are equal to 127 kN. When dividing this load over the entire surface, a pressure is obtained of 0.13 MPa. Only part of the surface is under compressions since the load is applied eccentrically. The results from the finite element analysis are in the same order of magnitude as the calculated pressure.

E.4 Buckling

FEA models assume perfection when calculating stresses. In real life, this is, most of the time, not the case. That is why additional checks are done to ensure the actual load in the cross-section is smaller than the buckling load.

For the calculation of the buckling load, Euler's column formula is used. See Equation E.4.4.

$$F = \frac{n\pi^2 EI}{l^2} \tag{E.4.4}$$

where:

F	Buckling load in (N)
n	End condition factor
E	Modulus of elasticity (N/m^2)
I	Moment of inertia (m^4)
l	Length of the column (m)

The assumption is made that the columns are somewhere between fixed and pivoted on both ends. The buckling length of the fixed column is equal to half of the total length, and the buckling length of the pivoted column is equal to the entire length. This result in the factor for end conditions to be equal to 4 for the fixed column and equal to 1 for the pivoted column.

The minimum cross-section in the model has a diameter of 150 mm, and the maximum length a column could have is 2.1 meter. This results in a buckling load of 2504 kN for a pivoted column and a buckling load of 14015 kN for a fixed column. This load is never exerted on the bridge, and thus, buckling is assumed to be safe.